Protein-Protein Interactions of Hsp27

by

Rebecca Emily Freilich

DISSERTATION

Submitted in partial satisfaction of the requirements for the degree of

DOCTOR OF PHILOSOPHY

in

Chemistry and Chemical Biology

in the

GRADUATE DIVISION

of the

UNIVERSITY OF CALIFORNIA, SAN FRANCISCO

Dedicated to Erica and David Freilich, Marion and Gerald Freilich, and Etan Schwartz.

Thank you for always believing in me.

Acknowledgements

I would like to thank my advisor Jason Gestwicki for his guidance and support throughout my PhD, for providing the space to explore and develop my scientific interests and curiosity, and for always being receptive to my unbridled enthusiasm. I would also like to thank my thesis committee members Kevan Shokat and Michelle Arkin for their support and guidance throughout my time at UCSF. Kevan was especially helpful to me during my first year of graduate school and helped me land in the Gestwicki lab, for which I will always be grateful.

I am grateful to work with all the members of the “Gestwicki Gang” past and present. In particular, I would like to thank Leah Makley, Jennifer Rauch, Sue-Ann Mok, Victoria Assimon and Matt Ravalin for their guidance and encouragement. I would also like to thank the many people at UCSF who have been willing to teach me new techniques and providing a different perspective, especially Daniel Elnatan, Miguel Betegon, Eric Tse, Olivier Julien, Adam Larson and Rose Citron.

I could not have completed this work without the love and support of my family and friends. I thank my parents for instilling the value of intellectual exploration within me and for their constant support; my grandparents, especially Poppy, for inspiring me to pursue a PhD; and to my husband, Etan Schwartz, who is my biggest cheerleader and is a constant source of encouragement.

Acknowledgement of Previously Published Material

Chapters 1, 2, and 3 are reprints of the material as it appears in:

Freilich, R., Arhar, T., Abrams, J.L., Gestwicki, J.E. Protein-protein interactions in the molecular chaperone network. ***Acc. Chem. Res****. 51(4): 940-949.*

Meister-Broekema, M.*, Freilich, R.*, Jagadeesan, C.*, Rauch, J.N.*, Minoia, M., Furtado, G., van Waarde, M., Carra, S., Bergink, S., Gestwicki, J.E., Kampinga, H.H. Myopathy associated BAG3 mutations lead to protein aggregation by stalling Hsp70 networks. ***Nat. Comm.*** Currently in revision.

Freilich, R., Betegon, M., Tse, E., Mok, S.A., Julien, O., Agard, D.A., Southworth, D.R., Takeuchi, K., Gestwicki, J.E. Competing protein-protein interactions regulate binding of Hsp27 to its client protein Tau. ***Nat. Comm.*** Currently in revision.

Protein-Protein Interactions of Hsp27

By Rebecca Emily Freilich

Abstract: Small Heat Shock Proteins (sHSPs), including Hsp27, are a non-enzymatic class of molecular chaperones that bind improperly folded proteins and maintain their solubility, acting as a first line of defense against cellular stress. Through their 'holdase' function, the sHSPs are implicated in a variety of diseases that involve imbalances in protein homeostasis, such as cancer and neurodegeneration. However, because they form highly dynamic, polydisperse oligomers, it has been difficult to study how they work and even what they interact with. This thesis explores the various protein-protein interactions (PPIs) that involve the sHSPs (particularly Hsp27) as a way to clarify sHSP function and guide future small-molecule development. Chapter one consists of a review of the various PPIs within the chaperone network and highlights the critical role of PPIs in facilitating cooperation between chaperone families, and how these individual PPIs represent important targets for small-molecule discovery. Chapter two describes a collaborative effort to characterize how point mutations within the Hsp70-sHSP adaptor protein BAG3 can upend the function of the entire network and lead to disease. Chapter three describes the characterization of Hsp27's interaction with client protein Tau and the important finding that client-binding sites are competitive with oligomeric PPIs. Taken together, this work emphasizes the importance of individual interaction interfaces in dictating function of a chaperone itself and in the context of the greater network.

Table of Contents

List of Figures

Chapter 1

Protein-protein interactions in the molecular chaperone network

Rebecca Freilich, Taylor Arhar, Jennifer L. Abrams and Jason E. Gestwicki

Conspectus. Molecular chaperones play a central role in protein homeostasis (aka proteostasis) by balancing protein folding, quality control and turnover. To perform these diverse tasks, chaperones need the malleability to bind nearly any "client" protein and the fidelity to detect when it is misfolded. Remarkably, these activities are carried out by only ~180 dedicated chaperones in humans. How do a relatively small number of chaperones maintain cellular and organismal proteostasis? Further, once a chaperone binds a client, how does it "decide" what to do with it? One clue comes from observations that individual chaperones engage in protein-protein interactions (PPIs) – both with each other and with their clients. These physical links coordinate multiple chaperones into organized, functional complexes and facilitate the "hand off" of clients between them. PPIs also link chaperones and their clients to other cellular pathways, such as those that mediate trafficking (*e.g.,* cytoskeleton) and degradation (*e.g.,* proteasome). Thus, the key to understanding chaperone-mediated proteostasis might be to understand how PPIs are regulated. This Account will discuss the efforts of our group and others to map, measure and chemically perturb the PPIs within the molecular chaperone network. Chemical biology has played a particularly important role in this effort, as molecules that either promote or inhibit specific PPIs have proven to be invaluable research probes. In addition, these molecules have provided leads for the potential treatment of protein misfolding diseases.

1 Introduction to the Chaperone Network. The largest class of molecular chaperones is the heat shock proteins[1], which are named for their apparent molecular mass (in kDa): Hsp90, Hsp70, Hsp60, Hsp40 and the small heat shock proteins (sHsps). The

heat shock proteins are abundant and conserved through all kingdoms of life, suggesting that they are an ancient way of protecting proteomes. In their simplest form, the “job” of the chaperones is to bind clients and protect them from aggregation. Some chaperones, such as Hsp70, accomplish this task by interacting reversibly with exposed hydrophobic regions, limiting aberrant (*i.e.,* non-native) contacts. Beyond this simple anti-aggregation activity, groups of chaperones are able to carry out more sophisticated functions, such as folding or dis-aggregating proteins. These activities are typically powered by ATP hydrolysis, and they often require the coordinated efforts of multiple chaperones and co-chaperones from different categories (*e.g.,* Hsp70s and Hsp40s) working together.

In this Account, we focus on the protein-protein interactions (PPIs) between chaperones. A map of the PPIs between chaperones shows that all of the major categories are physically linked to each other, either directly or through intermediary, scaffolding factors (Figure 1.1). For example, PPIs link the sHsps, such as Hsp27 and Hsp22, to Hsp70 and Hsp90 through the scaffolding co-chaperones BAG3 and HOP/Sti1. Other chains of PPIs link classes of chaperones, such as prefoldin and TriC, to Hsp70 and Hsp40s. In prokaryotes and yeast, PPIs (dashed lines in Figure 1.1) provide additional connectivity. However, it is important to note that these PPIs are not all the same. They occur with a wide range of affinity values, from strong (nM) to very weak (μM), and they involve contact surfaces that are either small or quite large (>2500 $Å^2$).

Our group, and many others, think that this PPI network architecture is critical to the ultimate functions of the chaperones[2]. It is known that some clients undergo "handoff" from one chaperone to another through these conduits, perhaps minimizing their exposure to bystanders. For example, steroid hormone receptors (SHRs) are shuttled between Hsp70 and Hsp90 through the action of HOP[3] (see Figure 1.1). In other examples, replacing one chaperone for another has been shown to "switch" the overall function. For example, while Hsp70 and HOP are linked to folding of SHRs, a complex of Hsp70 and CHIP is linked to their degradation[3]. Together, these observations give the impression of a dynamic, interconnected web of chaperones that coordinate their functions and share molecular information to maintain proteostasis.

Because PPIs are so critical in dictating chaperone functionality, chemical probes that target particular chaperone PPIs are extremely useful tools for understanding the role of chaperone co-chaperone pairs in overall network connectivity and specifying particular client interactions. Furthermore, it is possible that small-molecules targeting specific chaperone PPI pairs may impart more specificity than ATP-competitive inhibitors, as they may target only a subset of functions. The major chaperone classes have evolved to interact with many different proteins as to act as general anti-aggregation factors, and thus contain PPIs with broad affinity and surface areas. Our lab has used both direct and indirect high throughput screening (HTS) to identify small molecules that modulate chaperone PPIs. For example, we identified inhibitors of the Hsp70-BAG3 interaction using flow cytometry and capillary electrophoresis to directly detect disruption of PPIs[80,81]. Another approach is screening against the enzymatic activity of a multi-protein

complex, which we have used to identify inhibitors of Hsp70/J-protein/NEF interactions[82,83]. A variety of affinity- and stability-based methods are available for proteins that feature complex and not well-characterized PPIs[84]. For example, we used differential scanning fluorimetry (DSF) to identify chemical chaperones for small HSPs[62].

In the next sections, we briefly review the major classes of chaperones. We do not intend this discussion to be inclusive, because many reviews have covered the topics of chaperones[1], the stress response[4] and their roles in disease[5]. Rather, we focus here on the PPIs – the dynamic "glue" on which the chaperone network is assembled – and we highlight the important roles that small molecules have played.

2. Heat shock protein 70 (Hsp70). Hsp70 is a good starting-point for a discussion of chaperone PPIs, as it makes a number of well-characterized contacts (Figure 1.2). Hsp70 is composed of a nucleotide-binding (NBD) domain, which has ATPase activity, and a substrate-binding domain (SBD) that makes contact with the client. In the ATP-bound state, Hsp70 binds weakly to its clients, while nucleotide hydrolysis slows the off-rate and increases affinity[6-7]. Through this deceptively simple system of ATP-driven "catch-and-release", Hsp70 has been shown to be critical for a wide range of activities, including protein folding, chaperone-mediated autophagy and endocytosis. Because of its central role in delivering clients to so many different pathways, Hsp70 is often considered the "triage" chaperone.

How can one factor be involved in so many disparate processes? By design, Hsp70 and many other chaperones are promiscuous such that they can prevent bulk protein aggregation. It is thought that PPIs with co-chaperones are the key to providing specificity and functionality[2, 7]. Hsp70 binds to three major categories of co-chaperones: Hsp40s (also called J proteins), nucleotide exchange factors (NEFs) and tetratricopeptide repeat (TPR) proteins (Figure 1.2). There are ~50 Hsp40/J protein genes in humans, and dozens of NEFs and TPR proteins. Moreover, each of the individual co-chaperones brings its own functionality into the system, as outlined in the sections below. Thus, with the large number of Hsp70s and co-chaperones in the human genome, thousands of possible Hsp70-client-Hsp40-NEF-TPR combinations are possible.

Hsp40s/J Proteins. The Hsp40/J proteins are a group of co-chaperones that contain a conserved J-domain[8]. J-domains make contact with Hsp70s via electrostatic interactions between the positively charged helix II of the J-domain and negatively charged region composed of lobes IA and IIA of the NBD, the inter-domain linker, and the β sandwich domain in the SBD (Figure 1.2B)[9,10,85]. This PPI surface is strikingly "spread out" and polar, as well as weak (K_D estimated ~ 10 μM), placing it in a category of PPIs that is notoriously difficult to inhibit[11]. Despite this challenge, a class of dihydropyrimidines takes advantage of a relatively deep groove between the IA and IIA lobes of Hsp70 to either disrupt or promote the J-domain contact[12]. Work by our group and others have advanced these molecules as chemical probes for a number of disease systems[13-14].

The PPI between Hsp70 and its Hsp40s/J proteins has a number of important consequences. Firstly, it stimulates Hsp70's ATPase activity[10]. The intrinsic rate of nucleotide turnover is slow, so this stimulatory activity is important for converting Hsp70 to the tight-binding conformer. Second, the Hsp40s/J proteins often include second domains that bind directly to clients and recruit them to the Hsp70 system[8]. In this role, some Hsp40s/J proteins are highly specialized; for example, auxillin (DnaJC6) recruits Hsp70 specifically to clathrin-coated vesicles[15]. However, other Hsp40s/J proteins are relatively promiscuous, recognizing a wider range of proteins[16]. Some of the Hsp40s/J proteins also have additional domains that link them to other chaperones within the network; for example, DnaJC7 also binds Hsp90[17]. Finally, many of these co-chaperones engage in PPIs with themselves as part of oligomers, which might be important for certain functions, such as disaggregation[18]. Together, these diverse PPIs make Hsp40s/J proteins central adapters of the network.

Nucleotide Exchange Factors (NEFs). NEFs are co-chaperones that release ADP and clients from Hsp70[19]. There are four distinct structural categories of human NEFs, each of which uses a different binding mode. Although these categories of NEFs use different PPI interfaces, they all act to stabilize the "open" form of Hsp70's NBD, accelerating release of ADP and client. The prokaryotic GrpE and its human ortholog, GrpEL1 or HMGE, accomplish this goal using a β-domain to interact with lobes IB and IIB[20]. Members of the BAG family use a 3-helix bundle to make hydrophobic and electrostatic contacts with a similar region[21]. Recent work from our group has indicated that some

BAG family members, such as BAG1 and BAG3, make an additional, non-canonical interaction with Hsp70's SBD which is essential for release of clients[22]. Members of the Hsp110/Grp170 family use a completely different approach, making extensive contacts with lobe IIB of the NBD[23]. Finally, HspBP1/Sil1 family members use four armadillo-repeats to bind to lobe IIB, destabilizing the NBD[24]. HspBP1/Sil1 family members also contain an unstructured N-terminal domain which further facilitates client release by mimicking client and interacting with SBD[86,87]. The PPIs between Hsp70 and NEFs are relatively strong (K_D values in the low to mid nanomolar range), but the interaction surfaces have complex topology. Despite the complexity of these PPIs, inhibitors of Hsp70-NEF have been described. The best studied are the MKT-077 family of small molecules, which bind to a conserved allosteric site on Hsp70[25] and stabilize the ADP-bound state[26]. As discussed below, these molecules have been powerful probes for understanding the roles of Hsp70 and the NEFs in proteostasis.

In addition to their activity on Hsp70, some NEFs are multi-domain adapters that bind to proteins in other pathways. For example, Hsp110 binds to misfolded proteins, preferring aromatic residues and potentially expanding Hsp70's client pool[27]. Thus, NEFs are not only important for nucleotide cycling, but they also seem to be key in coordinating handoff to other chaperones and pathways.

Tetratricopeptide Repeat (TPR) Proteins. TPR domains are defined by three or more tandem TPR motifs that encode amphipathic helices[28-29]. There are hundreds of TPR domain-containing proteins expressed in humans, but a subset contains a conserved

lysine and two asparagines, which is termed a “carboxylate clamp”. These residues make hydrogen bonds with the extreme C-termini of the cytosolic Hsp70s and Hsp90s, in a shared motif defined by the amino acids EEVD-COOH[30]. While most of the binding energy for this interaction seems to come from the interaction of the EEVD with the carboxylate clamp[31], residues preceding the EEVD sequence have been shown to contribute to specificity; for example, FKBP51 and FKBP52 prefer Hsp90’s MEEVD, while CHIP and DnaJC7 prefer Hsp70’s IEEVD[17]. These differences provide a hierarchy of Kd values from ~10 μM to less than 1 μM. Because of the polar nature of the EEVD-TPR contact, few molecules have been reported to inhibit this PPI.

The defining feature of the TPR containing co-chaperones is that they bring specific enzymatic functions into the chaperone complexes[32]. For example, CHIP is an E3 ubiquitin ligase that acts on chaperone-bound clients, while PP5 is a protein phosphatase and FKBP51/52 are peptidyl prolyl isomerases. Thus, the identity of the bound TPR co-chaperone often seems to determine what ultimately happens to the chaperone’s client.

Putting It All Together. How do Hsp70 and its co-chaperones come together to make “decisions” about client fate? Our group has taken a chemical biology approach to this question, using small molecules to perturb individual PPIs and asking how client fate is impacted in cells and tissues. Recent reviews have described these chemical probes and their mechanisms in more detail[33-34]. Here, we focus on analogs of MKT-077, such as JG-48, which have been shown to inhibit the PPI between Hsp70-NEF[26]. Because

NEFs normally promote the release of clients, JG-48 significantly stabilizes the Hsp70-client complex, as shown *in vitro* and in cells. What is the consequence of this? Strikingly, a number of groups have found that JG-48 and its analogs promote the turnover of multiple Hsp70 clients, including tau[35], polyglutamine proteins[36], Dengue viral proteins[37] and oncoproteins[38]. Thus, it seems that Hsp70 and its NEFs may normally monitor the dwell time of clients and promote their degradation if they remain "too long"[39]. Chemical inhibitors promote turnover by limiting the ability of NEFs to release client, which could be a favorable activity in models of neurodegeneration and cancer.

Other Hsp70 Interactions in Prokaryotes. As mentioned above, Hsp70 co-chaperones, such as BAG3 and HOP, play an important "adapter" role in eukaryotes. However, many of these adaptors do not exist in prokaryotes, and there is some evidence that, in those systems, the major prokaryotic chaperones coordinate directly in their absence. For example, prokaryotic DnaK/Hsp70 directly interacts with prokaryotic Hsp90 (termed HptG) and ClpB[40-41]. These examples suggest that PPIs have always been used to build chaperone networks and that evolution has only further elaborated that scheme.

2. Hsp90. Hsp90 is another major "hub" of the chaperone network, interacting with a large number of co-chaperones and clients[42]. Based on pioneering work in SHRs, Hsp90 is thought to recognize clients in later stages of folding, functioning in their stability and activation[43]. Hsp90 has three domains: an amino-terminal domain (NTD)

that is responsible for binding to ATP[44], a middle domain (MD) that is required for ATPase activity[45], a carboxy-terminal domain (CTD) that is responsible for homodimerization[46] and terminates in the MEEVD motif that binds TPR co-chaperones[29]. The Hsp90 homodimer undergoes dramatic conformational rearrangements over the course of its ATPase cycle, in which binding of ATP promotes a closed state where the NTDs dimerize, allowing for ATP hydrolysis. A number of inhibitors, most notably geldanamycin and radicicol, have been found to compete for binding with ATP, thus inhibiting Hsp90 ATPase activity[47-48]. There have been reports of inhibitors, such as novobiocin, that bind to the CTD, potentially acting by interfering with allostery or dimerization[49].

Hsp90 Co-Chaperones. Hsp90 interacts with a number of co-chaperones that tune its ATPase activity and control its association with clients (Figure 1.3)[50]. The co-chaperone, Aha1, interacts tightly (Kd ~0.7 μM) through hydrophobic contacts with the first alpha-beta-alpha domain of the MD, as well as more widely distributed polar interactions and, by NMR, contact with the NTD[51]. Binding of Aha1 causes a conformational change in the catalytic loop of Hsp90, displacing HOP and releasing Arg 380 to access the ATP binding site in the NTD[52]. Another co-chaperone, p23, binds (Kd ~ 1 μM) as a dimer between the NTDs of two Hsp90s, inhibiting ATPase activity by stabilizing the ATP-bound, closed state[53]. Additional contacts are made between p23 and the inter-domain junction (where the MD of one protomer interacts with the NTD of the other protomer). Because this site is shared by Aha1, binding of p23 and Aha1 are mutually exclusive. Moreover, geldanamycin limits association of Hsp90 with p23[54], likely through an

allosteric mechanism. Finally, the co-chaperone, Cdc37, interacts with both the NTD and MD[55]. The major feature of Cdc37 is that it is required for maturation of kinases. Indeed, the structure of a kinase/Cdc37/Hsp90 complex reveals that this interaction occurs in the closed state of Hsp90, in which Cdc37 mimics interactions between p23 and the NTD while making additional, polar contacts with the MD. This interaction partially inhibits ATPase activity by limiting lid closure. Celastrol has been reported to disrupt the interaction of Cdc37 and Hsp90 by binding to the CTD[56], although its selectivity remains uncertain.

3. Small Heat Shock Proteins. The small heat shock proteins (sHsps) are a class of ~10 non-enzymatic chaperones that bind partially unfolded client proteins to maintain their solubility[57]. All sHsps contain a highly conserved α-crystallin domain (ACD) flanked by variable N- and C-termini (Figure 1.4A). A key feature is that these monomers assemble, using a series of PPIs described below, into large, polydisperse oligomers with sizes ranging from dimers to over 40 subunits[58]. Some studies suggest that smaller oligomers might be more potent chaperones, such that changes in oligomer size may be functionally important[59]. Thus, like other chaperone families, the biology of sHsps seems to be driven by dynamic PPIs, both with each other and with their clients.

Oligomeric Interactions of the sHsps. The simplest unit of the sHsps is the dimer, which is driven by the interaction of two ACDs. Each ACD is a highly conserved β-sandwich and two of them come together into a compact structure via anti-parallel β-sheets. Although similar in overall architecture, the dimer interfaces amongst the human

sHsps are not identical (Figure 1.4B). For example, the interface of αB crystallin's ACD dimer has many salt bridges that can act as a pH sensor[60], while that of Hsp27 contains a cysteine bridge that forms a redox sensor[61]. These observations support the idea that chaperone function is linked to regulation of this PPI. In addition, the ACD interface is the one PPI in this system that has a known chemical probe; our group discovered a class of oxysterols that stabilize this contact, with the lead molecule, C29, making contacts with both sides of the anti-parallel b-sheet[62]. Because mutational destabilization of this interface can lead to disease, C29 is currently in pre-clinical development as a non-surgical treatment for cataracts.

Other PPIs within sHsp oligomers are mediated by the highly variable and flexible C-terminal extensions (CTE). Specifically, some sHsps contain a conserved IXI (or IPV) motif within their CTEs. This motif binds to a groove formed by the β4/β8 strands on the edge of the ACD[63-64]. Thus, within an oligomer, the IXI/V motif of one sHsp is proposed to "reach back" and take part in a PPI with the ACD of another sHsp (Figure 1.4C), stabilizing large oligomers.

The final PPI involves the N-terminal domain (NTD). Because the NTD is the least conserved region and is highly flexible, this PPI is difficult to study and remains the most enigmatic. NTDs within an oligomer seem to make contact with other NTDs (Figure 1.4D), though it is possible that they interact transiently with other domains as well, including the ACD (Figure 1.4E). Regardless, it is clear that the NTD PPIs are important for oligomer formation based on deletion studies[65]. Moreover, the NTDs of different

sHsps seem to encode different oligomeric sizes and polydispersity, as transposition of the NTD from Hsp27 onto MjHsp16.5 can change the MjHsp16.5 oligomer to become more "Hsp27-like"[66].

Hetero-oligomerization of sHsps. The sHsps are known to form hetero-oligomers. This phenomenon has been extensively observed[67], most famously in lens α-crystallin hetero-oligomers that consists of αA and αB crystallin[68]. The functions of hetero-oligomers are not always clear but their properties seem to be distinct from that of homo-oligomers[68]. Hetero-oligomers are presumably held together by the same conserved PPIs, involving the IXI/V motifs and ACDs. However, the role of the NTD is less clear because it either promotes or disfavors hetero-oligomerization through unknown mechanisms[69].

Client Interactions with sHsps. How sHsps bind clients is not well understood, but an emerging model suggests that multiple domains are involved. Cross-linking studies in plant sHsps suggest that the NTD is the preferred client-binding site, with other regions involved in secondary interactions[70]. However, the ACD of αB crystallin, lacking an NTD, is sufficient to prevent aggregation of certain amyloid clients[71] and NMR studies indicate that the β4/β8 groove is an important binding site[72]. Thus, interactions outside the NTD might be critical for some systems. That being said, deletion of the NTD is sufficient to ablate chaperone activity for lysozyme[72]. For still other categories of clients, both the NTD and ACD have been shown to be important for chaperone activity[73].

Taken together, these data suggest that client binding can occur in multiple sites, depending on the type of client and the sHsp oligomeric state.

Connections with Other Chaperones: Because sHsps lack enzymatic activity, they must coordinate with other chaperone families to engage in complex functions. For example, sHsps are thought to create a reservoir of partially unfolded clients that are then refolded by the Hsp70/40 system[74] and Hsp100/ClpB system[75]. In humans, BAG3 seems to be the scaffolding factor that connects the sHsps with Hsp70 via its BAG domain and IPV motifs[76]. These PPIs are especially important in autophagy[77], where the BAG3/HspB8/Hsp70 complex has been shown to be required.

Conclusions. Protein−protein interactions are the “glue” that holds together the chaperone network (see Figure 1.1). However, this glue is not static; rather, dynamic changes in PPIs seem to accompany the major “decisions” of proteostasis. The dynamic nature of the system is by design, enabling the chaperone network to rapidly adapt to a number of different stresses by altering the equilibria of PPIs. For example, sudden high concentrations of a client protein can favor chaperone binding to the client while disfavoring particular co-chaperone/chaperone complexes. Because of the integration of the full chaperone network through PPIs, one change in a chaperone complex might reverberate through the entire network. While fascinating, this fluidity can make it challenging to study chaperone networks in a cellular context. In the next sections, we focus conclusions on the next-generation areas that we believe deserve further development.

Linking PPI Observations across Scales. Although we have focused primarily on structural examinations of individual PPIs in this Account, mass spectrometry has recently been used to globally profile PPIs within cells[78]. This approach is yielding unprecedented insight into the broader interactions of chaperones, co-chaperones, and clients. At the same time, advances in crystallography, NMR spectroscopy, and cryogenic electron microscopy have started to provide structures of larger and larger complexes, such as Hsp104− client[79]. These advances underscore the importance of understanding the affinities of specific chaperone complexes in vitro and then bridging those observations across larger scales: from biochemical to cellular to organismal. Integration of this knowledge will require biophysics, mathematical modeling, biochemistry, functional genomics, and other disciplines. In addition, it seems that chemical biology may play a particularly important role because of its ability to produce molecules that operate at each scale.

Cellular Context. While the core structure of the chaperone network seems to be maintained in different cell types and even cellular compartments, the specific co-chaperones can vary significantly, and the expression levels are varied. Recent work has identified a distinct chaperone complex (dubbed the epichaperome)[88] present in many cancer cells that is absent in normal cells and other cancer lines, suggesting that differences in the chaperone networks can contribute to disease. Furthermore, the makeup of the chaperone network might provide a therapeutic window for targeting specific cellular types, such as cancer cells.

Chemical Biology to Drug Discovery. Together, converging revolutions in structural

biology, proteomics, and other fields are creating new opportunities for chemical biology, as each of the newly characterized PPIs is a potential new site for perturbation. We suggest that drug-like molecules targeting these PPIs will continue to be invaluable tools for understanding chaperone networks, particularly because fast chemical perturbation of these highly dynamic interactions is critically important in understanding the overall network. Moreover, such molecules might be starting points for the development of next-generation therapeutics. To this end, it will be important that HTS methods and medicinal chemistry campaigns retain drug-like criteria in the selection schemes so that these important advances can be used to go beyond chemical probes and into clinical candidates. Recent successes in targeting PPIs in the clinic should embolden this effort and inform the specific challenges ahead.

References:

1. Hartl, F. U.; Bracher, A.; Hayer-Hartl, M., Molecular chaperones in protein folding and proteostasis. *Nature* **2011,** *475* (7356), 324-32.

2. Assimon, V. A.; Gillies, A. T.; Rauch, J. N.; Gestwicki, J. E., Hsp70 Protein Complexes as Drug Targets. *Current pharmaceutical design* **2012**.

3. Pratt, W. B.; Toft, D. O., Regulation of signaling protein function and trafficking by the hsp90/hsp70-based chaperone machinery. *Exp Biol Med (Maywood)* **2003,** *228* (2), 111-33.

4. Roth, D. M. et al., Modulation of the maladaptive stress response to manage diseases of protein folding. *PLoS Biol* **2014,** *12* (11), e1001998.

5. Balch, W. E.; Morimoto, R. I.; Dillin, A.; Kelly, J. W., Adapting proteostasis for disease intervention. *Science* **2008,** *319* (5865), 916-9.

6. Clerico, E. M.; Tilitsky, J. M.; Meng, W.; Gierasch, L. M., How hsp70 molecular machines interact with their substrates to mediate diverse physiological functions. *J Mol Biol* **2015,** *427* (7), 1575-88.

7. Zuiderweg, E. R.; Hightower, L. E.; Gestwicki, J. E., The remarkable multivalency of the Hsp70 chaperones. *Cell Stress Chaperones* **2017,** *22* (2), 173-189.

8. Kampinga, H. H.; Craig, E. A., The HSP70 chaperone machinery: J proteins as drivers of functional specificity. *Nat Rev Mol Cell Biol* **2010,** *11* (8), 579-92.

9. Ahmad, A. et al., Heat shock protein 70 kDa chaperone/DnaJ cochaperone complex employs an unusual dynamic interface. *Proceedings of the National Academy of Sciences of the United States of America* **2011,** *108* (47), 18966-71.

10. Greene, M. K.; Maskos, K.; Landry, S. J., Role of the J-domain in the cooperation of Hsp40 with Hsp70. *Proc Natl Acad Sci U S A* **1998,** *95* (11), 6108-13.

11. Cesa, L. C.; Mapp, A. K.; Gestwicki, J. E., Direct and Propagated Effects of Small Molecules on Protein-Protein Interaction Networks. *Frontiers in bioengineering and biotechnology* **2015,** *3*, 119.

12. Wisen, S. et al., Binding of a small molecule at a protein-protein interface regulates the chaperone activity of hsp70-hsp40. *ACS chemical biology* **2010,** *5* (6), 611-22.

13. Huryn, D. M. et al., Chemical methodology as a source of small-molecule checkpoint inhibitors and heat shock protein 70 (Hsp70) modulators. *Proc Natl Acad Sci U S A* **2011,** *108* (17), 6757-62.

14. Chafekar, S. M. et al., Pharmacological tuning of heat shock protein 70 modulates polyglutamine toxicity and aggregation. *ACS chemical biology* **2012,** *7* (9), 1556-64.

15. Bocking, T.; Aguet, F.; Harrison, S. C.; Kirchhausen, T., Single-molecule analysis of a molecular disassemblase reveals the mechanism of Hsc70-driven clathrin uncoating. *Nat Struct Mol Biol* **2011,** *18* (3), 295-301.

16. Schilke, B. A. et al., Broadening the functionality of a J-protein/Hsp70 molecular chaperone system. *PLoS genetics* **2017,** *13* (10), e1007084.

17. Assimon, V. A.; Southworth, D. R.; Gestwicki, J. E., Specific Binding of Tetratricopeptide Repeat Proteins to Heat Shock Protein 70 (Hsp70) and Heat Shock Protein 90 (Hsp90) Is Regulated by Affinity and Phosphorylation. *Biochemistry* **2015,** *54* (48), 7120-31.

18. Nillegoda, N. B. et al., Crucial HSP70 co-chaperone complex unlocks metazoan protein disaggregation. *Nature* **2015,** *524* (7564), 247-51.

19. Bracher, A.; Verghese, J., The nucleotide exchange factors of Hsp70 molecular chaperones. *Frontiers in molecular biosciences* **2015,** *2*, 10.

20. Harrison, C. J.; Hayer-Hartl, M.; Di Liberto, M.; Hartl, F.; Kuriyan, J., Crystal structure of the nucleotide exchange factor GrpE bound to the ATPase domain of the molecular chaperone DnaK. *Science* **1997,** *276* (5311), 431-5.

21. Sondermann, H.; Scheufler, C.; Schneider, C.; Hohfeld, J.; Hartl, F. U.; Moarefi, I., Structure of a Bag/Hsc70 complex: convergent functional evolution of Hsp70 nucleotide exchange factors. *Science* **2001,** *291* (5508), 1553-7.

22. Rauch, J. N.; Gestwicki, J. E., Binding of human nucleotide exchange factors to heat shock protein 70 (Hsp70) generates functionally distinct complexes in vitro. *J Biol Chem* **2014,** *289* (3), 1402-14.

23. Polier, S.; Dragovic, Z.; Hartl, F. U.; Bracher, A., Structural basis for the cooperation of Hsp70 and Hsp110 chaperones in protein folding. *Cell* **2008,** *133* (6), 1068-79.

24. Shomura, Y. et al, Regulation of Hsp70 function by HspBP1: structural analysis reveals an alternate mechanism for Hsp70 nucleotide exchange. *Mol Cell* **2005,** *17* (3), 367-79.

25. Rousaki, A.; Miyata, Y.; Jinwal, U. K.; Dickey, C. A.; Gestwicki, J. E.; Zuiderweg, E. R., Allosteric drugs: the interaction of antitumor compound MKT-077 with human Hsp70 chaperones. *J Mol Biol* **2011,** *411* (3), 614-32.

26. Young, Z. T. et al, Stabilizing the Hsp70-Tau Complex Promotes Turnover in Models of Tauopathy. *Cell chemical biology* **2016,** *23* (8), 992-1001.

27. Xu, X.; Sarbeng, E. B.; Vorvis, C.; Kumar, D. P.; Zhou, L.; Liu, Q., Unique peptide substrate binding properties of 110-kDa heat-shock protein (Hsp110) determine its distinct chaperone activity. *J Biol Chem* **2012,** *287* (8), 5661-72.

28. Zeytuni, N.; Zarivach, R., Structural and functional discussion of the tetra-trico-peptide repeat, a protein interaction module. *Structure* **2012,** *20* (3), 397-405.

29. D'Andrea, L. D.; Regan, L., TPR proteins: the versatile helix. *Trends Biochem Sci* **2003,** *28* (12), 655-62.

30. Scheufler, C. et al., Structure of TPR domain-peptide complexes: critical elements in the assembly of the Hsp70-Hsp90 multichaperone machine. *Cell* **2000,** *101* (2), 199-210.

31. Smith, M. C. et al., The E3 Ubiquitin Ligase CHIP and the Molecular Chaperone Hsc70 Form a Dynamic, Tethered Complex. *Biochemistry* **2013,** *52* (32), 5354-64.

32. Hohfeld, J.; Cyr, D. M.; Patterson, C., From the cradle to the grave: molecular chaperones that may choose between folding and degradation. *EMBO Rep* **2001,** *2* (10), 885-90.

33. Evans, C. G.; Chang, L.; Gestwicki, J. E., Heat shock protein 70 (hsp70) as an emerging drug target. *J Med Chem* **2010,** *53* (12), 4585-602.

34. Li, X.; Shao, H.; Taylor, I. R.; Gestwicki, J. E., Targeting Allosteric Control Mechanisms in Heat Shock Protein 70 (Hsp70). *Curr Top Med Chem* **2016,** *16* (25), 2729-40.

35. Abisambra, J. et al., Allosteric Heat Shock Protein 70 Inhibitors Rapidly Rescue Synaptic Plasticity Deficits by Reducing Aberrant Tau. *Biological psychiatry* **2013**.

36. Wang, A. M. et al., Activation of Hsp70 reduces neurotoxicity by promoting polyglutamine protein degradation. *Nature chemical biology* **2013,** *9* (2), 112-8.

37. Taguwa, S. et al, Defining Hsp70 Subnetworks in Dengue Virus Replication Reveals Key Vulnerability in Flavivirus Infection. *Cell* **2015,** *163* (5), 1108-23.

38. Colvin, T. A. et al., Hsp70-Bag3 interactions regulate cancer-related signaling networks. *Cancer Res* **2014,** *74* (17), 4731-40.

39. Pratt, W. B.; Gestwicki, J. E.; Osawa, Y.; Lieberman, A. P., Targeting hsp90/hsp70-based protein quality control for treatment of adult onset neurodegenerative diseases. *Annual review of pharmacology and toxicology* **2015,** *55*, 353-71.

40. Seyffer, F. et al., Hsp70 proteins bind Hsp100 regulatory M domains to activate AAA+ disaggregase at aggregate surfaces. *Nat Struct Mol Biol* **2012,** *19* (12), 1347-55.

41. Nakamoto, H. et al., Physical interaction between bacterial heat shock protein (Hsp) 90 and Hsp70 chaperones mediates their cooperative action to refold denatured proteins. *J Biol Chem* **2014,** *289* (9), 6110-9.

42. Whitesell, L.; Lindquist, S. L., HSP90 and the chaperoning of cancer. *Nature reviews* **2005,** *5* (10), 761-72.

43. da Silva, V. C.; Ramos, C. H., The network interaction of the human cytosolic 90 kDa heat shock protein Hsp90: A target for cancer therapeutics. *Journal of proteomics* **2012,** *75* (10), 2790-802.

44. Prodromou, C.; Roe, S. M.; O'Brien, R.; Ladbury, J. E.; Piper, P. W.; Pearl, L. H., Identification and structural characterization of the ATP/ADP-binding site in the Hsp90 molecular chaperone. *Cell* **1997,** *90* (1), 65-75.

45. Meyer, P. et al, Structural and functional analysis of the middle segment of hsp90: implications for ATP hydrolysis and client protein and cochaperone interactions. *Mol Cell* **2003,** *11* (3), 647-58.

46. Nemoto, T.; Ohara-Nemoto, Y.; Ota, M.; Takagi, T.; Yokoyama, K., Mechanism of dimer formation of the 90-kDa heat-shock protein. *Eur J Biochem* **1995,** *233* (1), 1-8.

47. Workman, P.; Burrows, F.; Neckers, L.; Rosen, N., Drugging the cancer chaperone HSP90: Combinatorial therapeutic exploitation of oncogene addiction and tumor stress. *Ann N Y Acad Sci* **2007**.

48. Shrestha, L.; Patel, H. J.; Chiosis, G., Chemical Tools to Investigate Mechanisms Associated with HSP90 and HSP70 in Disease. *Cell chemical biology* **2016,** *23* (1), 158-172.

49. Garg, G.; Khandelwal, A.; Blagg, B. S., Anticancer Inhibitors of Hsp90 Function: Beyond the Usual Suspects. *Adv Cancer Res* **2016,** *129*, 51-88.

50. Li, J.; Soroka, J.; Buchner, J., The Hsp90 chaperone machinery: conformational dynamics and regulation by co-chaperones. *Biochim Biophys Acta* **2012,** *1823* (3), 624-35.

51. Retzlaff, M. et al., Asymmetric activation of the hsp90 dimer by its cochaperone aha1. *Mol Cell* **2010,** *37* (3), 344-54.

52. Meyer, P. et al., Structural basis for recruitment of the ATPase activator Aha1 to the Hsp90 chaperone machinery. *EMBO J* **2004,** *23* (3), 511-9.

53. Ali, M. M. et al, Crystal structure of an Hsp90-nucleotide-p23/Sba1 closed chaperone complex. *Nature* **2006,** *440* (7087), 1013-7.

54. Sullivan, W. et al, Nucleotides and two functional states of hsp90. *J Biol Chem* **1997,** *272* (12), 8007-12.

55. Verba, K. A. et al., Atomic structure of Hsp90-Cdc37-Cdk4 reveals that Hsp90 traps and stabilizes an unfolded kinase. *Science* **2016,** *352* (6293), 1542-7.

56. Zhang, T. et al., A novel Hsp90 inhibitor to disrupt Hsp90/Cdc37 complex against pancreatic cancer cells. *Mol Cancer Ther* **2008,** *7* (1), 162-70.

57. Haslbeck, M.; Vierling, E., A first line of stress defense: small heat shock proteins and their function in protein homeostasis. *J Mol Biol* **2015,** *427* (7), 1537-48.

58. Delbecq, S. P.; Klevit, R. E., One size does not fit all: the oligomeric states of alphaB crystallin. *FEBS Lett* **2013,** *587* (8), 1073-80.

59. Giese, K. C.; Vierling, E., Changes in oligomerization are essential for the chaperone activity of a small heat shock protein in vivo and in vitro. *J Biol Chem* **2002,** *277* (48), 46310-8.

60. Rajagopal, P. et al., A conserved histidine modulates HSPB5 structure to trigger chaperone activity in response to stress-related acidosis. *eLife* **2015,** *4*.

61. Rajagopal, P.; Liu, Y.; Shi, L.; Clouser, A. F.; Klevit, R. E., Structure of the alpha-crystallin domain from the redox-sensitive chaperone, HSPB1. *J Biomol NMR* **2015,** *63* (2), 223-8.

62. Makley, L. N. et al., Pharmacological chaperone for alpha-crystallin partially restores transparency in cataract models. *Science* **2015,** *350* (6261), 674-7.

63. Jehle, S. et al., alphaB-crystallin: a hybrid solid-state/solution-state NMR investigation reveals structural aspects of the heterogeneous oligomer. *J Mol Biol* **2009,** *385* (5), 1481-97.

64. Delbecq, S. P.; Jehle, S.; Klevit, R., Binding determinants of the small heat shock protein, alphaB-crystallin: recognition of the 'IxI' motif. *EMBO J* **2012,** *31* (24), 4587-94.

65. Peschek, J. et al, Regulated structural transitions unleash the chaperone activity of alphaB-crystallin. *Proc Natl Acad Sci U S A* **2013,** *110* (40), E3780-9.

66. Shi, J.; Koteiche, H. A.; McHaourab, H. S.; Stewart, P. L., Cryoelectron microscopy and EPR analysis of engineered symmetric and polydisperse Hsp16.5 assemblies reveals determinants of polydispersity and substrate binding. *J Biol Chem* **2006,** *281* (52), 40420-8.

67. Arrigo, A. P., Human small heat shock proteins: protein interactomes of homo- and hetero-oligomeric complexes: an update. *FEBS Lett* **2013,** *587* (13), 1959-69.

68. Srinivas, P. N.; Reddy, P. Y.; Reddy, G. B., Significance of alpha-crystallin heteropolymer with a 3:1 alphaA/alphaB ratio: chaperone-like activity, structure and hydrophobicity. *Biochem J* **2008,** *414* (3), 453-60.

69. Heirbaut, M. et al, The preferential heterodimerization of human small heat shock proteins HSPB1 and HSPB6 is dictated by the N-terminal domain. *Arch Biochem Biophys* **2016,** *610*, 41-50.

70. Jaya, N.; Garcia, V.; Vierling, E., Substrate binding site flexibility of the small heat shock protein molecular chaperones. *Proc Natl Acad Sci U S A* **2009,** *106* (37), 15604-9.

71. Hochberg, G. K. et al., The structured core domain of alphaB-crystallin can prevent amyloid fibrillation and associated toxicity. *Proc Natl Acad Sci U S A* **2014,** *111* (16), E1562-70.

72. Mainz, A. et al, The chaperone alphaB-crystallin uses different interfaces to capture an amorphous and an amyloid client. *Nat Struct Mol Biol* **2015,** *22* (11), 898-905.

73. Basha, E.; Friedrich, K. L.; Vierling, E., The N-terminal arm of small heat shock proteins is important for both chaperone activity and substrate specificity. *J Biol Chem* **2006,** *281* (52), 39943-52.

74. Lee, G. J.; Vierling, E., A small heat shock protein cooperates with heat shock protein 70 systems to reactivate a heat-denatured protein. *Plant Physiol* **2000,** *122* (1), 189-98.

75. Haslbeck, M.; Miess, A.; Stromer, T.; Walter, S.; Buchner, J., Disassembling protein aggregates in the yeast cytosol. The cooperation of Hsp26 with Ssa1 and Hsp104. *J Biol Chem* **2005,** *280* (25), 23861-8.

76. Rauch, J. N. et al, BAG3 Is a Modular, Scaffolding Protein that physically Links Heat Shock Protein 70 (Hsp70) to the Small Heat Shock Proteins. *J Mol Biol* **2017,** *429* (1), 128-141.

77. Carra, S.; Seguin, S. J.; Landry, J., HspB8 and Bag3: a new chaperone complex targeting misfolded proteins to macroautophagy. *Autophagy* **2008,** *4* (2), 237-9.

78. Rizzolo, K. et al, Features of the Chaperone Cellular Network Revealed through Systematic Interaction Mapping. *Cell reports* **2017,** *20* (11), 2735-2748.

79. Gates, S. N. et al, Ratchet-like polypeptide translocation mechanism of the AAA+ disaggregase Hsp104. *Science* **2017,** *357* (6348), 273-279.

80. Ouimet, C. M. et al., Protein Cross-Linking Capillary Electrophoresis for Protein-Protein Interaction Analysis. *Anal. Chem.* **2016**, *88* (16), 8272–8278.

81. Rauch, J. N. et al., Development of a Capillary Electrophoresis Platform for Identifying Inhibitors of Protein–Protein Interactions. *Anal. Chem.* **2013**, *85* (20), 9824–9831.

82. Taylor, I. R. et al., High-Throughput Screen for Inhibitors of Protein–Protein Interactions in a Reconstituted Heat Shock Protein 70 (Hsp70) Complex. *J. Biol. Chem.* **2018**, *293* (11), 4014–4025.

83. Cesa, L. C. et al., Inhibitors of Difficult Protein-Protein Interactions Identified by High-Throughput Screening of Multiprotein Complexes. *ACS Chem. Biol.* **2013**, *8* (9), 1988–1997.

84. Makley, L. N.; Gestwicki, J. E. Expanding the Number of 'Druggable' Targets: Non-Enzymes and Protein-Protein Interactions. *Chem. Biol. Drug Des.* **2013**, *81* (1), 22–32.

85. Kityk, R.; Kopp, J.; Mayer, M. P. Molecular Mechanism of J-Domain-Triggered ATP Hydrolysis by Hsp70 Chaperones. *Mol. Cell* **2018**, *69* (2), 227–237.e4.

86. Gowda, N. K. C. et al., Nucleotide Exchange Factors Fes1 and HspBP1 Mimic Substrate to Release Misfolded Proteins from Hsp70. *Nat. Struct. Mol. Biol.* **2018**, *25* (1), 83–89.

87. Rosam, M. et al., Bap (Sil1) Regulates the Molecular Chaperone BiP by Coupling Release of Nucleotide and Substrate. *Nat. Struct. Mol. Biol.* **2018**, *25* (1), 90–100.

88. Rodina, A. et al., The Epichaperome Is an Integrated Chaperome Network That Facilitates Tumour Survival. *Nature* **2016**, *538* (7625), 397–401.

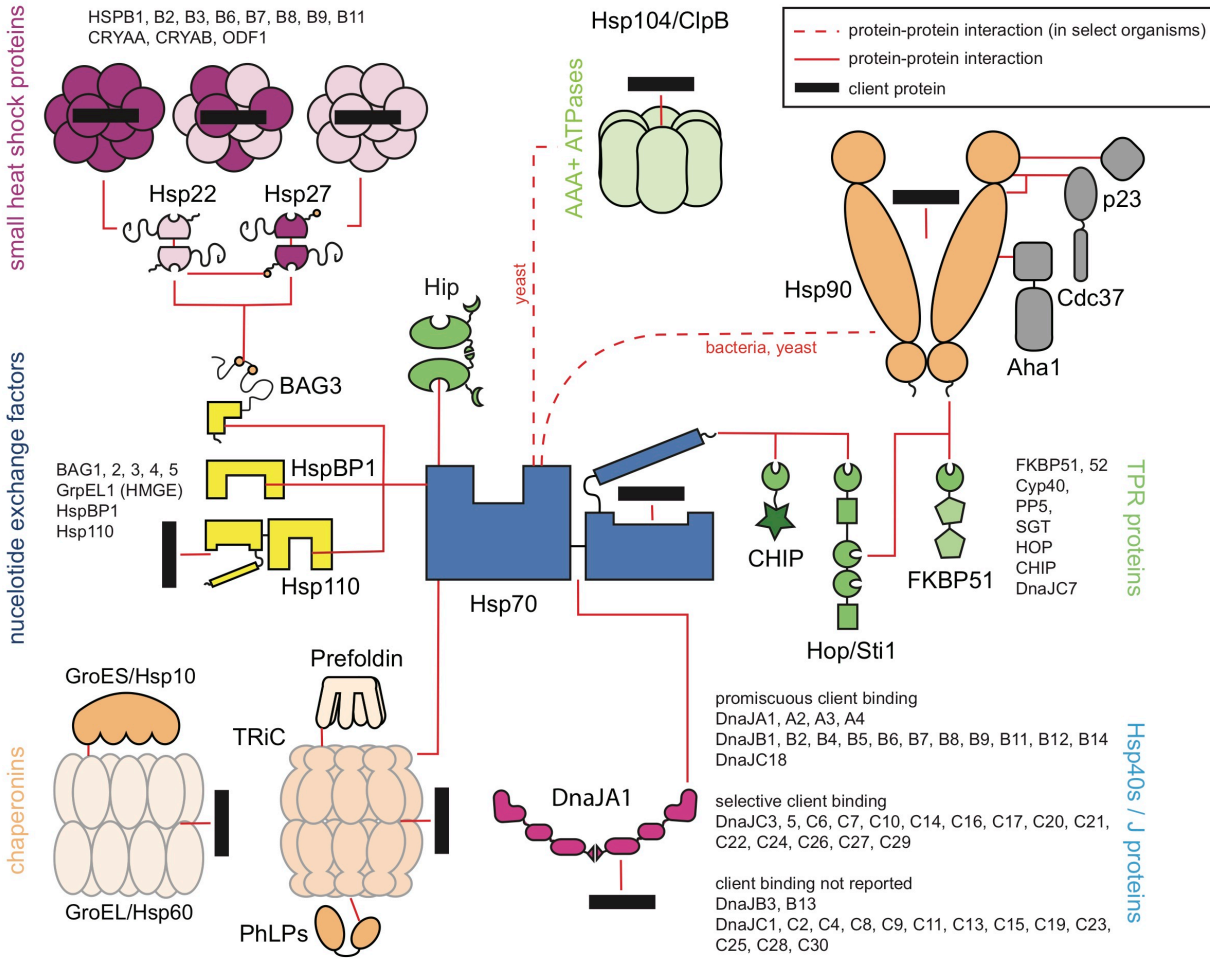

Figure 1.1. The physical interactions of the major chaperone families. PPIs are shown with red lines and the approximate surfaces indicated on the cartoons. Dotted lines indicated interactions that lack a high-resolution structure.

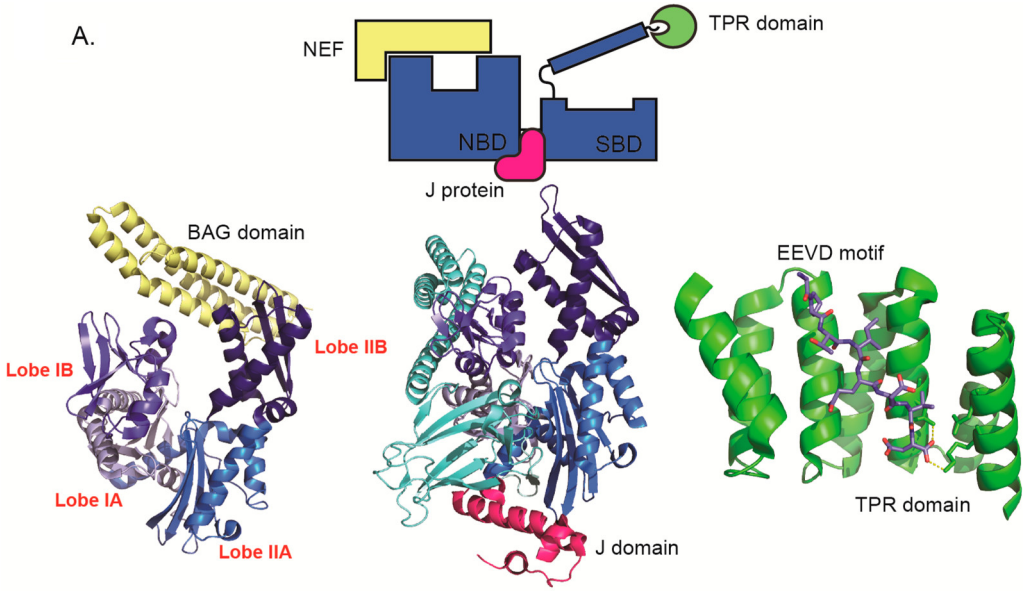

B.

PDB ID [ref]	Organism	Co-chaperone type	Co-chaperone	Regions of Hsp70 contact
2QWN	Bovine	J protein	Auxilin	NBD, lobes IA and IIA
5NRO	E. Coli	J protein	DnaJ	NBD lobe IIA, interdomain linker, SBDβ
3D2F	Human	NEF	Sse1 (Hsp110)	NBD, lobes IA, IB, and IIB
1DKG	E. Coli	NEF	GrpE	NBD, lobes IA, IB, and IIB
1HX1	Human	NEF	Bag1	NBD, lobes IB and IIB
3CQX	Human	NEF	Bag2	NBD, lobes IB and IIB
38AY	Human	NEF	Bag5	NBD, lobes IB and IIB
1XQS	Human	NEF	HspBP1	NBD, lobe IIB
1ELW	Human	TPR	HOP	EEVD
4KBQ	Human	TPR	CHIP	EEVD
4J8F	Human	TPR	HIP	NBD, lobes IA, IB, and IIB

Figure 1.2. Hsp70's interaction with co-chaperones. (A) Categories of co-chaperone PPIs in the Hsp70 sub-network, highlighting the different regions of Hsp70 that are involved. (B) Structures of Hsp70 complexes.

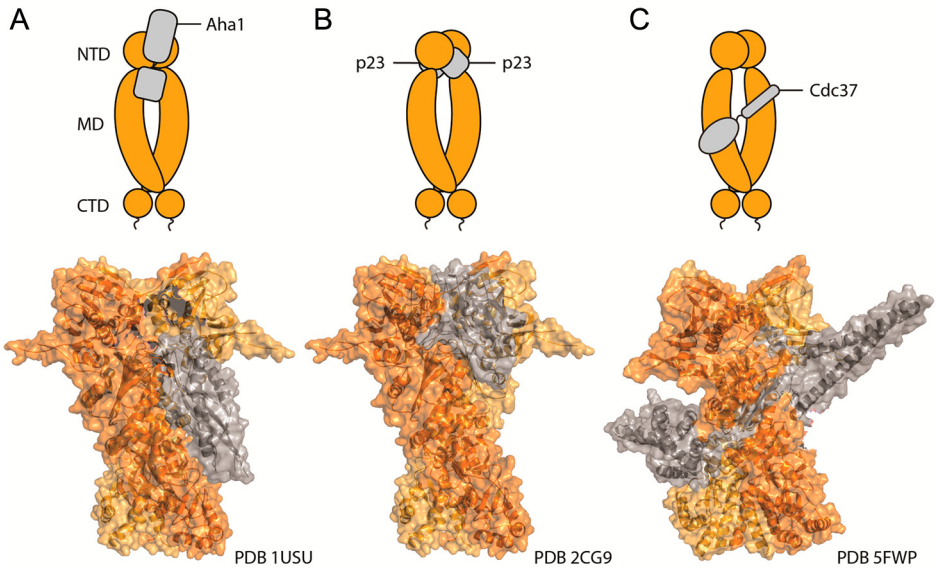

Figure 1.3. PPIs with Hsp90. (A) The interaction between Aha1 and Hsp90 is modeled by alignment of the co-crystal structure of the N-terminal domain of Aha1 and Hsp90 MD with the structure of full-length Hsp90 in the closed state (PDB 2CG9). The C-terminal domain of Aha1 (not shown) has been reported to interact with the Hsp90 NTD. (B) Two p23 molecules bind to the Hsp90 dimer, each binding between the Hsp90 NTDs. (C) Cdc37 wraps around Hsp90, splitting into two domains connected by a beta strand that packs against the Hsp90 MD.

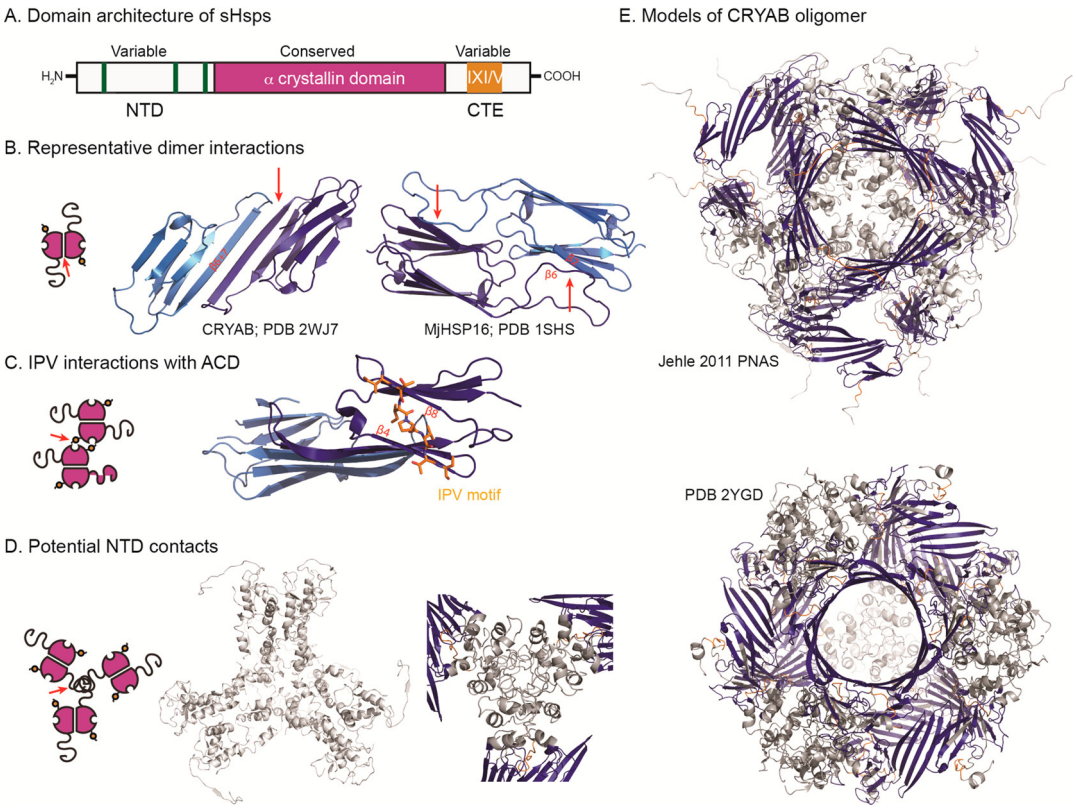

Figure 1.4. PPIs of the sHsps. (A) Domain architecture of sHsps. (B) Examples of dimer interfaces: αB crystallin (PDB: 2WJ7) an3d MjHSP16 (PDB: 1SHS). Key contacts are shown (red arrows). (C) Structure of an IPV peptide bound to Hsp27 β4/β8 groove (PDB: 4MJH). (D) Potential NTD contacts based on EM models. (E) Models of αB crystallin oligomers from electron microscopy.

Chapter 2

Myopathy associated BAG3 mutations lead to protein aggregation by stalling Hsp70 networks

Melanie Meister-Broekema*, Rebecca Freilich*, Chandhuru Jagadeesan*, Rocio Bengoechea, William W. Motley, Jennifer N. Rauch*, Melania Minoia, Gabriel V. Furtado, Maria A.W.H. van Waarde, Shawn J. Bird, Adriana Rebelo, Stephan Zuchner, Peter Pytel, Steven S. Scherer, Serena Carra, Conrad C. Weihl, Steven Bergink, Jason E. Gestwicki, and Harm H. Kampinga

Abstract. BAG3 is a multi-domain hub that connects two classes of chaperones, small heat shock proteins (sHSPs) via two isoleucine-proline-valine (IPV) motifs and Hsp70 via a BAG domain. It is the only stress-inducible BAG-family member and highly expressed in muscle. Mutations in BAG3 cause a dominant form of myopathy, characterized by protein aggregation in both skeletal and cardiac muscle tissues that undergo repeated cycles of shear stress. Most disease-causing BAG3 mutations reside in the second IPV motif. Here, we describe a new disease mutation that instead lies in the BAG domain. Surprisingly, for both IPV-motif and BAG-domain disease mutants, impaired chaperone binding is not sufficient to explain disease phenotypes. Recombinant mutants are correctly folded and show unaffected Hsp70 binding. However, stimulation of ADP-ATP exchange and client refolding of Hsp70 are impaired. As a consequence, the mutant BAG3 proteins become the node for a dominant gain of function causing aggregation of itself, Hsp70, Hsp70 clients and tiered interactors within the BAG3 interactome. Importantly, genetic and pharmaceutical interference with Hsp70 binding completely reverses stress-induced protein aggregation in cells and in fibroblasts derived from patients with both IPV motif and BAG domain mutations. Thus, the gain of function effects of BAG3 mutants acts as an Achilles heel of the entire HSP70 machinery.

Introduction. BAG3 is a multi-domain scaffolding protein composed of a WW domain, two IPV motifs, a PxxP domain, and a C-terminal BAG domain (Figure 1a), enabling it to engage in multiple protein-protein interactions[1]. Among the binding partners of BAG3 are two different classes of molecular chaperones; it binds Hsp70 (also called HSPAs)

via its C-terminal BAG domain and small heat shock proteins (also called HSPBs) via its IPV motifs (Figure 2.1A)[2,3]. Together, these molecular chaperones play a crucial role in protein quality control (PQC)[4]. In this process, Hsp70s rely on co-chaperones of the DNAJ- and HSPB-families to deliver clients[4-7], while nucleotide exchange factors (NEFs), including BAG3, promote client release[4,8-11]. BAG3 is thought to play a critical role because it can bind to Hsp70 and to HSPBs simultaneously[12,13], thereby forming a ternary complex. This type of adapter activity is expected to be critical because HSPBs lack enzymatic function and are not able to refold clients; rather, they rely on collaboration with other ATP- driven chaperones, such as Hsp70s[14]. Thus, the proper timing and architecture of this multi- chaperone complex is likely extremely important to ensure a proper chaperone function. Interestingly, BAG3 is generally expressed at low levels in addition to being the only stress- inducible member of the BAG-family of NEFs. In fact, multiple types of stress can induce the expression of BAG3[15,16], including mechanical stress as caused by muscle contraction[17].

Several mutations in the individual components of the HSP70 machinery have been shown to cause disease[18]. Whereas no disease-associated mutations have been found in Hsp70 genes, suggesting that these may be incompatible with life, most so-called ‘chaperonopathies’ are caused by mutations in either DNAJ or HSPB genes. The only two NEFs in which mutations are shown to cause disease are Sil1 and Bag3. Mutations in Sil1, the ER-resident NEF, causes Marinesco-Sjögren syndrome, which is an autosomal recessive cerebellar ataxia associated with a myopathy characterized by vacuoles and protein inclusions[19]. Mutations in BAG3 also cause a spectrum of disease

phenotypes[20-25]. For example, a proline to leucine substitution at position 209 within the HSPB binding motif (referred to as BAG3^{P209L}), causes a dominant, progressive myofibrillar myopathy (MFM) in which patients suffer from progressive muscle weakening, followed by sudden death due to heart failure in early adulthood[20-24,26]. A striking feature of this disease is the accumulation of protein aggregates in patient muscle, suggesting a collapse of protein homeostasis[21,27,28]. In addition, other missense mutations at the same P209 position (P209Q or P209S) within the IPV motif have been identified in multiple families with MFM and/or neuropathy[25,29]. Because these BAG3 mutations lie in the second IPV motif, loss of HSPB binding has been suggested as a molecular mechanism underlying disease[30,31]. However, in this study we report on a novel mutation in the BAG domain (BAG3^{P470S}) as the cause of MFM, in two unrelated families. This observation calls into question whether the BAG3 mutants merely disrupt HSPB binding. Therefore, we set out to study the mechanism by which mutations in BAG3 protein drive such a devastating disease.

In contrast to the initial expectation, we show that a disturbed binding of BAG3 mutants to either HSPBs or Hsp70 does not underlie the dramatic collapse of PQC. In fact, for both the BAG3^{P209L} and BAG3^{P470S} mutants, binding to Hsp70 was found to be required for the phenotypic effects. These mutations caused aggregation of Hsp70 client protein and subsequent sequestration of PQC-proteins into insoluble aggregates. Importantly the function of co- aggregating chaperones is severely hampered. Together, these events lead to a self-perpetuating progressive collapse of PQC. We found that the genetic or pharmacological disruption of the interaction between the mutant BAG3

proteins and Hsp70 is sufficient to revert this process.

Thus, our data reveal how two different types of mutations in BAG3 lead to MFM in a similar manner that goes beyond a simple loss of function but is mediated by a dominant-gain of function on the Hsp70 chaperone machines. These findings suggest that BAG3 in particular, and maybe NEFs in general, are a potential Achilles heel of the Hsp70 machinery, where minor malfunctioning results in the entrapment of the whole chaperone complex with disastrous consequences for protein homeostasis. Inhibiting the BAG3-Hsp70 interaction using small molecules relieves this collapse and offers the first potential strategy to help these patients.

Results

Loss of HSPB binding does not result in the cellular BAG3^{P209L} phenotype. It is striking that several BAG3 mutations that lead to early onset MFM reside in the second IPV domain. To gain insight into what mechanism may underlay this, we initially focused on BAG3^{P209L} as a prime example of fulminant BAG3 related MFM. Our first hypothesis was that the P209L mutation might prevent binding of BAG3 to HSPBs because it is located in the second IPV motif[30-32]. To test this idea, we measured the interaction of BAG3^{WT} and BAG3^{P209L} with a model, human HSPB fragment (HSPB1c/Hsp27c) using isothermal titration calorimetry (ITC). We found that Hsp27c binding to BAG3^{P209L} is indeed reduced 3.6-fold as compared to BAG3^{WT}(Figure 2.1B). This loss of affinity was similar to the complete deletion of the IPV2 motif, but less pronounced than the deletion of both IPV motifs (Figure 2.1B). Further, the estimated stoichiometry (N) of the complex

was reduced from ~2:1 to ~1:1, which is consistent with the loss of one IPV interaction. To test if this loss of affinity was sufficient to affect BAG3-HSPB8 interactions in cells, we performed immunoprecipitations and found that $BAG3^{P209L}$ binding to HSPB8 was only mildly reduced (Figure 2.1C). Rather, it took mutation of both IPV-motifs ($BAG3^{IPV1mut,IPV2mut}$) to prevent the interaction. Mutating the first IPV motif in the $BAG3^{P209L}$ background ($BAG3^{IPV1mut,P209L}$) did not further affect HSPB8-binding, supporting the idea that the P209L substitution can still partially interact with HSPBs (Figure 2.1C).

The $BAG3^{P209L}$ mutation has been associated with the aggregation of sarcomeric proteins, including $BAG3^{P209L}$ itself[21]. Accordingly, a significant portion of ectopically expressed $BAG3^{P209L}$ is detergent insoluble in human cells, whereas $BAG3^{WT}$ is primarily detergent soluble (Figure 2.1D and S2.1A). Furthermore, whereas $BAG3^{WT}$ was found to be distributed homogenously throughout the cell, ~50% of cells expressing $BAG3^{P209L}$ showed a decrease in the amount of nuclear BAG3 and a punctae-like distribution pattern (Figure 2.1E,F and S2.1B). These punctae appeared to be detergent insoluble (Figure S2.1B) and reminiscent of cellular aggregates observed in patients with $BAG3^{P209L}$- associated MFM/DCM[21]. Intriguingly, a complete loss in HSPB binding ($BAG3^{IPV1mut,IPV2mut}$) did not affect BAG3 solubility (Figure 2.1D and S2.1C,D) and did not cause formation of BAG3 punctae (Figure 2.1E,F). Further going against expectations, we noticed that mutating IPV1 in the presence of the P209L mutation ($BAG3^{IPV1mut,P209L}$) only modestly reduced punctae formation and improved solubility (Figure 2.1 D,F and S2.1C,D). Together, these results surprisingly contradicted the

initial hypothesis and, instead, support the idea that loss of HSPB binding is insufficient to cause the cellular BAG3^{P209L} phenotype.

Recombinant BAG3^{P209L} loses its native-quaternary fold in a temperature-dependent manner. Next, we considered a model in which the P209L mutation makes the BAG3 protein prone to aggregation. Using PepFold predictions, we had noticed that substituting leucine for proline at amino acid 209 switched the predicted secondary structure of BAG3 from random coil to strongly b-sheet (Figure 2.2A). In line with this prediction, purified BAG3^{P209L} showed a marked increase in Sypro staining (Figure 2.2B), indicative of exposed hydrophobic regions. Also, BAG3^{P209L} but not BAG3^{WT} showed a temperature-dependent increase in staining with the fluorescent b-sheet dye thioflavin-T (Figure 2.2C). To further explore this thermal instability, we measured the melting temperature of BAG3^{WT} and BAG3^{P209L} by differential scanning fluorimetry (DSF) and found that BAG3^{P209L} was nearly 4 °C less stable (BAG3^{WT} 49.6 °C +/- 0.78 versus BAG3^{P209L} 46 °C +/- 0.58). Strikingly, other hydrophobic mutations at position 209, such as Ile and Trp, were also predicted to increase b-sheet content (Figure S2.2A), which was supported by the thioflavin-T positive staining of the corresponding mutants (BAG3^{P209I} and BAG3^{P209W}) (Figure S2.2B). This behavior is restricted to hydrophobic mutations, as substitutions that were predicted to be strongly random coil in this region (BAG3^{P209A}, BAG3^{P209D}, BAG3^{P209G} and BAG3^{P209K}) did neither have an increased predicted b-sheet content (Figure S2.2A) nor were the corresponding proteins thioflavin-T positive (Figure S2.2B). Like BAG3^{P209L}, the other hydrophobic mutants and to a lesser extent the other control mutants, had reduced affinity for Hsp27c (Figure

S2.2C), suggesting that they all impair the second IPV motif. In summary, most substitutions at the 209-position weaken the interaction with HSPB.

Although these results initially suggested that BAG3^{P209L} might form insoluble aggregates, we found that recombinant BAG3^{P209L} is soluble under a wide range of conditions and that its overall fold is indistinguishable from BAG3^{WT} by circular dichroism (CD) (Figure 2.2D). However, in SEC- MALS experiments, BAG3^{WT} and all control mutants (BAG3^{P209A}, BAG3^{P209D}, BAG3^{P209G} and BAG3^{P209K}) were monomeric (~62 kDa), whereas BAG3^{P209L} and the hydrophobic mutants (BAG3^{P209I} and BAG3^{P209W}) primarily formed soluble, higher order oligomers (Figure S2.2D). Indeed, BAG3^{P209L} showed partial resistance to chymotrypsin and trypsin digestion (Figure 2.2E), further suggesting a higher order structure. Consistent with these *in vitro* data, we separated detergent- soluble cell lysates on sucrose gradients and found that BAG3^{P209L} sediments at higher densities than BAG3^{WT} (Figure 2.2F). Together, these results show that BAG3^{P209L} itself is not prone to forming insoluble aggregates, but that it does have a non-native quaternary structure.

BAG3^{P209L} is impaired in stimulating the ATPase activity of Hsp70. We next wondered how the soluble BAG3^{P209L} oligomers might affect Hsp70-interactions. *In vitro* and in cells, BAG3 and Hsp70 are known to coordinate cycles of client-binding and client-release, creating the delicate balance required for re-folding[33,34]. To probe for a putative effect of the P209L mutation on its functional interaction with Hsp70, we initially measured the affinity of BAG3^{WT} and BAG3^{P209L} for the nucleotide-binding domain

(NBD) of a representative Hsp70 family member, HSPA8, by isothermal calorimetry (ITC). Under these conditions, both $BAG3^{WT}$ and $BAG3^{P209L}$ bound normally to $HSPA8^{NBD}$ (K_D ~ 0.3 μM) (Figure 2.2G). Further, all of the point mutants had normal activity in releasing fluorescent nucleotide from $HSPA8^{NBD}$ (Figure S2.2E). Together, these data imply that, despite their non-native quaternary structure, all mutants can bind equally well to Hsp70.

Next, we wondered whether the oligomeric and metastable structure of $BAG3^{P209L}$ might have an impact on the functionality of full length HSPA8. $BAG3^{WT}$ shows a concentration-dependent bell-shaped curve for stimulating the ATPase activity of HSPA8, characteristic for all BAG proteins (Figure 2.2H)[35]. Despite the similar binding affinity, $BAG3^{P209L}$ was inactive in ATPase assays using HSPA8 (Figure 2.2H). This loss of activity of $BAG3^{P209L}$ is temperature dependent, consistent with the ThT and DSF assays (data not shown). To investigate the consequence of this defect, we used denatured firefly luciferase as a model. We first replicated the known behaviour of $BAG3^{WT}$, in which low levels (~0.2 μM) of the co-chaperone enhance the yield of folded luciferase by ~4-fold, while this stimulatory activity is lost at higher concentrations (Figure 2.2I), mirroring the effect of BAG proteins in the Hsp70-ATPase assays (Figure 2.2H). Strikingly, $BAG3^{P209L}$ was severely compromised in this assay, only inhibiting the reaction (Figure 2.2I). To test whether the Hsp70- $BAG3^{P209L}$ axis might be disrupted in living cells as well, we expressed $BAG3^{WT}$ or $BAG3^{P209L}$ and measured overall cellular folding capacity. It is known that over-expression of NEFs, such as BAG3, reduces the cellular luciferase folding capacity[36], likely because NEFs are constitutively expressed at

or near their optimal concentration (*e.g.* the equivalent of 0.2 μM in Figure 2.2I). Despite this difficult backdrop, we found that elevated expression of BAG3^{P209L} reduced Hsp70-mediated folding capacity even further than high levels of BAG3^{WT} (Figure 2.2J). In summary, hydrophobic mutations in BAG3 at position 209 induce a mild temperature dependent local unfolding that still allows proper Hsp70 binding but stalls the Hsp70 cycle at the client release stage.

Disruption of Hsp70 binding to BAG3^{P209L} suffices to rescue aggregation. Next, we wondered whether in living cells at 37^{o}C the thermal instability of BAG3^{P209L} alone suffices to induce protein aggregation or if the failure to coordinate with Hsp70 underlies the aggregation phenotype. Therefore, we deleted the BAG domain, which is required for Hsp70 binding [13,35,37], from BAG3^{WT} and BAG3^{P209L} and tested whether these proteins affect aggregation in cells (Figure S2.3A). As controls, we also deleted the WW- and PxxP-domains, which are not involved in Hsp70 binding. When over-expressed in cells, none of the BAG3^{WT} deletions (BAG3$^{WT\text{-}\Delta WW}$, BAG3$^{WT\text{-}\Delta PXXP}$, or BAG3$^{WT\text{-}\Delta BAG}$) resulted in punctae formation or insolubility (Figure 2.3A-C and S2.3B). Also, expression of the BAG3$^{WT\text{-}\Delta WW}$ and BAG3$^{WT\text{-}\Delta PXXP}$ double mutants yielded punctae-formation that were indistinguishable from the effects of the BAG3^{P209L} single mutant alone (Figure 2.3A-C and S2.3B). These results suggest that interactions with BAG3-binding partners, such as synaptopodins (WW domain)[38] and SH3 domain-containing proteins, such as dynein motors (PxxP-motif)[39], are not involved. Moreover, loss of Hsp70 interaction alone (BAG3$^{WT\text{-}\Delta BAG}$) is not sufficient to cause an obvious aggregation phenotype. However, abrogating the ability of BAG3^{P209L} to interact with

Hsp70 (BAG3$^{P209L-\Delta BAG}$), fully prevented the BAG3^{P209L}-characteristic punctae formation and loss of solubility (Figure 2.3A-C and S2.3B). Immunoprecipitation experiments confirmed that BAG3$^{P209L-\Delta BAG}$ could no longer bind Hsp70s (Figure 2.3D). These results confirm our *in vitro* data showing that recombinant BAG3^{P209L} is soluble despite its thermal instability (Figure 2.2) and strongly suggest that, in cells, Hsp70- engagement is required for the BAG3^{P209L} aggregation phenotype.

The requirement of Hsp70 interaction for BAG3^{P209L}-mediated aggregation was confirmed by experiments with a single point mutation, R480A, in the BAG domain. This BAG3^{R480A} mutant is strongly impaired in Hsp70 binding (Figure 2.3D) but is otherwise normal[40]. When expressed in cells, the R480A mutation could suppress the effects of P209L, as the double mutant (BAG3$^{P209L, R480A}$) is neither insoluble (Figure 2.3E), nor localized in punctae (Figure 2.3A,B). Further, BAG3$^{P209L, R480A}$, unlike BAG3^{P209L}, did not have an adverse effect on the folding capacity in cells (Figure 2.2J). To independently test this idea, we treated BAG3^{P209L} expressing cells with YM01 and JG98 molecules that pharmacologically impair binding of Hsp70 to BAG3 (Figure 2.3F)[41]. Consistent with the double mutant data, both compounds reduced the BAG3^{P209L} -associated insolubilization in a dose dependent manner (Figure 2.3G,H), whilst an inactive, structurally similar control compound had no effect (data not shown). Together, these results reveal that the protein aggregation caused by BAG3^{P209L} requires the recruitment of Hsp70. The slight decrease in BAG3^{P209L} stability (Figure S2.2D and 2.2E) seems to be insufficient to induce aggregation by itself *in vitro* (Figure 2.2E) or in cells (Figure 3). Rather, upon binding to Hsp70, which is undisturbed in BAG3^{P209L},

BAG3^{P209L} is recruited to mis- or unfolded Hsp70-clients. Because of its inability to stimulate Hsp70-mediated function this leads to co-aggregation. It is difficult to monitor this type of higher order process *in vitro*, but we found that recombinant BAG3^{P209L} (but not BAG3^{WT}) binds unfolded peptides such as the LVEAVY amyloid peptide from IAPP (Figure 2.2K), possibly via its non-canonical interaction surface[35]. Thus, multivalent interactions between BAG3^{P209L}, Hsp70s, HSPBs and clients, driven by aberrant BAG3^{P209L}-client contacts and avidity effects through multiple BAG domain-Hsp70^{NBD} contacts may disrupt dynamic protein-protein interactions and trigger aggregation.

BAG3^{P209L} aggregation leads to co-aggregation of proteasomal substrates. BAG3 has been found to be up-regulated by various forms of stresses that overload the proteasomal capacity[15-17] and to redirect ubiquitinated Hsp70-clients from the proteasome to the autophagy-lysosome system[15]. During this process, termed BAG-induced proteasome to autophagy switch and sorting (BiPASS), BAG3 and Hsp70, along with ubiquitinated clients, temporarily localize to p62/LC3-positve punctae before being degraded by autophagy[15]. Intriguingly, the punctae formed by BAG3^{P209L} under non-stress conditions stain positive for p62, but not LC3 (Figure 2.4A), suggesting that, although BAG3^{P209L} remains partially functional in initiating BIPASS, the process is somehow impaired or stalled. Expression of either BAG3^{WT} or BAG3^{P209L} caused a similar increase in the LC3-II:LC3-I ratio (Figure 2.4B,C) as previously [reported12,42] and indicating no major impact of the P209L mutation on BAG3-dependent increases the autophagic flux. However, compared to BAG3^{WT}, the ability of BAG3^{P209L} to support the autophagic disposal of protein aggregates initiated by polyglutamine (polyQ) was much

reduced (Figure 2.4D,E and S2.4A)[3]. This result indicates that delivery of cargo to the autophagic system is impaired in BAG3^{P209L} -expressing cells. In-line with this hypothesis, BAG3^{P209L} expression led to the accumulation of ubiquitin-positive punctae that co-localized with BAG3^{P209L} (Figure 4f; Figure S4b). Moreover, NP40-insoluble ubiquitinated proteins accumulated upon BAG3^{P209L} -expression (Figure S2.4C)[15]. To further investigate whether BAG3^{P209L} affects the disposal of proteasomal clients, we co-expressed the proteasomal reporters Ub-R-GFP (degraded following proteasome via the N-end-rule pathway) and GFP-ODC (delivered to the proteasome via ubiquitin-independent pathways)[43] with BAG3^{WT} or BAG3^{P209L}. Expression of BAG3^{WT} led to small increases in both reporters (Figure 2.4G), which reflects its role in re-routing proteasomal HSP70-clients to autophagosomes[15]. Mirroring its effects on endogenous ubiquitin, BAG3^{P209L} dramatically increased the levels of both reporters, revealing a dramatic loss in the cellular capacity to degrade proteasomal clients. Further, BAG3^{P209L}, but not BAG3^{WT}, led to the insolubilization of both proteasomal reporters (Figure 2.4G). Experiments using a cell line stably expressing the proteasomal reporter Ub-G76V-YFP, which is degraded via the UFD-pathway[44], showed qualitatively similar results (Figure S2.4D). Expression of BAG3^{IPV1,IPV2} did not lead to the insolubilization of ubiquitinated proteins or their accumulation in BAG3^{P209L} punctae, while BAG3^{IPV1,P209L} led to less insolubilization and punctae formation of ubiquitinated proteins than BAG3^{P209L} (Figure S2.4E,F), again showing that loss of HSPB binding is not responsible for the functional defect in BAG3^{P209L}.

Also, in line with our previous results (Figure 2.3), Hsp70 binding is essential for the

dominant defect evoked by expression of BAG3^{P209L}: besides abrogating the BAG3^{P209L}-insolubilization itself (Figure 2.3), deletion of the BAG domain (but not the WW or PxxP domain) in the background of the P209L mutation also negated the BAG3^{P209L} effects on the insolubilization of ubiquitinated proteins (Figure S2.4G) and their accumulation into the BAG3^{P209L} punctae (Figure S2.4B). In addition, the BAG3^{P209L,R480A} double mutant neither led to the insolubilization of ubiquitinated proteins (Figure 2.4H), nor to the accumulation and precipitation of the UFD reporter (Figure S2.4D). Finally, JG98 or YM01 treatment counteracted the effects of BAG3^{P209L} on the insolubilization of ubiquitinated proteins (Figure S2.4H,I). Together, these results indicate that BAG3^{P209L} leads to a general impairment of processing and aggregation of a wide range of ubiquitin-tagged client proteins of HSPB or/and HSP70.

PQC proteins co-aggregate with BAG3^{P209L}. How the accumulation of aggregates in cells can lead to toxic effects has been a matter of dispute for many years and may involve several, perhaps parallel acting, events[45]. One consequence of aggregation is the sequestration of components of the PQC systems, which leads to a vicious and progressive decline in protein homeostasis that subsequently impairs many cellular functions and eventually results in cell death[45]. Indeed, upon expression of BAG3^{P209L}, we found several chaperones (HSPA1A, HSPA8, HSPB1, HSPB8, DNAJB1, and DNAJB6), albeit not all (HSPB5 and HSPA6), to be enriched in the same detergent-insoluble fraction as BAG3^{P209L} (Figure 2.5A and S2.5A) and co-localizing with ubiquitinated proteins and BAG3^{P209L}-punctae (Figure 2.5B and S2.5B,C). This co-aggregation was also highly dependent on the BAG3^{P209L}-Hsp70 interaction as

disruption of the BAG domain abrogated the co-aggregation (Figure 2.5A and S2.5A-C). Many DNAJs are known to have their own client-binding ability that is not dependent on Hsp70-interactions. We found that the recruitment of DNAJB1 and DNAJB6 into aggregates is independent of the J-domain, which is needed to bind Hsp70s (Figure 2.5C and data not shown), suggesting that their co-localization with punctae is Hsp70 independent. One possibility is that co-chaperones are recruited by clients and trapped when they become insoluble. In line with such a trapping model, only the mainly cytosolic DNAJB6 isoform (DNAJB6b, 26 kDa) became insoluble in $BAG3^{P209L}$-expressing cells, while the exclusively nuclear isoform (DNAJB6a, 40 kDa) remained soluble (Figure 2.5A).

Sequestration of chaperones into insoluble aggregates suppresses their function. Trapping of (co-)chaperones could contribute to disease by reducing their effective pool in the cell. To test this idea, we measured the ability of DNAJB6b to suppress polyQ aggregation in the background of $BAG3^{WT}$ or BAG3 mutants[46,47]. $BAG3^{WT}$ can reduce aggregation initiated by short $polyQ_{43}$ expansions (Figure 2.3)[3] but not aggregation initiated by long $polyQ_{119}$ fragments, while DNAJB6 co- expression alone almost completely suppresses $polyQ_{119}$ aggregation (Figure 2.5D)[46,47]. In line with the hypothesis of a dominant negative effect via sequestration of other chaperones into $BAG3^{P209L}$ aggregates, co-expression of $BAG3^{P209L}$ -but not $BAG3^{WT}$ or $BAG3^{P209L,R480A}$-inhibited DNAJB6- mediated anti-aggregation (Figure 2.5D). Together, these data reveal that $BAG3^{P209L}$ directly stalls the Hsp70 function, which -as a result- perpetuates into a dominant effect on the function of other chaperones.

Stalling of Hsp70 is a common feature of BAG3 myopathy related mutations. To test if impediment of Hsp70 functioning by single amino acid substitutions in BAG3 occurs more frequently, we turned to two other mutations at the P209 position, BAG3^{P209Q} and BAG3^{P209S} that cause MFM or neuropathy, respectively[25,29]. Like BAG3^{P209L}, both BAG3^{P209Q} and BAG3^{P209S} form multiple punctae when expressed in cells. Likewise, genetic abrogation of the Hsp70 interaction (BAG3^{P209Q,R480A} and BAG3^{P209S,R480A}) reverts this phenotype as well (Figure 2.6A and S2.6A), implying that all P209 disease-causing mutants operate via a similar dominant Hsp70-stalling mechanism.

In order to further understand BAG3 associated MFM pathogenesis and identify potentially novel BAG3 genetic variants that are associated with MFM, we performed exome sequencing on patients with muscle weakness and features of MFM on muscle biopsy. This approach identified two unrelated MFM patients carrying an unreported BAG3 c.1408C>T; p.P470S missense mutation (Figure S2.6B,C). Neither patient had a family history of muscle weakness or other neuromuscular disorder. Whole exome sequencing of patient 2's living parents failed to identify the BAG3 c.1408C>T; p.P470S variant, suggesting that it was a de novo mutation in this patient. It was only possible to obtain DNA samples from Patient 1's mother, confirming that she was a non-variant carrier (Figure S2.6B). Muscle tissue from both patients demonstrated features characteristic for MFM patient tissue with sarcoplasmic inclusions and rimmed vacuoles as visualized on hematoxylin and eosin staining and gomori trichrome (Figure 2.6B).

Amino acid P470 is conserved in all human BAG proteins, except BAG2, and amongst various BAG3 from other vertebrate species (Figure S2.6D). The P470S variant is predicted to be damaging by Polyphen2 and Mutation Taster. Moreover, it is not found within public databases, including the EXAC browser and GNOMAD, further supporting its pathogenicity. Unlike the previously reported BAG3 mutations, which reside within the second IPV motif, the P470 residue lies within the HSP70 binding region or BAG domain. Since our proposed model of BAG3 mutant dysfunction suggested that mutations in the IPV motif destabilize the protein and alter HSP70 kinetics that require HSP70 binding, we tested whether the P470S missense mutation within the BAG domain has affected HSP70 binding as well. Surprisingly, the $BAG3^{P470S}$ mutant maintained HSP70 association, albeit with a slight loss in binding, unlike the $BAG3^{R480A}$ mutant that abolishes HSP70 binding (Figure 6c). In addition, similar to $BAG3^{P209L}$, $BAG3^{P209Q}$, and $BAG3^{P209S}$, $BAG3^{P470S}$ aggregated in cell culture, which was corrected by a secondary R480A mutation (Figure 2.6A and S2.6A). Together these results suggest that all MFM related BAG3-mutants tested require interaction with Hsp70 to become pathological and result in a dominant gain of impairment of the functions of Hsp70 related networks.

Abrogation of BAG3-Hsp70 by pharmaceutical intervention as a potential therapeutic approach. To address whether endogenous, rather than over-expressed, BAG3 mutations results in similar phenotypes, we performed experiments with fibroblasts derived from control patients or patients carrying the $BAG3^{P209L}$ and $BAG3^{P470S}$ mutations. Endogenous expression of BAG3 is low in most cell types,

including fibroblasts, which may be the reason why no spontaneous mutant BAG3-related punctae were observed in the patient fibroblasts (Figure 2.6D,E). However, as stated above, BAG3 is the only stress-inducible BAG-protein[48] and is up-regulated by a variety of stress signalling cascades, including those initiated by treatment with proteasome inhibitors[15]. Indeed, a short treatment with bortezomib produced persistent ubiquitin-positive BAG3 punctae in fibroblasts from both $BAG3^{P209L}$ and $BAG3^{P470S}$ carriers but not in fibroblasts from patients without the mutation (Figure 2.6D,E). To test whether this punctae formation can be reversed by disrupting BAG3-Hsp70 interactions, we co-treated the BAG3 mutated, MFM patient-derived fibroblasts with bortezomib and the drug JG98 that disturbs Hsp70-BAG3 interactions (Figure 2.3F)[41] and reverts aggregates formation when the mutants are overexpressed (Figure 2.3 and S2.4). As predicted, this treatment indeed reduced the frequency of persistent BAG3 punctae in the lines from both $BAG3^{P209L}$ and $BAG3^{P470S}$ carriers (Figure 2.6D,E). This confirms that they cause aggregation via similar mechanisms and imply that pharmaceutically targeting the Hsp70-Bag3 interaction could be a first therapeutic strategy for patients carrying P209L/Q/S or P470S substitutions.

Discussion

Mutations in BAG3 are associated with a devastating syndrome that includes MFM, dilated cardiomyopathy and neuropathy. Why certain mutations result in a more severe clinical outcome is unclear. Thus far MFM was associated with mutations at P209 position that lies in the second IPV motif[21-24]. Here we describe a second mutation site (P470S) that lies in the BAG domain. The notion that both are localized in domains that

connect this central co-chaperone to other chaperone systems initially led us to hypothesize that the mutation might block binding to HSPBs or Hsp70, leading to loss-of-function as has been suggested. However, our results suggest a more nuanced mechanism characterized by only mildly impaired chaperone binding but a more intense outcome, i.e. a dramatic stalling of Hsp70 client processing via a disruption in their ability to functionally stimulates the ATP activity of HSP70s. In cells, these molecular defects result in the formation of protein aggregates via interactions with Hsp70. These aggregates next trap chaperones that subsequently become partly non-functional, which is exemplified by the BAG3^{P209L}-effects on DNAJB6 function. Intriguingly, just like BAG3 mutations, mutations in DNAJB6 have been linked to myopathies as well[49,50].

Interestingly, whereas absence or loss of function of BAG3 result in an increase in insoluble proteins[51], this is not sufficient to cause the formation of large aggregates triggered by BAG3^{P209L}, BAG3^{P209Q}, BAG3^{P209S} or BAG3^{P470S} mutations. Apparently, loss (or partial loss) of BAG3 function does affect PQC, but dominant gain of function mutations, including the MFM-related BAG3 mutations, are more deleterious by triggering the negative spiral of trapping and co- aggregating of Hsp70-clients, Hsp70 itself, and other PQC components. The latter results in loss of function of other chaperones. Our data reveal a completely novel molecular mechanism that would explain the far more progressive and early onset aspects related to MFM pathology. This concept has potentially broad implications because multiple myopathies and neuropathies are caused by dominant mutations in PQC components as well.

It is also interesting to compare the BAG3 related diseases to other chaperonopathies, like those caused by recessive or dominant mutations in other Hsp70 co-chaperones such as DNAJ or HSPB proteins[18]. Mutations in DNAJs or HSPBs are typically associated with late onset cardiomyopathies or neuropathies. In contrast, mutations in the NEFs (Sil-1 and BAG3) often cause early onset or congenital disease[19,21-25]. The reason for this is not known but could reside in the fact that DNAJs and HSPBs primarily select the input of clients into Hsp70 chaperones machines. This implies that only a certain number of substrates are affected. Moreover, the handling of these substrates can, at least for some time, be taken care of by alternative PQC mechanisms as has been suggested for DNAJB6 mutations[52]. In contrast, mutations in BAG proteins, as being NEFs, are responsible for the output of a larger range and number of substrates. Therefore, impairment of NEF functions like that of Sil1 and BAG3 may impede on more clients and thus have a more drastic impact. For, BAG3 loss of heterozygosity already leads to widespread and early onset diseases[21-25]. Even more so, BAG3 is involved in what already seems to be a back-up PQC mechanism that compensates for an overload of the proteasome (BIPASS)[15] and the dominant effects as we found for the mutants here rapidly culminates in the collapse of the entire machinery.

The high vulnerability of skeletal and cardiac muscle cells to BAG3 mutations may be linked to the fact that BAG3 is constitutively expressed at relatively high levels in these tissues. Stress situations that overload the proteasome increase BAG3 levels without affecting expression of other members of the BAG family[48], probably helping cells to re-route proteasomal clients to autophagosomes[15]. Muscle cells are repeatedly exposed to

cellular stress (*e.g.* mechanic stress from exercise) that may elevate BAG3 expression to levels sufficient for the primary defects of mutants, like BAG3^{P209L}, to start take effect. Amongst the BAG family members, BAG3 has the highest affinity for Hsp70s[34], meaning that a stress-related imbalance in relative BAG levels may suffice to initiate the negative cascade described here. Indeed, the data on patient-derived fibroblasts provides a proof-of-concept for this idea.

The perspectives of our study are that either genetics or small molecules that specifically interfere with the Hsp70-BAG3 interaction not only attenuated the negative cascade but also minimized its toxic, downstream effects. Inhibitors of the Hsp70-BAG3 interaction, some of which have been advanced in pre-clinical safety studies[34], may thus have the potential to serve as treatments in BAG3-related myopathies.

Materials and methods

Plasmid construction. Plasmids encoding myc-tagged human HSPB8[53] and peGFP-HDQ74, which was kindly provided by Dr. D.C. Rubinsztein were described before[54]. FLAG-BAG3 WT and P209L constructs were kindly provided by Dr. S. Takayama. The primers and plasmids used in this study are listed in Supplementary **Table S2.1** and Supplementary **Table S2.2**. To generate Flag tagged human BAG3 (pcDNA3 FLAG-BAG3), BAG3 delta BAG (pcDNA3 FLAG-B BAG3$^{\Delta BAG}$), and BAG3 delta PxxP (pcDNA3 FLAG- BAG3$^{\Delta PXXP}$), the BAG3 encoding sequences of the following constructs were amplified by polymerase chain reaction (PCR) with Phusion polymerase, purified by agarose gel electrophoresis and ligated to EcoRI and XhoI digested pcDNA FLAG-

Parkin: BAG3 (pCN His- BAG3), BAG3 ΔBAG (pCN His- BAG3$^{\Delta BAG}$) and BAG3 ΔPxxP (pCN His- BAG3$^{\Delta PXXP}$). Using specific primers, the P209L mutation was introduced into Flag-tagged BAG3 constructs with the *Pfu* turbo DNA polymerase site directed mutagenesis kit to generate the following constructs: BAG3P209L (pcDNA3 FLAG-BAG3^{P209L}), BAG3 delta BAG P209L (pcDNA3 FLAG-BAG3$^{\Delta BAG,P209L}$), BAG3 delta PxxP P209L (pcDNA3 FLAG-BAG3$^{\Delta BAG,P209L}$), BAG3 delta WW (pcDNA3 FLAG-BAG3$^{\Delta WW}$), and BAG3 delta WW P209L (pcDNA3 FLAG-BAG3$^{\Delta WW,P209L}$). BAG3 IPV1 (pcDNA3 FLAG-BAG3$^{IPV1>AAA}$), BAG3 IPV2 (pcDNA3 FLAG-BAG3$^{IPV2>AAA}$), BAG3 IPV1 P209L (pcDNA3 FLAG-BAG3$^{IPV1>AAA,P209L}$), and BAG3 IPV1 IPV2 (pcDNA3 FLAG-BAG3$^{IPV1>AAA,IPV2>AAA}$) were constructed in a similar fashion; all constructs were sequence verified. All domain deletion constructs used for *in vitro* studies were sub-cloned from the BAG3 pMCSG7 parent vector and confirmed with DNA sequencing. Mutations were constructed using standard mutagenesis protocols.

Recombinant protein production. All constructs were transformed into BL21(DE3) cells and single colonies were used to inoculate TB medium containing ampicillin (50 μg/mL). Cultures were grown at 37 °C to an OD_{600} 0.6, when NaCl and betain were added to a final concentration of 500 mM and 10 mM respectively. The cultures were cooled to 18 °C and induced overnight with 500 μM IPTG. BAG3-expressing cells were pelleted, resuspended in BAG3 lysis buffer (50 mM Tris, 100 mM NaCl, 1 mM EDTA, and 15 mM β-mercaptoethanol (pH 8.0)), microfluidized, and applied to Ni-NTA resin. After Ni-NTA columns, all proteins were subjected to TEV protease cleavage overnight and dialyzed into MonoQ buffer A (20 mM HEPES, 10 mM NaCl, and 15 mM β-

Mercapthoethanol (pH 7.6)). Proteins were applied to a MonoQ column (GE Healthcare) and eluted by a linear gradient of MonoQ buffer B (buffer A + 1 M NaCl). Fractions were dialyzed into BAG buffer (25 mM HEPES, 5 mM MgCl2, and 150 mM KCl (pH 7.5)) and concentrated. Hsc70, $Hsc70_{NBD}$, $Hsc70_{SBD}$, J proteins, and Hsp27c were purified as described elsewhere[13].

DSF and ThT Melt curve. Samples of $BAG3^{WT}$ or $BAG3^{P209L}$ in BAG3 buffer (20 µL samples of 0.3 mg/mL) with a 5x final concentration of SYPRO Orange (Sigma) were placed into a white 96-well plate with optically clear caps. DSF melt curves were acquired on a Stratagene Mx300P RT-PCR using the SYPRO filter set. Samples were heated from 25 °C to 95 °C in 1 °C increments, and the melting temperature was determined using a Boltzmann fit. For ThT melt curves, 100 µL samples of 10 µM $BAG3^{WT}$ or $BAG3^{P209L}$ with 10 µM ThT were heated in a thermocycler from 20 °C to 90 °C in 10 °C increments and removed from heating at each temperature. Samples were cooled to 20 °C and plated in a low volume, black 384-well plate (Corning) and ThT fluorescence was read with 444 nm excitation, 485 nm emission and a 475 nm cutoff using a SpectraMax5 M5 multi-mode plate reader. All experimental data were analyzed using Prism 7.0 software (Graphpad Software).

Circular Dichroism. $BAG3^{WT}$ and $BAG3^{P209L}$ were dialyzed overnight against 20 mM NaP_i with 100 mM NaF (pH 7.5). 0.1 mg/mL samples were placed in a low volume (250 µL) cuvette. Measurements were taken at 25 °C using a Jasco710 instrument.

Partial Proteolysis. $BAG3^{WT}$ or $BAG3^{P209L}$ (0.8 mg/mL or ~13 μM) in BAG buffer was subjected to partial proteolysis with either chymotrypsin (1/5000 ratio BAG3/enzyme) or trypsin (1/10000). The samples were incubated at 37 °C for specified time and reactions were quenched by adding SDS sample loading dye and boiling at 98 °C for five minutes. Protein fragments were separated by SDS-PAGE and stained with Coomassie.

ITC. BAG3 constructs, Hsp27c and $Hsp72^{NBD}$ were dialyzed overnight against ITC buffer (25 mM HEPES, 5 mM $MgCl_2$, 100 mM KCl [pH 7.5]). Concentrations were determined using a BCA Assay (Thermo Scientific), and the experiment was performed with a MicroCal microITC (GE Healthcare) at 25 °C. $Hsp72^{NBD}$ (100 μM) or Hsp27c (200 μM) in the syringe was titrated into a 10 μM cell solution of BAG3 protein. Calorimetric parameters were calculated using Origin® 7.0 software and fit with a one-site binding model.

Antibodies and reagents. Antibodies (dilutions are indicated in brackets for western blot (WB), immunofluorescence (IF) or immunoprecipitation (IP)) against FLAG (Sigma, clone M2; Sigma, produced in Rabbit, IP 3ul/sample, IF 1:100, WB 1:1000), FLAG (Sigma, clone M2; Sigma, M, Wb 1:1000, IF 1:200), ubiquityl-histone H2A (Millipore, clone E6C5), ubiquitin (Norvus Biologicals, FK2, M, WB 1:1000, IF 1:1000; Dako WB), K48-linkage specific polyubiquitin (Enzo lifesciences, WB 1:1000), K63- linkage specific polyubiquitin (Cell Signalling, clone D7A11, 1:1000), myc (MBL, clone PL14, WB 1:3000, IF 1:100), HSC70 (Stressgen, WB 1:5000, IF 1:100), HSC70 (Stressmarq biosciences), HSP70 (Stressgen, clone SPA-810, WB 1:1000, IF 1:50), HSPA1A (Enzo

life sciences, Rb, WB 1:1000), HSPB1 (Stressmarq biosciences), GAPDH (Fitzgerald, clone 6C5, WB 1:50000), histone H2A (Abcam, WB 1:5000), MYC (Clonetech, Mountain View, CA, USA), DNAJB1/Hsp40 (Stressgen, San Diego, CA, USA, Rb, 1:1000) were used.
MG132 (20 μM for 3-6 hours), rapamycin, Pepstatin A (10 μg/ml), E64d (10μg/ml), 3-Methyladenine (3-MA, 10 mM) ammonium chloride (NH_4Cl, 20 mM) were purchased from sigma.

Cell culture and transfection. Standard cell culture techniques were used. HeLa (human cervical cancer), HEK293, and HEK293T (human embryonal kidney) cells were grown at 37C° and 5% CO_2 in Dulbecco's modified Eagle's medium with high glucose supplemented with 10% fetal calf serum and 1% penicillin/streptomycin (Gibco). Cell lines stably expressing GFP-ubiquitin (Dantuma) were generated by transfecting GFP-ubiquitin into HEK293-cells with lipofectamine using standard procedures[46]. HEK293T and HeLa-cells were transfected with calcium phosphate precipitation, as previously described[44]; for higher efficiency in immunofluorescence experiments, HEK293 and HeLa cells were transfected with lipofectamine (Invitrogen) or polyethylenimine (PEI) (Sigma- Aldrich, St Louis, MO, USA) according to manufacturer's protocols.

Chaperone Assays. The steady-state ATPase activity of Hsc70 was measured by malachite green as previously reported[55]. For ATPase activity, Hsc70 (final concentration 1 μM), DnaJA2 (final concentration 0.5 μM) and various concentrations of BAG3 WT or P209L were added to clear 96-well plates to give a volume of 15 μL. The

reaction was initiated by adding 10 µL of 2.5 mM ATP to give a final concentration of 1 mM. Plates were covered and incubated at 37 °C for 1 hour. The reactions were developed with malachite green, quenched with sodium citrate, and plate absorbance was measured at 620 nm.

Luciferase refolding assay. The refolding of chemically denatured firefly luciferase was measured by recovered luminescence, as described[34]. Briefly, working stocks of denatured luciferase were prepared by mixing 10 µL of 200 µM native firefly luciferase (Promega) with 30 µL of 8 M GnHCl for 1 hour at room temperature. Denatured luciferase stocks were stored at −80 °C until use. To white 96-well plates, was added denatured luciferase (final concentration of 100 nM), Hsc70 (final concentration of 1 µM), DnaJB4 (final concentration of 0.5 µM), and various concentrations of $BAG3^{WT}$ or $BAG3^{P209L}$ to give a final volume of 25 µL in refolding buffer (20 mM HEPES, 120 mM KAc, 1.2 mM MgAc, 15 mM DTT, 60 mM creatine phosphate, 35 U/mL creatine kinase, 5 ng/µL BSA, pH 7.4). The reaction was initiated by adding 10 µL of 2.5 mM ATP to give a final concentration of 1 mM. Plates were covered and incubated at 37 °C for 1 hour. Finally, 25 µL of Steady-Glo reagent (Promega) was added to each well and luminescence values were measured immediately.

SEC-MALS. Solutions of $BAG3^{WT}$ or $BAG3^{P209L}$ (30 µM) were separated by size exclusion chromatography (Shodex 804), as previously described[13]. Molecular weights were determined by multi-angle laser light scattering using an in-line DAWN HELEOS detector and an Optilab rEX differential refractive index detector (Wyatt Technology

Corporation). Calculation of molecular weights was performed using the ASTRA software package (Wyatt Technology Corporation).

Fluorescent peptide assay. Experiments were performed in 384-well, black, low volume, round-bottom plates (Corning) using a SpectraMax5 M5 multi-mode plate reader, as previously described[56]. To each well, was added specified amount of protein and the 5-carboxyfluorescein (5-FAM) labeled LVEALY tracer (20 nM) to a final volume of 20 µL in the assay buffer (50 mM HEPES, 75 mM NaCl, 0.01% Triton X-100, pH 7.4). The plate was incubated at room temperature for 30 minutes to reach equilibrium. The polarization values in millipolarization units (mP) were measured at an excitation wavelength at 485 nm and an emission wavelength at 535 nm.

Protein-pull down. For immunoprecipitation, cells were lysed on ice in IP lysis buffer 24 hours post transcriptional activation (buffer: 60/80mM KCl, 50mM HEPES pH 7.5, 1.5 mM MgCl2, 0,4% Nonidet P-40, 10/3% glycerol, 0.5mM DTT, complete EDTA-free (Roche Applied Sciences) and 10mM NEM). Cell lysates were homogenized by passing lysates 5/6 times through a 26G needle and the total or 'whole cell lysate' was collected. Lysates were centrifuged at maximum speed for 15 minutes at 4C° in order to separate the supernatant (input or soluble fraction) from the pellet fraction (insoluble fraction). In the meantime, magnetic beads complexed with FLAG-antibodies (14ul beads/sample; Sigma, FLAG M2, clone) were washed with IP lysis buffer. Pellet fractions were resolubilized with 2%SDS buffer containing beta-mercapthoethanol, boiled and stored for future use. Co-immunoprecipitation was performed by adding the input fraction onto

the washed magnetic beads and incubating them at slow rotation (5 RPM) for at least 2 hours at 4C°. The first wash was performed using the IP-volume in lysis buffer and a magnetic stand. In between washes, beads were incubated on the rotator for 5 minutes at slow rotation at 4C°. Further 3 washes were performed in a similar way using 1ml of IP lysis buffer. During the last wash, beads were transferred into new cups and washed with IP lysis buffer without detergent. Proteins were eluted using 1⁄2 volume 2%SDS buffer and 1⁄2 volume 4x2%SDS buffer and 10% beta- mercapthoethanol. Samples were kept on ice until they were boiled for 5 minutes. Co-immunoprecipitated proteins and input fractions were resolved on SDS-PAGE the same day as the IP was performed.

Fractionations. Protein measurement was performed using the nanophotometer (company), protein content was equalized and equal amounts of volume and protein were used for subsequent fractionation. SDS fractionation was performed as previously described[57]. For NP40 fractionations, cell-pellets were resuspended in NP40 fractionation buffer (Fractionation buffer: 50 mM HEPES, pH 7.4, 2 mM $MgCl_2$, 60 mM KCl, 0.4% NP-40, 10% glycerol, complete EDTA-free (Roche, 11873580001) and 10 mM NEM). The cell extracts were homogenized by sonication for 5 seconds. NP-40 soluble and insoluble fractions were separated by centrifugation at 14,000 RPM for 20 min at 4°C. Whole cell lysates (pre-centrifugation), soluble (supernatant, post-centrifugation) and insoluble fractions (pellet fraction, post-centrifugation) were captured, supplied with SDS, boiled and resolved on SDS-PAGE.

Filter trap assay (FTA). To determine protein aggregation, the filter trap assay was performed as previously described[37]. Briefly, cell lysates were made one day after transfection in FTA buffer (10 mM Tris-Cl,150 mM NaCl; pH=8.0) containing 2% SDS. Serial dilutions of the protein extracts (typically 1:5 and 1:25) were applied onto a 0.2 µm pore cellulose-acetate membrane prewashed with FTA-buffer containing 0.1% SDS. Aggregated proteins trapped in the membrane were immuno-detected using mouse anti-GFP antibody JL-8 (Clontech) and visualized as in Western Blotting.

Western Blotting. Following the preparation of protein samples, proteins were resolved by SDS-PAGE, transferred to nitrocellulose membrane and processed for Western blotting. Primary antibodies (at concentrations mentioned above) were prepared in 3% BSA/PBSTween, secondary antibodies (Invitrogen, horse peroxidase conjugated IGG or IGM) in 5% milk/PBSTween. For visualization membranes were incubated with ECL western blotting substrate (Pierce, cat. No. 32106) for 2 minutes and developed (Sigma, cat. No. P7042-1GA) and fixed (Sigma, cat. No. P7167-1GA) using luminescent films (Amersham hyperfilm, GE-healthcare, cat. No. 28906837).

Immunofluorescence. HeLa cells were seeded on poly-D-lysine coated glass slides and fixed 48 hours post transfection. HeLa cells were washed once with PBS (Gibco) and fixed with 2% formaldehyde (Sigma-Aldrich, St Louis, MO, USA) for 15 minutes at room temperature. Fluorescent staining's were performed as previously described[58]. Primary antibody incubation was performed overnight at 4C° in a humid chamber and Alexa-conjugated dyes (Invitrogen, Carlsbad, CA, USA; Alexa Fluor 488 goat- anti-

Rabbit, Alexa Fluor 488 donkey-anti-Rabbit, Alexa Fluor 594 goat-anti-Rabbit, Alexa Fluor 594 donkey-anti-Rabbit, Alexa Fluor 488 goat-anti-mouse, Alexa Fluor 594 goat-anti-mouse, Alexa Fluor 594 chicken-anti-rat) were applied for 1.5 hrs at room temperature to visualize primary antibodies. Nuclear counterstaining was perfomed with 4',6-diamidino-2- phenylindole(DAPI; Invitrogen) or Hoechst 33258 for 5 minutes, and samples were and embedded in glycerol (CitiFluor, Agar Scientific).

Imaging. Immunofluorescence (IF) images were captured using confocal laser scanning microscope (Leica TCS SP8) with a 63X/1.40 objective lens. Z-stack images were obtained to check for the aggregates in different Z-planes. Quantification of the aggregates in various mutants was carried out manually using Leica DM6000 microscope. Imaris, photoshop, and Image J software was used for image processing.

Clinical Data. Standard protocol approvals, registrations, and patient consents. Clinical data and sample collection: The families were seen by one of the authors (SSS or CCW) in an outpatient clinic, where clinical neurophysiology was also performed.

Clinical data and sample collection. IRB approval was obtained from the University of Pennsylvania for these studies. Written informed consent was obtained from each patient that participated. Each family member was seen by one of the authors (SSS, or CCW) in an outpatient clinic, where clinical neurophysiology was performed with standard methods.

Whole exome sequencing (WES) and analysis. Genomic DNA was isolated from peripheral blood from all participants. Exome DNA was captured using the SureSelect, Human All Exon5 50 Mb kit (Agilent, Stanta Clara, CA) and sequenced on a HiSeq 2000 (Illumina, San Diego, CA). Paired-end reads of 100 bp length were generated and alignment and variant calls were made using BWA (Li and Durbin, 2010) and GATK software packages (McKenna et al., 2010). Data were then imported into GEM.app, a web-based collaborative genome analysis tool (Gonzalez et al., 2013), where variants were filtered for de novo non-synonymous or splice site variants with frequency in public databases (MAF <0.01 in NHLBI EVS), conservation (GERP>2, PhastCons Score>0.5, or phyloP Score>0.75). The BAG3 variant was confirmed by bidirectional Sanger sequencing using forward (CCCAAGAGTGTGGCTACAGAA) and reverse (GTGTGGGGATCTTCTGCATT) primers.

Acknowledgements

We are grateful to Telethon Genetic BioBank (GTB12001D to Elena Pegoraro) and Eurobiobank Network for providing the patient fibroblasts.

Funding

HHK was involved in a regional initiative (SNN project Transitie II & Pieken) called ChaperoneAge, a consortium with commercial partners Syncom, ABL, Axon MedChem, Nyken, Brains-on-line, Angita Pharma and the RuG/UMCG. HHK and SC received research grants from Prinses Beatrix Spierfonds; HHK received grants from the Hersenstichting, the High-Q foundation, the Ministry of Economic Affaires

(senternoven.nl), the National Ataxia Foundation, and the Dutch Heart Society (Hartedroom project 2013T088 and CVON-2014-40). SC was supported for initiating this work by an AFM trampoline grant (14492-MNM1 2012-Funding Myologie). SB received grants from the Hersenstichting and NWO-ALW. MMB was a graduate student at the University Medical Center Groningen at the time the study was conducted and is currently employed by PAREXEL International. JEG received grants from the US National Institutes of Health (NS059690) and the Tau Consortium. CCW is supported by NIH R01 AR068797 and a research grant from the MDA.

Author contributions

M.M-B., R.F., C.J., J.N.R., C.C.W. S.B, J.E.G., and H.H.K. designed and conceived the research plan; M.M-B., R.F., C.J., J.N.R., contributed equally to the experimental work. R.B., W.W.M, M.M., G.F., M.A., W.H.W., and S.C. providing additional data and materials. W.W.M, S.J.B, A.R, S.Z, P.P, S.S.S., and C.C.W, provided the new patients data, clinical material and genetic sequencing data. M.M- B., R.F., C.J., J.N.R., C.C.W., S.B, J.E.G., and H.H.K. analysed the data and wrote the initial draft of the paper. The other authors provided feedback and editorial comments on the manuscript.

References

1. Rosati, A., Graziano, V., De Laurenzi, V., Pascale, M. & Turco, M. C. BAG3: a multifaceted protein that regulates major cell pathways. *Cell Death Dis.* **2,** e141 (2011).

2. Bracher, A. & Verghese, J. The nucleotide exchange factors of Hsp70 molecular chaperones. *Front. Mol. Biosci.* **2,** (2015).

3. Carra, S., Seguin, S. J., Lambert, H. & Landry, J. HspB8 chaperone activity toward poly(Q)- containing proteins depends on its association with Bag3, a stimulator of macroautophagy. *J. Biol. Chem.* **283,** 1437–1444 (2008).

4. Kampinga, H. H. & Craig, E. A. The HSP70 chaperone machinery: J proteins as drivers of functional specificity. *Nat. Rev. Mol. Cell Biol.* **11,** 579–592 (2010).

5. Bukau, B., Deuerling, E., Pfund, C. & Craig, E. A. Getting newly synthesized proteins into shape. *Cell* **101,** 119–122 (2000).

6. Boncoraglio, A., Minoia, M. & Carra, S. The family of mammalian small heat shock proteins (HSPBs): implications in protein deposit diseases and motor neuropathies. *Int. J. Biochem. Cell Biol.* **44,** 1657–1669 (2012).

7. Garrido, C., Paul, C., Seigneuric, R. & Kampinga, H. H. The small heat shock proteins family: the long forgotten chaperones. *Int. J. Biochem. Cell Biol.* **44,** 1588–1592 (2012).

8. Brehmer, D., Gässler, C., Rist, W., Mayer, M. P. & Bukau, B. Influence of GrpE on DnaK- substrate interactions. *J. Biol. Chem.* **279,** 27957–27964 (2004).

9. Polier, S., Dragovic, Z., Hartl, F. U. & Bracher, A. Structural basis for the cooperation of Hsp70 and Hsp110 chaperones in protein folding. *Cell* **133,** 1068–1079 (2008).

10. Schuermann, J. P. *et al.* Structure of the Hsp110:Hsc70 nucleotide exchange machine. *Mol. Cell* **31,** 232–243 (2008).

11. Cyr, D. M. Swapping nucleotides, tuning Hsp70. *Cell* **133,** 945–947 (2008).

12. Carra, S., Seguin, S. J. & Landry, J. HspB8 and Bag3: a new chaperone complex targeting misfolded proteins to macroautophagy. *Autophagy* **4,** 237–239 (2008).

13. Rauch, J. N. *et al.* BAG3 Is a Modular, Scaffolding Protein that physically Links Heat Shock Protein 70 (Hsp70) to the Small Heat Shock Proteins. *J. Mol. Biol.* **429,** 128–141 (2017).

14. Mogk, A. & Bukau, B. Role of sHsps in organizing cytosolic protein aggregation and disaggregation. *Cell Stress Chaperones* (2017). doi:10.1007/s12192-017-0762-4

15. Minoia, M. *et al.* BAG3 induces the sequestration of proteasomal clients into cytoplasmic puncta: Implications for a proteasome-to-autophagy switch. *Autophagy* **10,** 116–134 (2014).

16. Knezevic, T. *et al.* BAG3: a new player in the heart failure paradigm. *Heart Fail. Rev.* **20,** 423– 434 (2015).

17. Hishiya, A., Kitazawa, T. & Takayama, S. BAG3 and Hsc70 Interact With Actin Capping Protein CapZ to Maintain Myofibrillar Integrity Under Mechanical Stress. *Circ. Res.* **107,** 1220–1231 (2010).

18. Kakkar, V., Meister-Broekema, M., Minoia, M., Carra, S. & Kampinga, H. H. Barcoding heat shock proteins to human diseases: looking beyond the heat shock response. *Dis. Model. Mech.* **7,** 421–434 (2014).

19. Senderek, J. *et al.* Mutations in SIL1 cause Marinesco-Sjögren syndrome, a cerebellar ataxia with cataract and myopathy. *Nat. Genet.* **37,** 1312–1314 (2005).

20. Selcen, D. Myofibrillar myopathies. *Curr. Opin. Neurol.* **23,** 477–481 (2010).

21. Selcen, D. *et al.* Mutation in BAG3 Causes Severe Dominant Childhood Muscular Dystrophy. *Ann. Neurol.* **65,** 83–89 (2009).

22. Odgerel, Z. *et al.* Inheritance patterns and phenotypic features of myofibrillar myopathy associated with a BAG3 mutation. *Neuromuscul. Disord. NMD* **20,** 438–442 (2010).

23. Jaffer, F. *et al.* BAG3 mutations: another cause of giant axonal neuropathy. *J. Peripher. Nerv. Syst. JPNS* **17,** 210–216 (2012).

24. Konersman, C. G. *et al.* BAG3 myofibrillar myopathy presenting with cardiomyopathy. *Neuromuscul. Disord. NMD* **25,** 418–422 (2015).

25. Shy, M. *et al.* Mutations in BAG3 cause adult-onset Charcot-Marie-Tooth disease. *J. Neurol. Neurosurg. Psychiatry* **89,** 313–315 (2018).

26. Avila-Smirnow, D. *et al.* Cardiac arrhythmia and late-onset muscle weakness caused by a myofibrillar myopathy with unusual histopathological features due to a novel missense mutation in FLNC. *Rev. Neurol. (Paris)* **172,** 594–606 (2016).

27. Arimura, T., Ishikawa, T., Nunoda, S., Kawai, S. & Kimura, A. Dilated cardiomyopathy- associated BAG3 mutations impair Z-disc assembly and enhance sensitivity to apoptosis in cardiomyocytes. *Hum. Mutat.* **32,** 1481–1491 (2011).

28. Ruparelia, A. A., Oorschot, V., Vaz, R., Ramm, G. & Bryson-Richardson, R. J. Zebrafish models of BAG3 myofibrillar myopathy suggest a toxic gain of function leading to BAG3 insufficiency. *Acta Neuropathol. (Berl.)* **128,** 821–833 (2014).

29. Semmler, A.-L. *et al.* Unusual multisystemic involvement and a novel BAG3 mutation revealed by NGS screening in a large cohort of myofibrillar myopathies.

Orphanet J. Rare Dis. **9,** 121 (2014).

30. McCollum, A. K., Casagrande, G. & Kohn, E. C. Caught in the middle: the role of Bag3 in disease. *Biochem. J.* **425,** e1-3 (2009).

31. Norton, N. *et al.* Genome-wide studies of copy number variation and exome sequencing identify rare variants in BAG3 as a cause of dilated cardiomyopathy. *Am. J. Hum. Genet.* **88,** 273–282 (2011).

32. Fuchs, M. *et al.* Identification of the key structural motifs involved in HspB8/HspB6-Bag3 interaction. *Biochem. J.* **425,** 245–255 (2010).

33. Brehmer, D. *et al.* Tuning of chaperone activity of Hsp70 proteins by modulation of nucleotide exchange. *Nat. Struct. Biol.* **8,** 427–432 (2001).

34. Rauch, J. N. & Gestwicki, J. E. Binding of Human Nucleotide Exchange Factors to Heat Shock Protein 70 (Hsp70) Generates Functionally Distinct Complexes in Vitro. *J. Biol. Chem.* **289,** 1402–1414 (2014).

35. Rauch, J. N., Zuiderweg, E. R. P. & Gestwicki, J. E. Non-canonical Interactions between Heat Shock Cognate Protein 70 (Hsc70) and Bcl2-associated Anthanogene (BAG) Co-Chaperones Are Important for Client Release. *J. Biol. Chem.* **291,** 19848–19857 (2016).

36. Nollen, E. A., Brunsting, J. F., Song, J., Kampinga, H. H. & Morimoto, R. I. Bag1 functions in vivo as a negative regulator of Hsp70 chaperone activity. *Mol. Cell. Biol.* **20,** 1083–1088 (2000).

37. Sondermann, H. *et al.* Structure of a Bag/Hsc70 complex: convergent functional evolution of Hsp70 nucleotide exchange factors. *Science* **291,** 1553–1557 (2001).

38. Ulbricht, A. *et al.* Cellular Mechanotransduction Relies on Tension-Induced and

Chaperone- Assisted Autophagy. *Curr. Biol.* **23,** 430–435 (2013).

39. Doong, H., Vrailas, A. & Kohn, E. C. What's in the 'BAG'?--A functional domain analysis of the BAG-family proteins. *Cancer Lett.* **188,** 25–32 (2002).

40. Gentilella, A. & Khalili, K. BAG3 Expression in Glioblastoma Cells Promotes Accumulation of Ubiquitinated Clients in an Hsp70-dependent Manner. *J. Biol. Chem.* **286,** 9205–9215 (2011).

41. Lee, B.-H. *et al.* Enhancement of Proteasome Activity by a Small-Molecule Inhibitor of Usp14. *Nature* **467,** 179–184 (2010).

42. Quintana, M. T. *et al.* Cardiomyocyte-Specific Human Bcl2-Associated Anthanogene 3 P209L Expression Induces Mitochondrial Fragmentation, Bcl2-Associated Anthanogene 3 Haploinsufficiency, and Activates p38 Signaling. *Am. J. Pathol.* **186,** 1989–2007 (2016).

43. Hipp, M. S. *et al.* Indirect inhibition of 26S proteasome activity in a cellular model of Huntington's disease. *J. Cell Biol.* **196,** 573–587 (2012).

44. Bowman, A. B., Yoo, S.-Y., Dantuma, N. P. & Zoghbi, H. Y. Neuronal dysfunction in a polyglutamine disease model occurs in the absence of ubiquitin-proteasome system impairment and inversely correlates with the degree of nuclear inclusion formation. *Hum. Mol. Genet.* **14,** 679–691 (2005).

45. Kampinga, H. H. & Bergink, S. Heat shock proteins as potential targets for protective strategies in neurodegeneration. *Lancet Neurol.* (2016). doi:10.1016/S1474-4422(16)00099- 5

46. Hageman, J. *et al.* A DNAJB chaperone subfamily with HDAC-dependent activities suppresses toxic protein aggregation. *Mol. Cell* **37,** 355–369 (2010).

47. Kakkar, V. *et al.* The S/T-Rich Motif in the DNAJB6 Chaperone Delays Polyglutamine Aggregation and the Onset of Disease in a Mouse Model. *Mol. Cell* **62,** 272–283 (2016).

48. Franceschelli, S. *et al.* Bag3 gene expression is regulated by heat shock factor 1. *J. Cell. Physiol.* **215,** 575–577 (2008).

49. Nam, T.-S. *et al.* A novel mutation in DNAJB6, p.(Phe91Leu), in childhood-onset LGMD1D with a severe phenotype. *Neuromuscul. Disord. NMD* **25,** 843–851 (2015).

50. Couthouis, J. *et al.* Exome sequencing identifies a DNAJB6 mutation in a family with dominantly-inherited limb-girdle muscular dystrophy. *Neuromuscul. Disord. NMD* **24,** 431– 435 (2014).

51. Fang, X. *et al.* Loss-of-function mutations in co-chaperone BAG3 destabilize small HSPs and cause cardiomyopathy. *J. Clin. Invest.* **127,** 3189–3200 (2017).

52. Sandell, S. *et al.* Diagnostically important muscle pathology in DNAJB6 mutated LGMD1D. *Acta Neuropathol. Commun.* **4,** 9 (2016).

53. Carra, S., Sivilotti, M., Chávez Zobel, A. T., Lambert, H. & Landry, J. HspB8, a small heat shock protein mutated in human neuromuscular disorders, has in vivo chaperone activity in cultured cells. *Hum. Mol. Genet.* **14,** 1659–1669 (2005).

54. Rubinsztein, D. C., Codogno, P. & Levine, B. Autophagy modulation as a potential therapeutic target for diverse diseases. *Nat. Rev. Drug Discov.* **11,** 709–730 (2012).

55. Chang, C.-H. *et al.* Different angiotensin receptor blockers and incidence of diabetes: a nationwide population-based cohort study. *Cardiovasc. Diabetol.* **13,** 91 (2014).

56. Young, Z. T. *et al.* Stabilizing the Hsp70-Tau Complex Promotes Turnover in Models of Tauopathy. *Cell Chem. Biol.* **23,** 992–1001 (2016).

57. Bergink, S. *et al.* Recognition of DNA damage by XPC coincides with disruption of the XPC- RAD23 complex. *J. Cell Biol.* **196,** 681–688 (2012).

58. Bergink, S. *et al.* DNA damage triggers nucleotide excision repair-dependent monoubiquitylation of histone H2A. *Genes Dev.* **20,** 1343–1352 (2006).

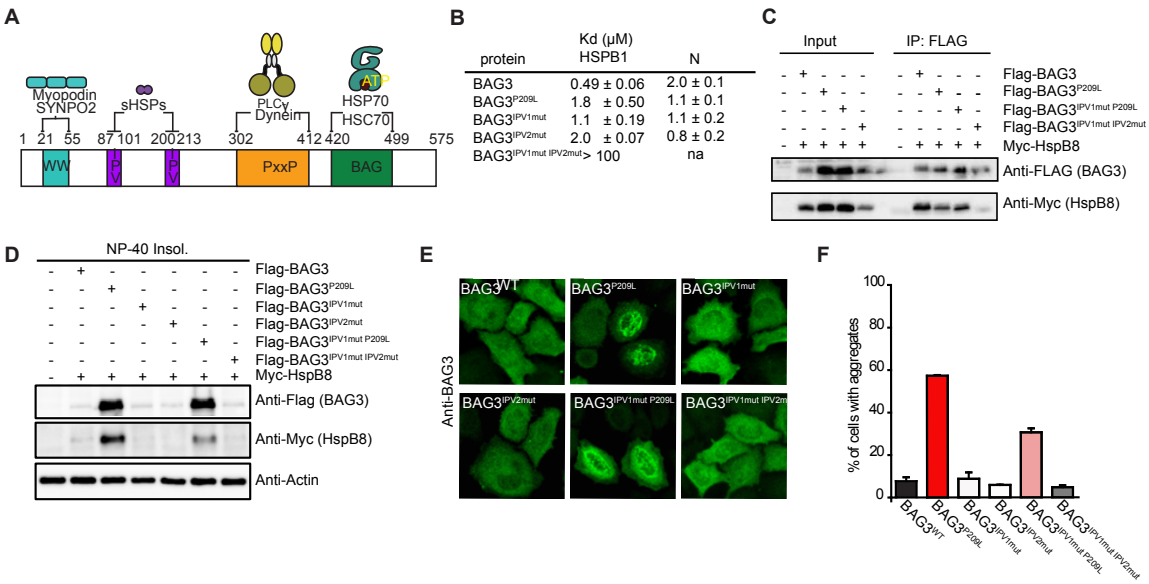

Figure 2.1. Protein aggregation by BAG3P209L is not caused by a loss of HSPB binding. (A) Schematic representation of BAG3 depicting the WW domain, the IPV motifs, the PxxP domain and the BAG domain. The disease-causing mutation P209L resides in the second IPV domain (residues 200- 213). (B) Binding of BAG3 to HSPB1c (Hsp27c) is partially disrupted by P209L. Binding affinity and estimated stoichiometry were measured by ITC. Results are the average of at least three independent experiments and error is standard deviation (SD). (C) Immunoprecipitation from cells expressing FLAG-BAG3^{WT} or mutant variants using anti-FLAG beads. Western blots for FLAG (BAG3) and MYC (HSPB8) is shown. (D) NP-40 insoluble fraction of cells expressing indicated FLAG- BAG3 variants. Western blot against the indicated antibodies is shown. The soluble fraction can be found in supplemental figure 2.1D. (E) Immunofluorescence pictures of FLAG-BAG3^{WT} and indicated mutants, using a BAG3 antibody (green). (F) Quantification of the percentage of cells with BAG3 aggregates expressing the indicated variants of BAG3. Data represent the mean and standard deviation of two independent experiments (at least 100 cells were counted per experiment).

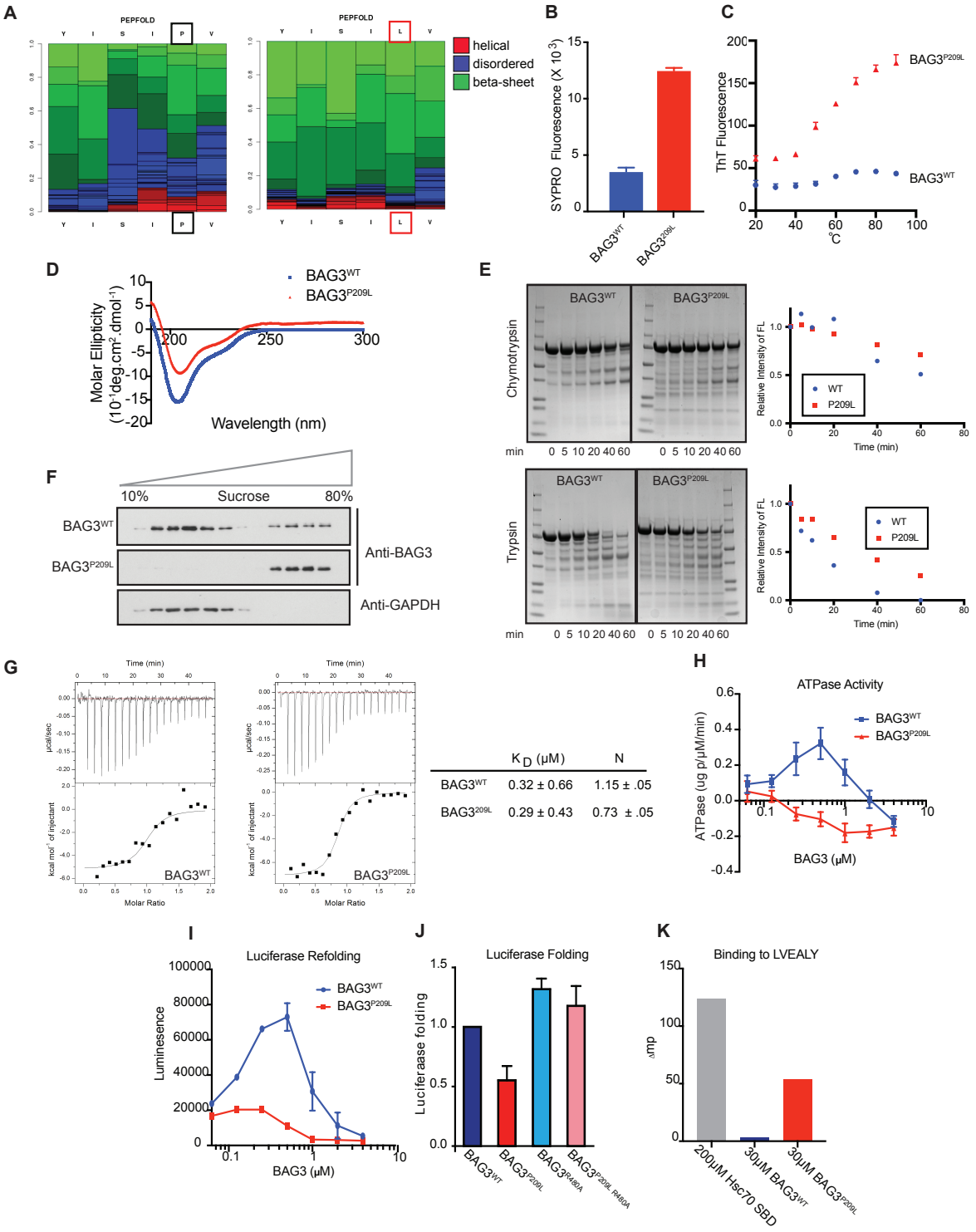

Figure 2.2. BAG3^{P209L} forms soluble oligomers that fail to collaborate with Hsp70 in client refolding. (A) Replacing proline for leucine at residue 209 is predicted to increase local beta-sheet content. PepFold was used to estimate propensity to form secondary structure. (B) Solutions containing recombinant BAG3^{WT} or BAG3^{P209L} were stained with SYPRO orange and fluorescence was measured. Results are the average

of at least three independent experiments performed in triplicate each. Error bars represent SD. (C) Recombinant $BAG3^{WT}$ or $BAG3^{P209L}$ solutions were labeled by the beta-sheet dye, thioflavin T. Results are the average of at least three independent experiments performed in triplicate each. Error bars represent SD. (D) $BAG3^{P209L}$ does not have gross changes in secondary structure, as estimated from CD measurements. Results are representative of measurements performed in triplicate. (E) $BAG3^{WT}$ or $BAG3^{P209L}$ solutions were subjected to partial proteolysis with either chymotrypsin or trypsin and samples were loaded on SDS-PAGE for separation. Coomassie stained gels are shown. (F) Fractionation of cells expressing FLAG- $BAG3^{WT}$ or FLAG-$BAG3^{P209L}$ over a sucrose gradient. Western blot against BAG3 and GAPDH is shown. (G) Recombinant $BAG3^{WT}$ and $BAG3^{P209L}$ have normal affinity to $HSPA8^{NBD}$**.** (H-I) Recombinant $BAG3^{P209L}$ is not functional in promoting HSPA8 steady state ATP hydrolysis (H) and Hsp70-mediated refolding assays (I). Measurement of ATPase activity and denatured luciferase refolding was carried out in the presence of Hsc70, DnaJA2 and various concentrations of $BAG3^{WT}$ and $BAG3^{P209L}$. Results are the average of at least three independent experiments performed in triplicate each. Error bars represent SD. (J) Relative luciferase folding capacity of HEK293 cells expressing HSPB8 and $BAG3^{WT}$ or indicated mutants of BAG3. Luciferase levels were normalized to those in cells expressing $BAG3^{WT}$. Data represents the mean and standard error of two independent experiments. (K) Non-canonical interaction of $BAG3^{P209L}$ with LVEAVY amyloid peptide.

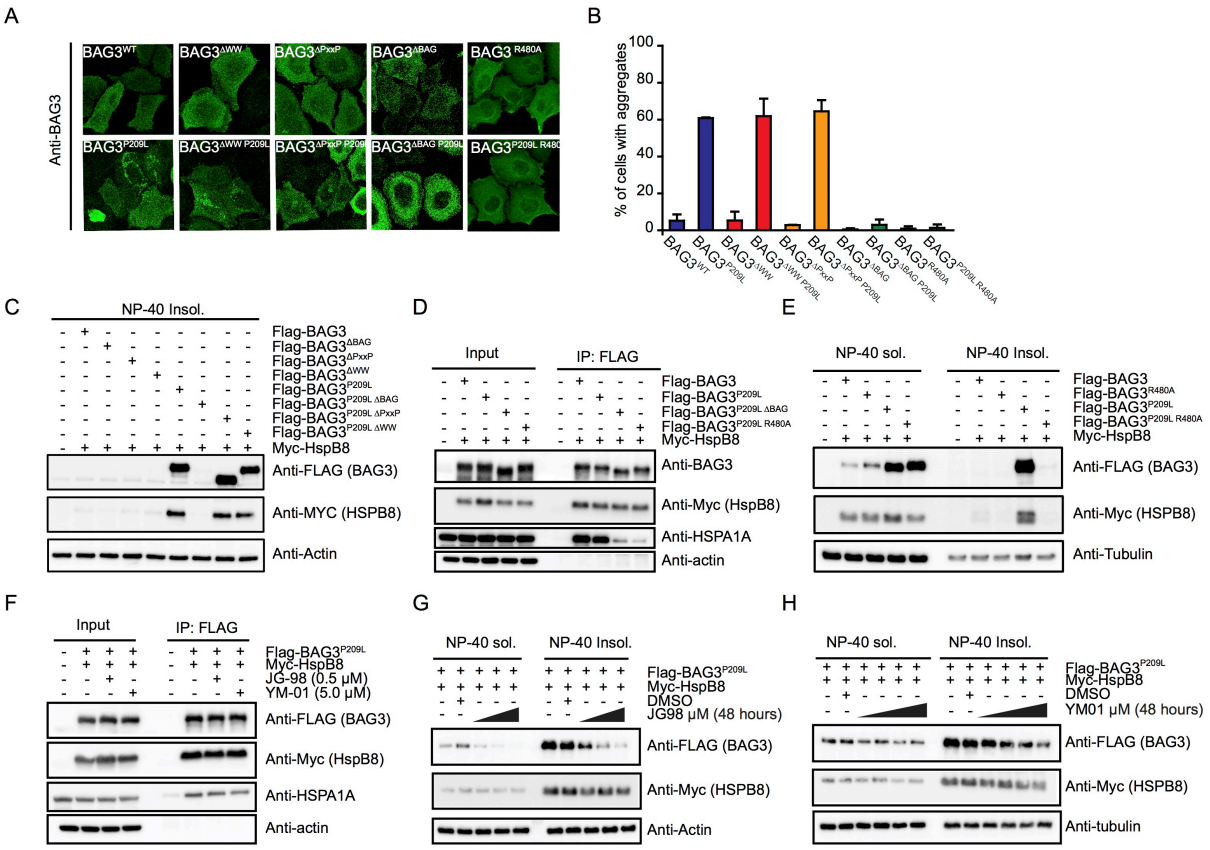

Figure 2.3: BAG3^{P209L} aggregation requires an interaction with Hsp70. (A) Immunofluorescence images of HeLa cells expressing FLAG-BAG3^{WT} and indicated mutants using an antibody recognizing BAG3 (green). (B) Quantification of the fraction of cells expressing the indicated BAG3 variants with immunofluorescence detectable punctae (2 experiments, at least 100 cells were counted per experiment, error bars represent SD). (C) Western blot of the NP-40 insoluble fraction of cells expressing BAG3^{WT} and indicated variants of BAG3. (D) Immunoprecipitation of FLAG-BAG3 variants from cells expressing both Myc-HSPB8 and indicated FLAG-BAG3 variants. Western blots using the indicated antibodies is shown. (E) Western blot of NP-40 soluble and insoluble fractions of cells expressing indicated BAG3 variants; FLAG (BAG3), Myc (HSPB8) and tubulin antibodies were used. (E) Western blot of immunoprecipitates using anti FLAG beads from HEK293 cells expressing both FLAG-BAG3^{P209L} and Myc-HSPB8 in cells treated with either 0.5 M JG-98, 5 M YM-01 or DMSO; FLAG (BAG3), Myc (HSPB8), HSPA1A and actin antibodies were used. (G-H) Western blot of NP-40 soluble and insoluble fractions of cells expressing both FLAG-BAG3^{P209L} and Myc-HSPB8, treated with DMSO or increasing concentration of the drug JG-98 (0.25, 0.5 or 1.0 μM) (G) or YM-01 (1.25, 2.5, 5.0 or 10 μM) (H).

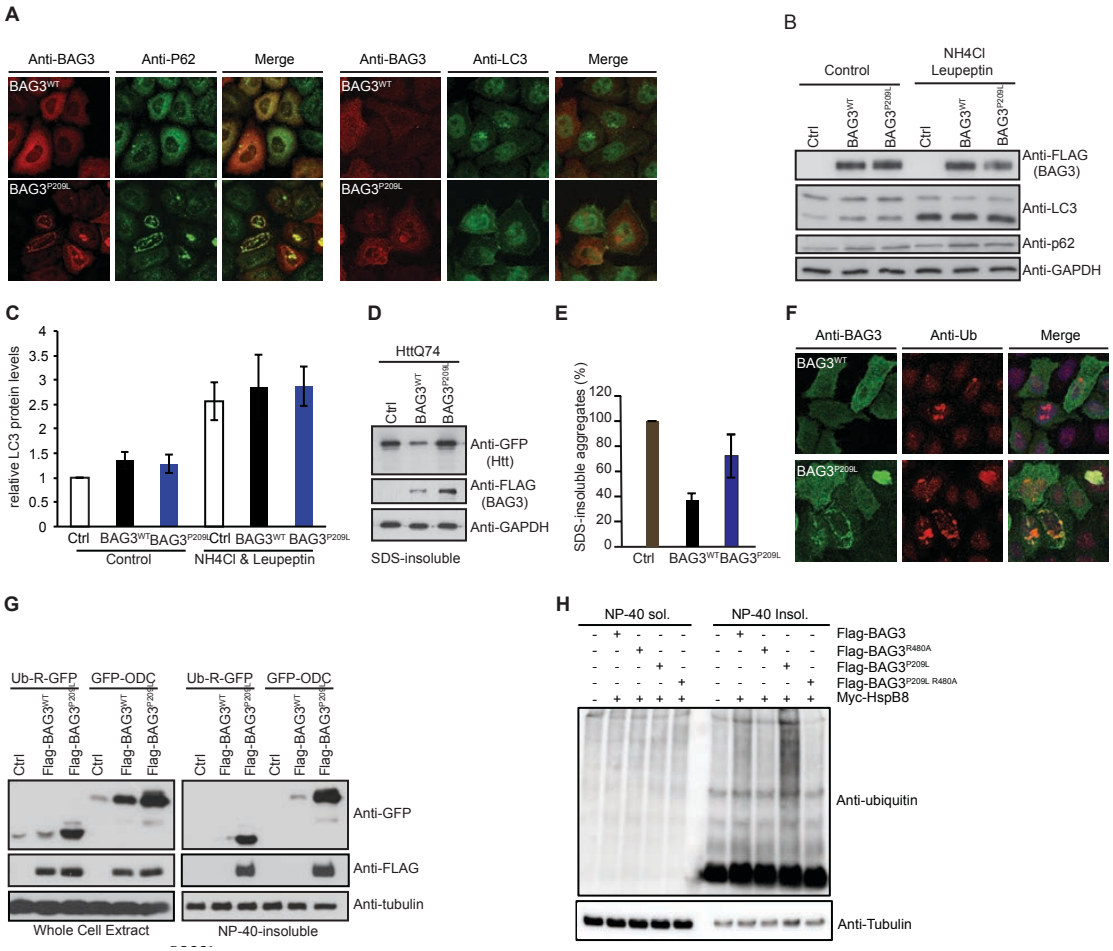

Figure 2.4. BAG3^{P209L} aggregation leads to co-aggregation of proteasomal substrates. (A) Immunofluorescence pictures of HeLa cells expressing FLAG-BAG3^{WT} or FLAG-BAG3^{P209L} using antibodies against BAG3 (green) or ubiquitin (red). (B) Induction of autophagy in cells expressing empty vector, FLAG-BAG3^{WT} or FLAG-BAG3^{P209L}; cells were treated with NH4Cl and Leupeptin or not. Western blot against the indicated antibodies is shown. (C) Quantification of autophagy induction of experiments similar to b. Relative LC3 proteins levels are shown. Data represents the mean and standard deviation of three independent experiments. (D) Suppression of GFP-HttQ74 aggregation of cells expressing a control, FLAG-BAG3^{WT} or FLAG-BAG3^{P209L}. Western blot against indicated antibodies is shown. (E) Quantification of GFP-HttQ74 aggregation of experiments similar to D. Relative percentage of SDS-insoluble protein levels are shown. Data represents the mean and standard deviation of three independent experiments. (F) Immunofluorescence pictures of HeLa cells expressing FLAG-BAG3^{WT} or FLAG-BAG3^{P209L} using antibodies against BAG3 (green) or ubiquitin (red). Left column BAG3, middle column ubiquitin and right column is the merge of BAG3 (green), ubiquitin (red) and DAPI (blue). (G) Fractionation of HEK293 cells expressing HSPB8, a control or BAG3^{WT} or BAG3^{P209L}, together with either Ub-R-GFP or GFP-ODC (ornithine decarboxylase). Western blot against GFP, FLAG (BAG3), Myc (HSPB8) and tubulin are shown. (H) Fractionation of cells expressing HSPB8 and indicated BAG3 variants. Western blot using ubiquitin (FK2) and tubulin antibodies are

shown.

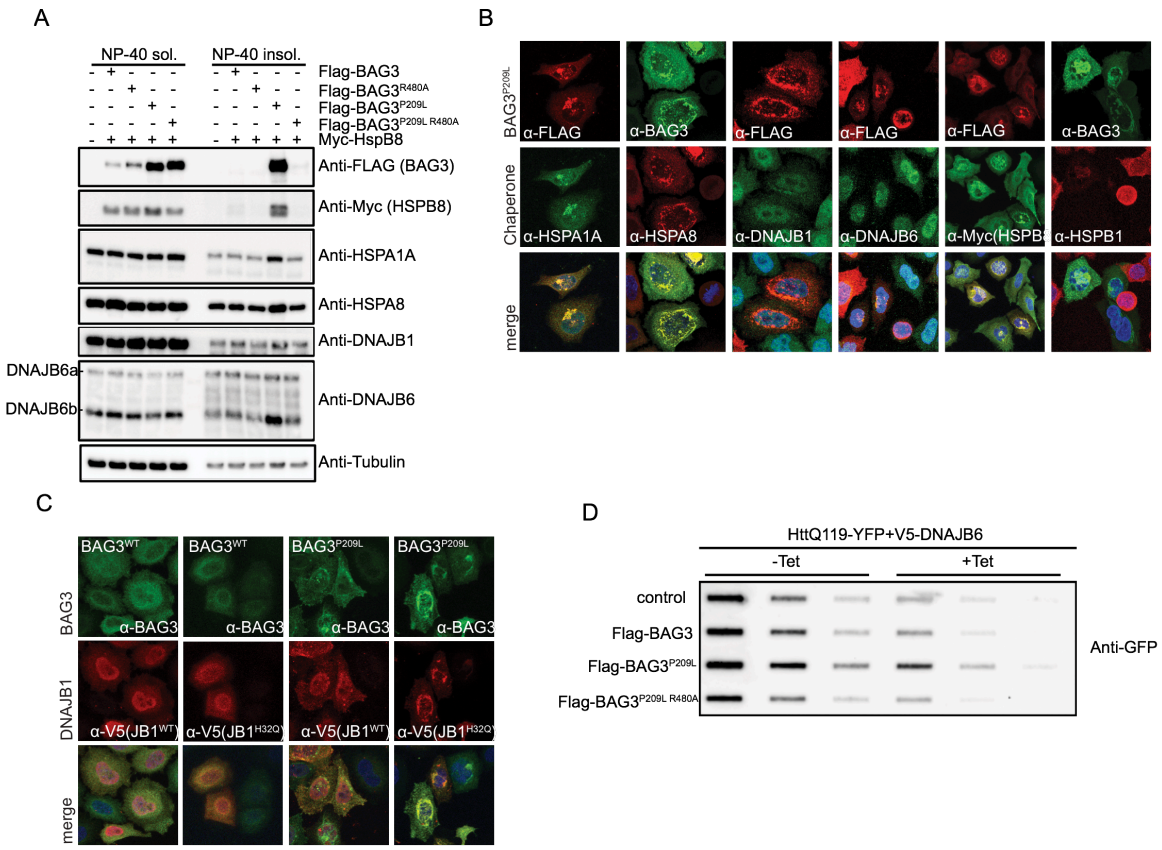

Figure 2.5. PQC proteins co-aggregate with BAG3^{P209L}. (A) Fractionation of HEK293 cells expressing Myc-HSPB8 and BAG3 variants. Western blots using the indicated antibodies is shown. (B) Immunofluorescence pictures of HeLa cells expressing FLAG-BAG3^{P209L}. Cells were stained with the indicated antibodies for staining endogenous chaperones except HSPB8 (which was stained using antibodies against myc after expression of myc-HSPB8). (C) Immunofluorescence pictures of HeLa cells expressing BAG3^{WT} or BAG3^{P209L} (upper row in green) with V5-DNAJB1^{WT} or V5- DNAJB1^{H32Q} (middle row in red). Lower row depicts the merge with DAPI. (D) Filter trap assay of cells expressing HttQ119-YFP together with Tetracyclin-inducible DNAJB6b and the indicated FLAG-BAG3 variants. Immunoblot using a GFP antibody is shown.

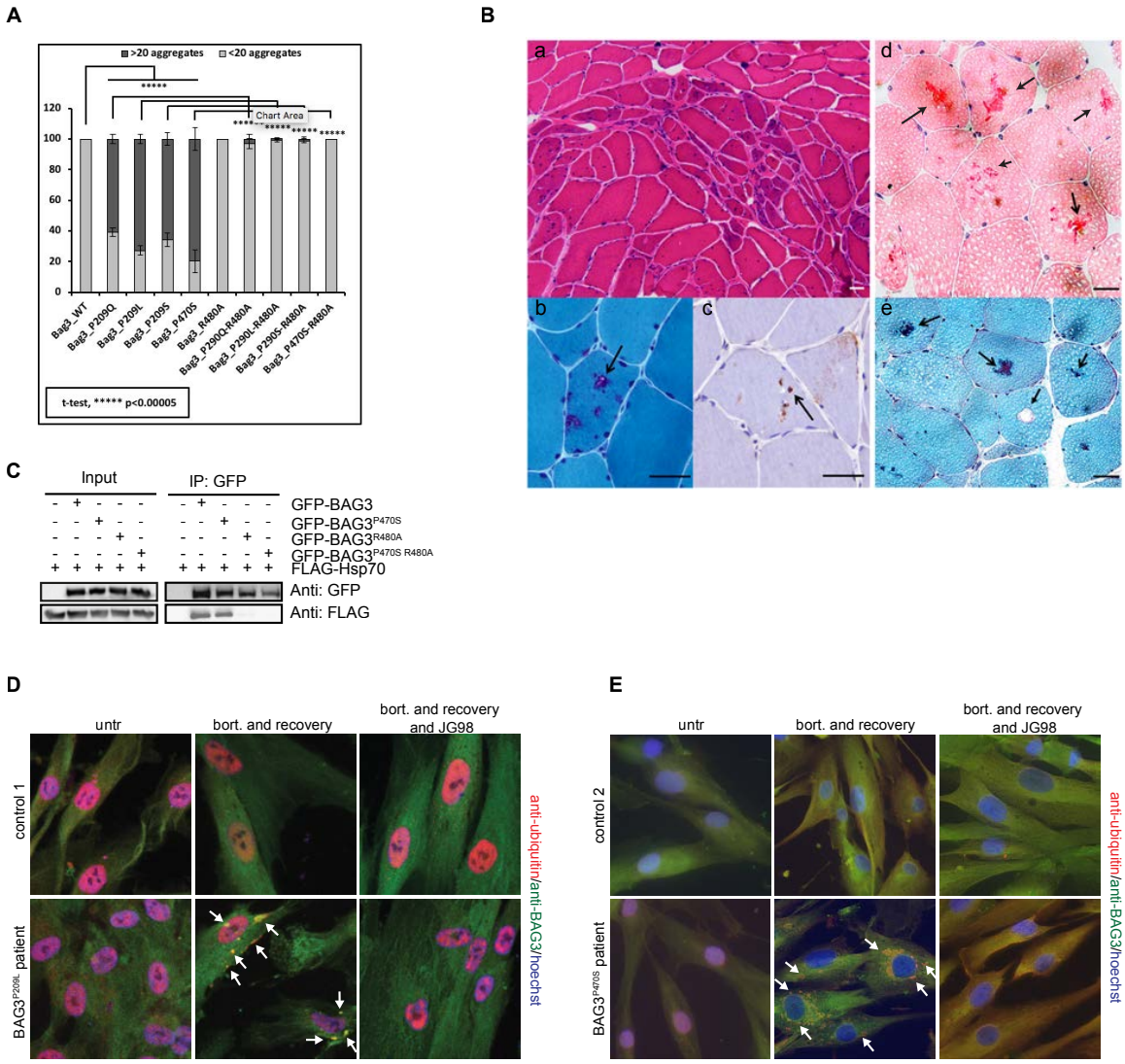

Figure 2.6. Novel MFM-causing BAG-domain mutations in BAG3 also cause HSP70-dependent aggregation; abrogation of BAG3-Hsp70 by pharmaceutical intervention as a potential therapeutic approach. (A) Analyses of the number of cells expressing the indicated BAG3-disease causing mutants (with or without the additional R480A mutation that abrogates their ability BAG3s to interact with Hsp70) that contain over 20 punctae. Typical immunofluorescent images are provided in Figure S2.6A. (B) Histochemical and immunohistochemical analysis of muscle biopsies from two novel MFM patients carrying a P470S mutation in the BAG domain of BAG3: Patient 1 (a-c) and Patient 2 (d,e) (see figure S2.6B,C for further patient info); (a) Hematoxylin and eosin (H & E) staining demonstrates region of grouped atrophy with small fibers harboring vacuoles; (b) Modified gomori trichrome (GT) staining demonstrating both cytoplasmic inclusion and rimmed vacuoles; (c) Immunohistochemistry with an antibody to TDP-43 demonstrates protein accumulation; (d) H & E staining shows large centrally located eosinophilic inclusion; (e) GT staining shows dark centrally located inclusions and a fiber with a centrally located vacuole. Arrows denote protein inclusions or vacuoles. Scale is 50 μM. **c,** Immunoprecipitation of GFP- tagged BAG3 variants from

cells expressing both GFP-BAG3 variants and FLAG-tagged HSP70. Western blots using the indicated antibodies is shown. (D,E) Immunofluorescence pictures of primary control versus BAG3^{P209L} patient fibroblasts (D) or primary control versus BAG3^{P470S} patient fibroblasts (E)**.** Cells were either untreated, treated for 6 hours with bortezamib followed by a 20 hours recovery or treated for 6 hours with bortezamib followed by a 20 hour recovery in the presence of 0.05 μM JG98. Arrows indicate BAG3-punctae.

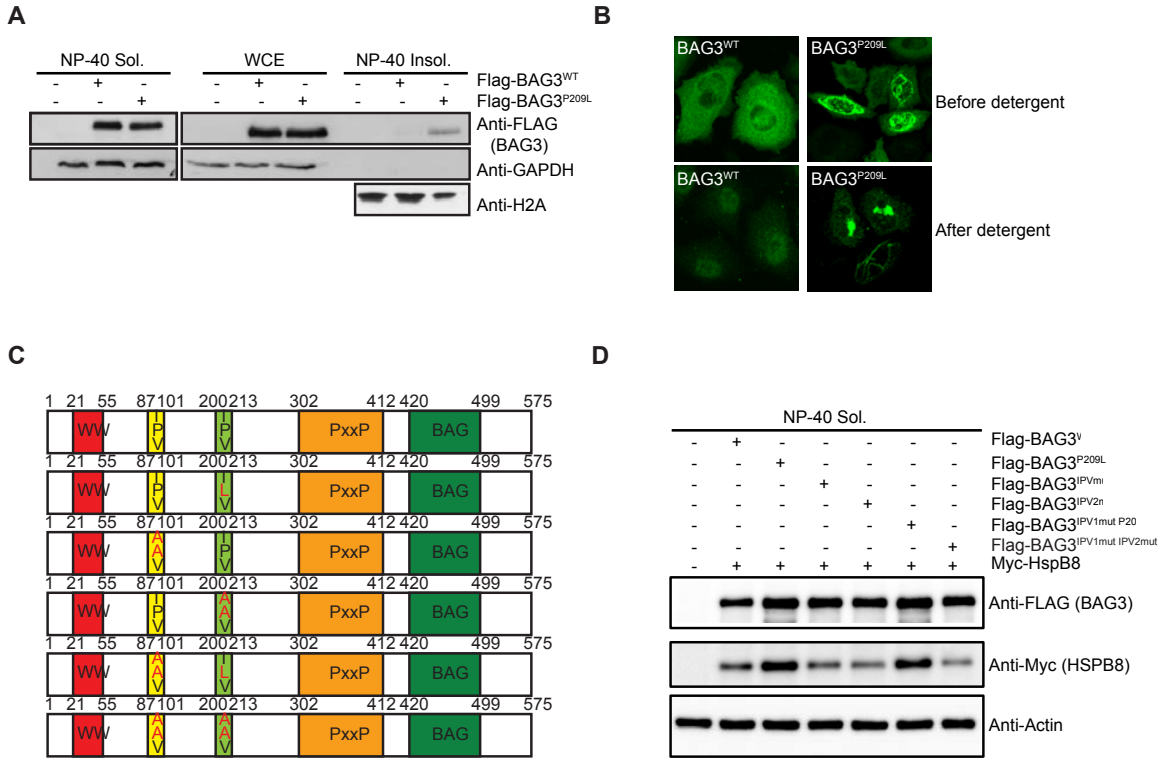

Figure S2.1. BAG3^{P209L} aggregation is not caused by a loss of HSPB binding. (A) Whole cell extracts (WCE) and NP-40 soluble and insoluble fractions of cells expressing indicated FLAG-BAG3 variants. Western blot against the indicated antibodies is shown. (B) Immunofluorescence pictures of FLAG-BAG3^{WT} and FLAG-BAG3^{P209L}, using a BAG3 antibody (green) before and after detergent treatment prior to fixation. (C) Schematic representation of BAG3 mutants used. (D) NP- 40 soluble fractions belonging to Figure 2.1D of cells expressing indicated FLAG-BAG3 variants. Western blot against the indicated antibodies is shown.

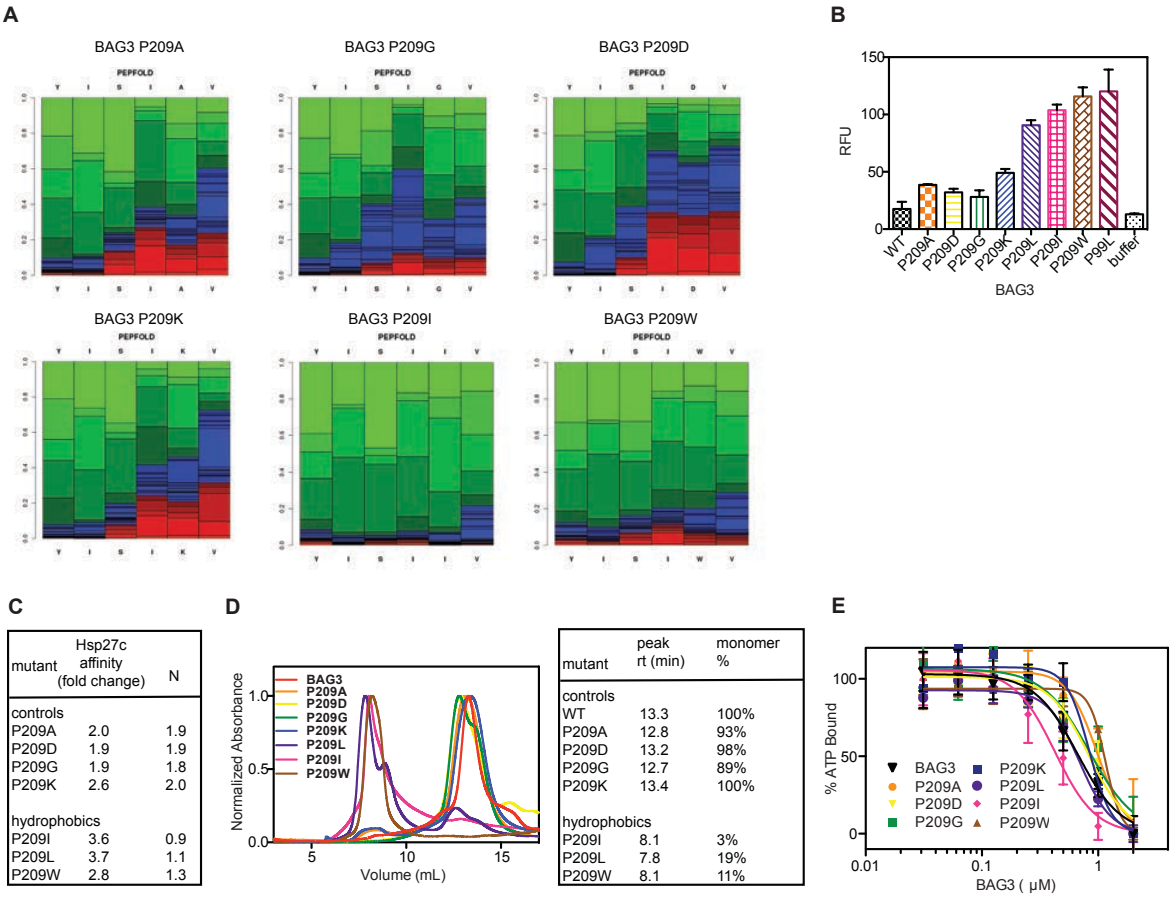

mutant	Hsp27c affinity (fold change)	N
controls		
P209A	2.0	1.9
P209D	1.9	1.9
P209G	1.9	1.8
P209K	2.6	2.0
hydrophobics		
P209I	3.6	0.9
P209L	3.7	1.1
P209W	2.8	1.3

mutant	peak rt (min)	monomer %
controls		
WT	13.3	100%
P209A	12.8	93%
P209D	13.2	98%
P209G	12.7	89%
P209K	13.4	100%
hydrophobics		
P209I	8.1	3%
P209L	7.8	19%
P209W	8.1	11%

Figure S2.2. BAG3^{P209L} forms soluble oligomers that fail to collaborate with Hsp70 in client refolding. (A) PepFold predictions for additional hydrophobic and control mutants at position 209. (B) Hydrophobic BAG3 mutants, but not controls, bind to ThT *in vitro*. Results are the average of at least three independent experiments performed in triplicate each. Error bars represent SD. Relative ThT fluorescence is shown. (C) Normalized (to BAG3^{WT}) affinity and stoichiometric ratio (N) for Hsp27c/HSPB1c of indicated BAG3 mutants. (D) BAG3^{P209L} and hydrophobic BAG3 mutants, but not controls, are soluble oligomer, as observed by SEC-MALS. Protein solutions (230 µM) were separated by SEC and the size of particles estimated by light scattering. Retention times and percent monomer are shown. Results are representative of measurements performed in triplicate. (E) All of the BAG3 variants are capable of releasing fluorescent nucleotide from Hsc70/HSPA9. Results are the average of at least three experiments performed in triplicate. Error bars represent SD. See the methods for details.

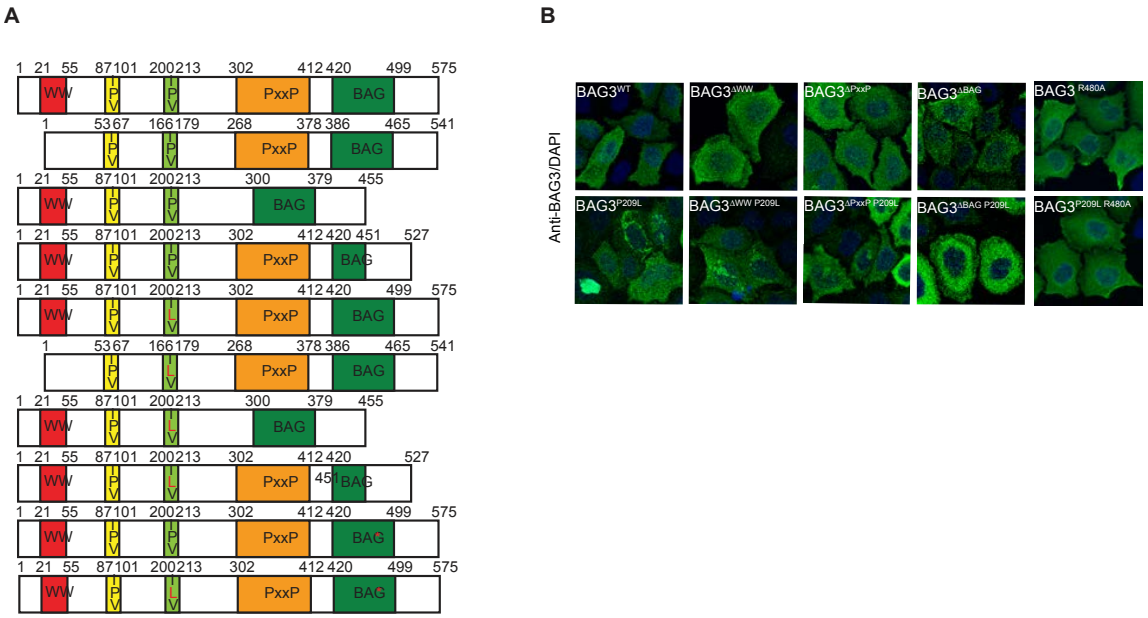

Figure S2.3. BAG3^{P209L} aggregation requires Hsp70 interaction. (A) Schematic representation of BAG3 mutants used. (B) Immunofluorescence images of HeLa cells expressing FLAG-BAG3^{WT} and indicated mutants using an antibody recognizing BAG3 (green) and DAPI staining (blue).

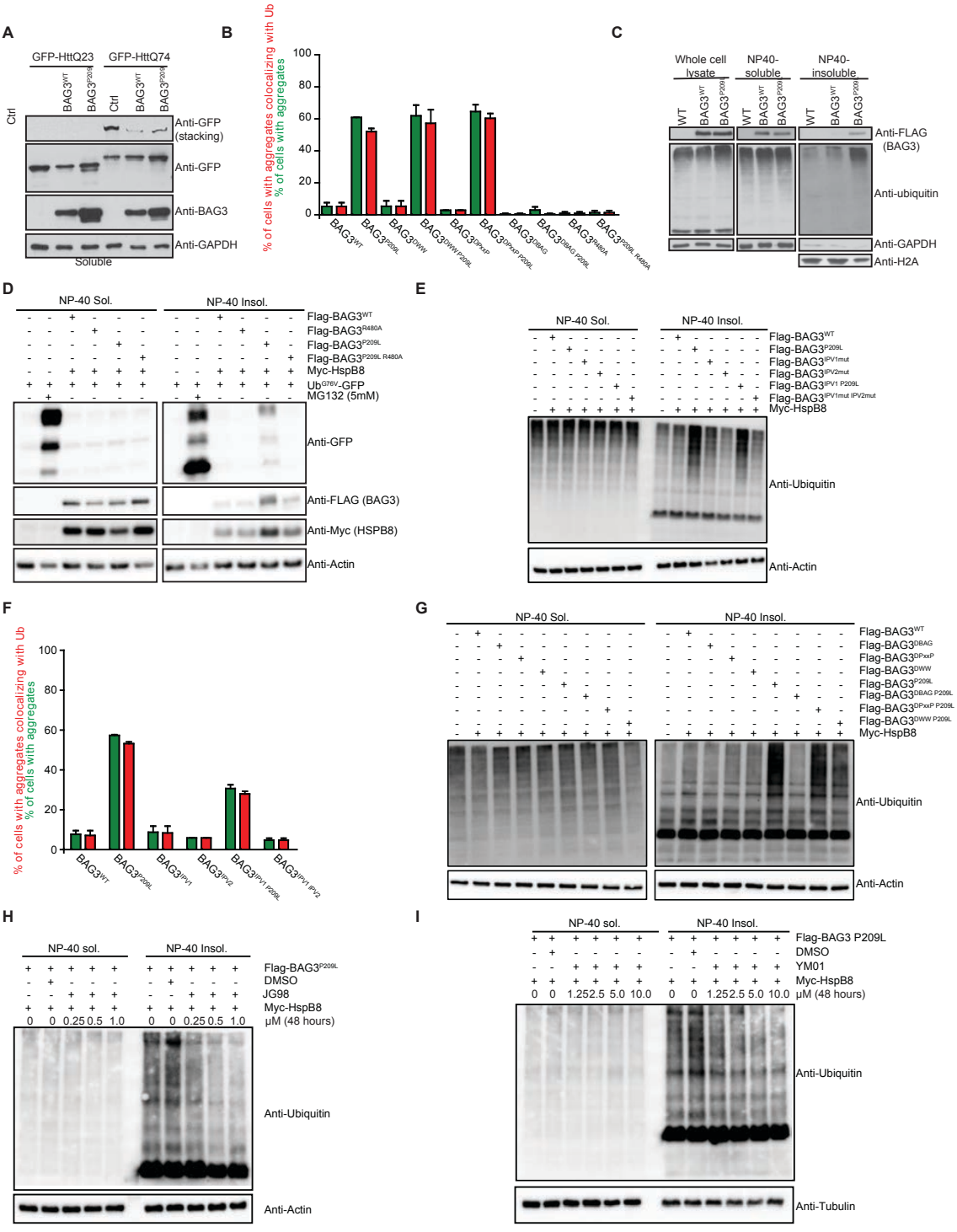

Figure S2.4. BAG3^{P209L} mutant is partially dysfunctional as Hsp70 co-chaperone. (A) Effect of FLAG- BAG3^{WT} or FLAG-BAG3^{P209L} on expression levels of GFP-HttQ23 and GFP-HttQ74 (exon-1 of the huntingtin gene) and on GFP-HttQ74 aggregation (stacking). Western blot against indicated antibodies is shown (belongs to Figure 2.4D,E). (B) Quantification of the percentage of cells with BAG3 aggregates (green) and percentage of cells with BAG3 aggregates that co-localize with ubiquitin (red). Cells

expressed HSPB8 and BAG3 or the indicated variants of BAG3. Data represents the mean and standard deviation of two independent experiments at least 100 cells were counted per experiment. (C) Fractionation of HEK293 cells expressing a control, FLAG-BAG3^{WT} or FLAG-BAG3^{P209L}. Western blot against FLAG (BAG3), ubiquitin, GAPDH and H2A are shown. (D) Fractionation of HEK293 cells expressing HSPB8, a control or BAG^{WT} or BAG3^{P209L}, together with either Ub-R-GFP or GFP-ODC (ornithine decarboxylase). Western blot against GFP, FLAG (BAG3), Myc (HSPB8) and tubulin is shown**.** (E) Fractionation of HEK293 cells expressing a control, FLAG-BAG3^{WT} or various FLAG-BAG3 –IPV mutants as indicated. Western blot against FLAG (BAG3), ubiquitin and actin are shown. (F) Quantification of the percentage of cells with BAG3 aggregates (green) and percentage of cells with BAG3 aggregates that co-localize with ubiquitin (red). Cells expressed HSPB8 and BAG3 or the indicated variants of BAG3. Data represents the mean and standard deviation of two independent experiments at least 100 cells were counted per experiment. (G) Fractionation of HEK293 cells expressing HSPB8, a control or BAG3^{WT} or BAG3^{P209L} or the indicated single or double deletion mutants. Western blot against indicated antibodies is shown. (H) Fractionation of HEK293 cells expressing HSPB8 and BAG3^{P209L} in the presence of increasing concentration of JG98. Western blot against indicated antibodies is shown. (I) Fractionation of HEK293 cells expressing HSPB8 and BAG3^{P209L} in the presence of increasing concentration of YM01. Western blot against indicated antibodies is shown.

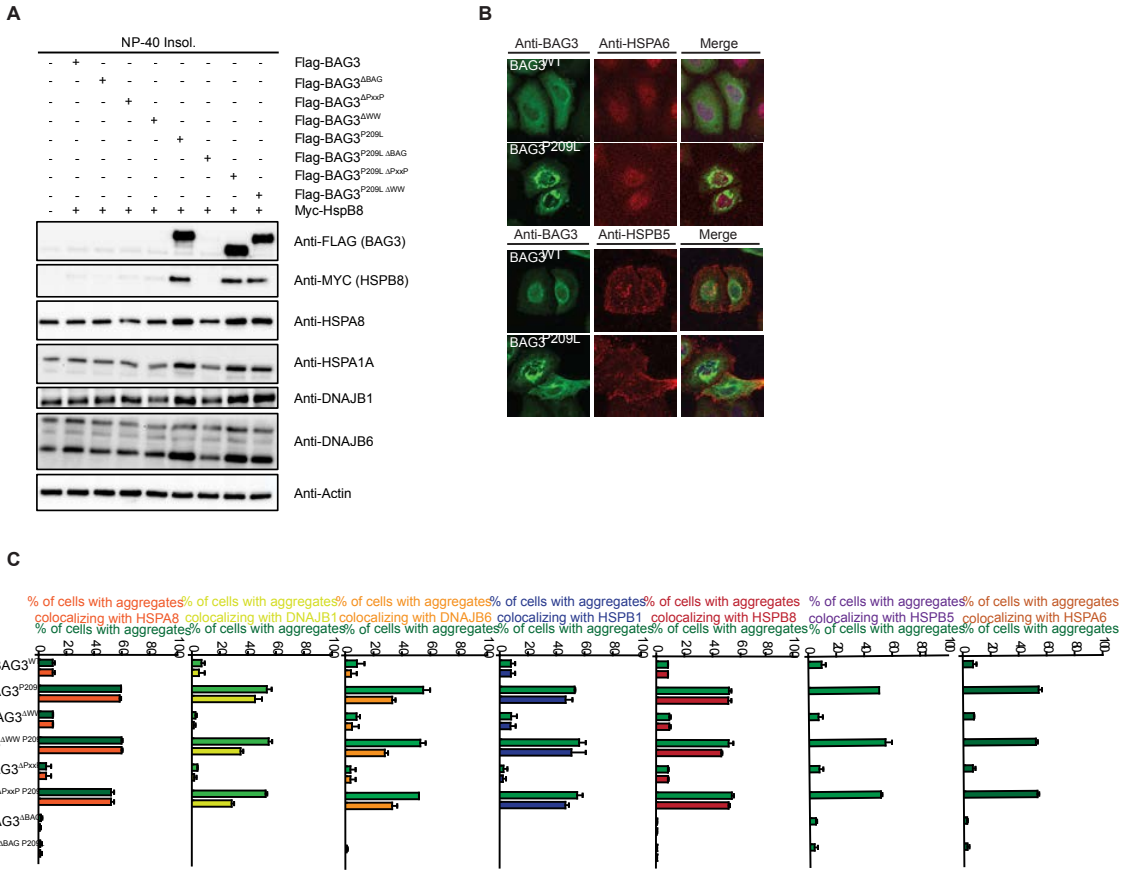

Figure S2.5: BAG3^{P209L} aggregates sequester chaperones in an HSP70-binding dependent manner. (A) Fractionation of HEK293 cells expressing Myc-HSPB8 and BAG3 variants. Western blots using the indicated HSP antibodies is shown (additional data to Figure 2.5A). (B) Immunofluorescence pictures of HeLa cells expressing FLAG-BAG3^{P209L}. Cells were stained with the indicated antibodies for staining endogenous chaperones. (C) Quantification of the percentage of cells with aggregates and cells with aggregates that colocalize with the indicated chaperones. Data represents the mean and standard deviation of two independent experiments (at least 100 cells were counted per experiment).

A

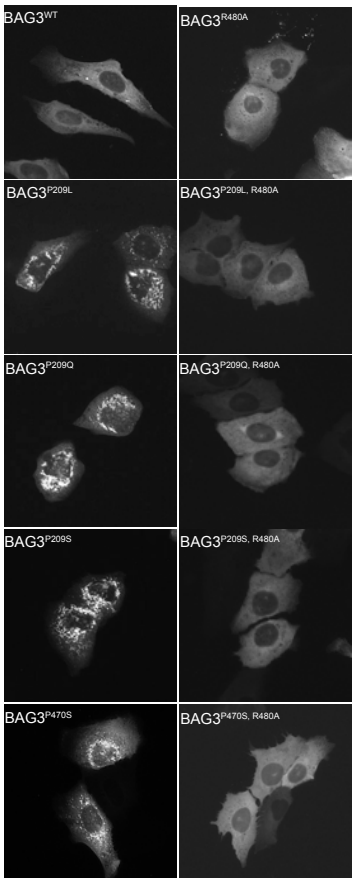

B

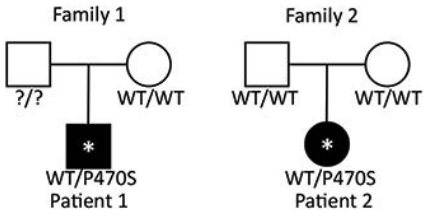

C

	Patient 1	Patient 2
BAG3	c.1408C>T p.Pro407Ser	c.1408C>T p.Pro407Ser
Sex	Male	Female
Age	45	37
Onset	35	28
Weakness	Symmetric	Mild assymmetry
Deltoid	4+	5
Biceps	5	5
Triceps	5	5
Wrist extensors	5	5
Hand intrinsics	5	5
Iliopsoas	4	5
Quadriceps	5	5
Hamstrings	5	5
Gastrocnemius	5	4-
Tibialis anterior	4	2-3
Sensation	NL	NL
Reflexes	Trace throughout	Absent at the ankles
Creatine kinase	618 (nl 30-200)	306 (nl 30-200)
EMG	Myopathic changes in proximal muscles and neurogenic features in distal leg muscles.	Acute and chronic denervation in the peroneal and tibial nerve innervated muscles and moderate to chronic denervation in the vastus.
Biopsy	Quadriceps and Deltoid with small angular fibers, rimmed vacuoles and TDP-43 inclusions. **RV myopathy**	Fiber atrophy with centrally located eosinophilic and trichrome positive inclusions, RVs and Z-disc streaming on EM. **Myofibrillar Myopathy**

D

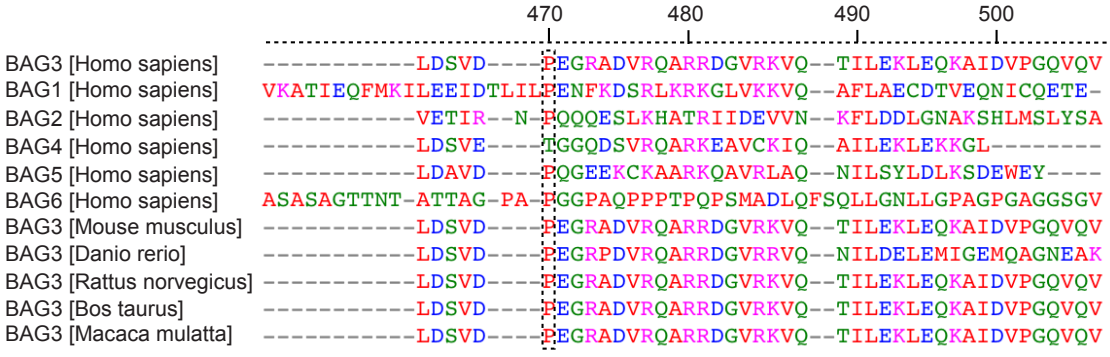

Figure S2.6. Abrogation of BAG3-Hsp70 by pharmaceutical intervention as a potential therapeutic approach. (A) Immunofluorescence pictures cells of cells expressing the indicated BAG3-disease causing mutants, with or without the additional R480A mutation that abrogates the ability of the (mutant) BAG3s to interact with Hsp70 (quantification provided in Figure 2.6A). (B) Pedigree structures and known genotype of the proband (*) and parents in Family 1 and Family 2 with a P470S mutation in the BAG-domain. (C) Patient characteristics. (D) Alignment of BAG3 proteins show the high conservation of proline at position 470.

Chapter 3

Competing protein-protein interactions regulate Hsp27's interactions with its client protein Tau

Rebecca Freilich, Miguel Betegon, Eric Tse, Sue-Ann Mok, Olivier Julien, David A. Agard, Daniel R. Southworth, Koh Takeuchi and Jason E. Gestwicki

Abstract: Small heat shock proteins (sHSPs) are a class of oligomeric molecular chaperones that limit the aggregation of partially unfolded proteins. Despite recent insights, it is often not clear where sHSPs bind on their "client" proteins, or how these protein-protein interactions (PPIs) are regulated. Here, we mapped the PPIs between human Hsp27 and an important native client, the microtubule-associated protein tau (MAPT/tau). We found that Hsp27 selectively recognizes two aggregation-prone regions of tau, using the conserved β4-β8 cleft of its alpha-crystallin domain (ACD). The β4-β8 region is also known to be important for Hsp27-Hsp27 interactions within oligomers, suggesting that competitive PPIs between Hsp27-Hsp27 and Hsp27-tau may be an important regulatory paradigm. Indeed, we found that each of the individual PPIs are relatively weak and that competition for shared sites seems to control both client binding and Hsp27 oligomerization. Moreover, we found that an additional, distinct PPI between tau and Hsp27's unstructured N-terminal domain (NTD) is critical to chaperone activity, suggesting a model in which Hsp27's NTD is a functional chaperone domain while the β4-β8 groove acts as a tunable sensor for unfolded clients. These findings highlight the importance of multiple, competitive PPIs in the function of Hsp27.

Introduction. Molecular chaperones maintain cellular protein homeostasis (proteostasis)[1]. Among these chaperones, the small heat shock proteins (sHSPs) play a key role by preventing the aggregation of partially unfolded proteins[2–4]. Specifically, sHSPs are thought to maintain their "client" proteins in a soluble, folding-competent state for subsequent processing by ATP-dependent chaperones[5,6], such as Hsp70. In

this way, the sHSPs act as sentinels of protein unfolding, especially in response to stress or conditions that would promote protein aggregation.

Hsp27 is a broadly expressed member of the sHSP family, which prevents aggregation of a large number of putative clients[7]. As a consequence of these interactions, Hsp27 has been implicated in many diseases, including neurodegeneration[8–10]. Despite its important roles, the molecular mechanisms of Hsp27 function remain mysterious. Like all sHSPs, Hsp27 contains a highly conserved α-crystallin domain (ACD) flanked by disordered N- and C- terminal domains (NTD and CTD) (Figure 3.1A). The ACD has an anti-parallel β-sandwich fold and cross β-sheet interactions between two of these domains mediate the dimerization of sHSPs[11,12]. These dimers are then assembled into larger species (up to ~30mers) through a series of distinct PPIs that involve different regions of the ACD, as well as the NTD and CTD. The best characterized of these oligomer-stabilizing PPIs is the one between IXI motifs in the CTD and the β4-β8 groove of the ACD[12–15]. This interaction involves binding of the linear, disordered IXI motif into a shallow groove between β-sheets 4 and 8. The IXI interaction with β4-β8 is important in homo-oligomer formation but it can also facilitate heterodimer formation between different members of the sHSP family[16]. Separate PPIs involving the NTD are also thought to contribute to oligomer formation[16–18], but the specific interaction sites are not known. However, Hsp27's NTD is clearly important because three phosphorylation sites in that region regulate oligomer assembly[19].

One of the major roles of Hsp27 is to prevent aggregation of its client proteins. However, it is not yet clear where Hsp27 binds to clients or how it stabilizes them. Work in other sHSPs, such as α-crystallin[20], yeast Hsp42[5] and plant Hsp18[21–23] has suggested that different surfaces can be used to engage clients. It has been shown that the highly conserved ACD is sufficient to prevent aggregation of certain clients[12,20], while the NTD is necessary for others[20,24–27] . However, the factors that determine what types of clients are bound and what parts of Hsp27 are involved (*i.e.* ACD, NTD and CTD) remain ambiguous. One of the key issues is that the natural clients of the sHSPs are often not known. Model proteins, such as firefly luciferase, citrate synthase and malate dehydrogenase, have been used to study mechanisms of sHSP function[5,28,29], but biophysical information on native interactions is sparse[7,30,31].

In this study, we characterized the interactions between Hsp27 and microtubule-associated protein tau (MAPT/tau). We selected tau for these studies because Hsp27 has been shown to regulate tau's aggregation *in vitro* and *in vivo*[32,33], making it one of the few well-validated, natural clients. Moreover, tau is an intrinsically disordered protein, a feature that removes the complication of considering both folded and unfolded states. Finally, tau is known to aggregate in a number of progressive, untreatable neurodegenerative disorders[34], including some forms of Alzheimer's disease (AD), so mechanistic information about how Hsp27 acts on it would be of biomedical interest. Indeed, over-expression of Hsp27 has been found to be partially protective in animal models of tauopathy[32].

Using a combination of biophysical techniques, we characterized Hsp27's interactions with tau. We found that Hsp27 binds two sites on tau (PHF6 and PHF6*) that are well known to be required for aggregation. The location of these interactions helps explain the strong anti-aggregation activity of Hsp27 and suggests that the chaperone may be tuned to prefer the most problematic regions in tau. On the other side, we found that Hsp27 used both its NTD and β4-β8 groove to bind tau. The involvement of the β4-β8 groove was unexpected and interesting because, as mentioned above, this region is also known to bind IXI motifs within the oligomer. Thus, this result suggested that competition between client and IXI might limit chaperone function. Indeed, we found that Hsp27-Hsp27 interactions, mediated by the IXI motifs, seemed to partially counteract tau binding. We speculate that this set of competing PPIs may normally hold Hsp27 in a latent, inactive oligomer prior to accumulation of sufficient levels of misfolded client to overcome the self-limiting interactions. Finally, we found that binding alone was not sufficient to prevent tau aggregation and that additional contacts in the NTD were required. Together, these results suggest that, at least for tau, Hsp27's NTD plays a major role in chaperone function, while the β4-β8 groove serves as an important client sensor. This model advances our understanding of sHSP structure-function and suggests potential ways of targeting Hsp27 for drug discovery.

Results:

Hsp27's β4/β8 groove is a PPI hotspot for both client and homotypic interactions. Because the ACD has been shown to have chaperone activity for some clients[20], we first measured the interaction of ^{15}N-labelled Hsp27 ACD with tau by HSQC NMR[11]. In

this experiment, we utilized two isoforms of tau (Figure 3.1A): the full length splice variant 0N4R tau, which is commonly expressed in adult brain and K18, a construct containing just the four microtubule binding repeats (MTBRs) that is known to contain the binding sites of other chaperones[35,36]. We found that both tau isoforms caused chemical shift perturbations (CSPs; > 0.4 ppm) within the hydrophobic β4-β8 groove of the ACD, in addition to sporadic shifts along the dimer interface (Figure 3.1B). The β4-β8 groove is a conserved binding site for IXI motifs[14], as well as the Hsp70 co-chaperone BAG3[37] and some other clients[20]. Moreover, a recent study also suggested that tau binds to this region of Hsp27's ACD[33]. To better understand how tau and the IXI motif (which is isoleucine, proline, valine (IPV) in Hsp27) might compete for the same region, we first synthesized the 9-mer peptide of Hsp27 (EITIPVTFE) and confirmed its binding site in the HSQC assay (Figure 3.1C). We found that the peptide caused peak broadening, indicating that it is in an intermediate exchange. As expected, the affected peaks were localized to the β4-β8 groove, confirming that both IPV/IXI and tau bind the same region.

Next, we used isothermal calorimetry (ITC) to measure the affinity of Hsp27's IPV motif for the β4-β8 groove (Figure 3.1D and S3.2A). We found that the native Hsp27 IPV sequence had a weak affinity for ACD (>25 μM), but that swapping the penultimate phenylalanine residue for a histidine, which is the identity of this position in the IXI motif of the co-chaperone BAG3, improves affinity to 11.5 ± 0.43 μM. Next, we examined the other residues that might contribute to affinity using alanine scanning, in the context of the His-containing sequence. We were particularly intrigued by the fact that Hsp27's

motif contains an unusual, extended IXIXV sequence (ITIPV; see Figure 3.1D). However, alanine scanning revealed that the isoleucine and valine of the canonical IPV are the major contributors to affinity; mutating either one of these residues completely ablated the interaction (K_d > 25 μM). On the contrary, mutating either X residue in the IXIXV motif (EIATIPVTHE or EITIAVTHE) modestly improved, rather than reduced, affinity (K_d ~ 5 μM). The ITC titrations indicated that all of the peptides have a binding stoichiometry of between 0.5 and 1, suggesting that the peptides do not always occupy all available β4-β8 binding sites on the ACD.

To understand how this IXI interaction might compete with tau binding at the β4-β8 groove, we attempted to measure tau's affinity for the ACD by ITC and BLI. However, we found that this interaction was quite weak (>100 μM). Thus, while both IPV motifs and tau bind at the β4-β8 groove, the self-interaction is significantly (~10-fold) tighter.

Multiple domains of Hsp27 interact with tau and binding can be obscured by oligomeric self-interactions. Next, we wanted to study the other side of the interaction and learn where Hsp27 binds on tau**.** Because our earlier study suggested that K18 and 0N4R tau bind similarly to Hsp27's ACD (see Figure 3.1), we focused on the shorter K18 region as likely to contain the major site(s). Accordingly, we used ^{15}N-labelled K18 in HSQC NMR experiments to map putative interactions with unlabeled Hsp27 ACD. We found that addition of Hsp27's ACD caused peak broadening in two remarkably discrete locations (Figure 3.2). These binding sites include the well documented PHF6 (275-VQIINK-280) and PHF6* (306-VQIVYK-311) regions, which are known to be

required for tau aggregation[38]. To confirm whether the β4-β8 groove was involved in this binding, we purified an Hsp27 ACD mutant, L157A. This residue was previously identified as being important in IXI interactions[14] and we confirmed that mutation blocks binding to BAG3 (Figure S3.3). Surprisingly, we found that the L157A mutation ablated the interaction with the first motif, but not the second (Figure 3.2), suggesting that the binding modes of the two peptide regions may not be equivalent.

In order to estimate the relative affinity for the two sites, we carried out a detailed titration analysis using a TROSY scheme with better chemical shift resolution[39]. Titration of Hsp27 ACD into ^{15}N labeled K18 tau confirmed that the main binding interaction occurs at the two PHF6 and PHF6* motifs, with minor interactions at residues 292-297 and 349-353 (Figure S3.4A). Consistent with this model, deletion of residues 277/8 and 308/9 in both aggregation motifs entirely abolished the interaction with Hsp27's ACD (Figure S3.4B). Then, to understand which site might be preferred, we generated the single deletions of 277/8 or 308/9 in K18 tau and found that the first aggregation motif has a much stronger affinity than the second (Figure S3.4C). Specifically, the ACD's interaction with the first aggregation motif is saturable at a 1:2 K18:ACD stoichiometry, while the interaction at the second aggregation motif was not saturable within the constraints of protein solubility. Then, we tried to measure the relative affinity of the 6-mer peptides corresponding to the first (VQIINK) and second (VQIVYK) aggregation motifs, but found that they were unable to produce saturable chemical shift changes in the ^{1}H-^{15}N ACD spectra, signifying that the isolated motifs, by themselves, have weak affinity for Hsp27 (Figure S3.4D).

The NTDs of sHSPs have also been implicated in recognition of various model clients. To determine whether it is involved in tau binding, we purified Hsp27's NTD and tested its binding to ^{15}N K18 by HSQC. This experiment revealed broadening in a large number of residues across the K18 sequence (Figure 3.2). Compared to the discrete ACD interaction, the NTD contacts seemed to involve multiple parts of K18 tau, including the PHF6 and PHF6* aggregation motifs, as well as broad regions corresponding to residues 246-268 and 342-361.

The evidence so far suggested that Hsp27 interacts with multiple regions of tau, using both its ACD and NTD. We hypothesized, therefore, that the full-length Hsp27 protein, containing both the NTD and the ACD, might have tight affinity due to multivalent interactions. However, when we tested binding of full-length Hsp27 to K18 tau (Figure 3.2 and S3.5), we observed no broadening or CSPs. This result is consistent with an alternative model in which the Hsp27-Hsp27 interactions, mediated by the IXI motifs locking together with β4-β8 grooves in adjacent ACDs, largely "hides" this PPI surface from interacting with tau. Indeed, previous structural studies[15] have shown that Hsp27's IXI motifs engage in extensive PPIs with itself in the context of large oligomers. Based on these results and our binding studies, we speculate that the weaker interactions of tau cannot, under these conditions at least, compete with Hsp27's IXI motifs, which have higher individual affinity.

Hsp27's NTD plays a functional role in chaperoning tau. So then, how does Hsp27 become activated as a chaperone? To explore this question, we first focused on the NTD because phosphorylation of this region has been shown to reduce oligomer size and increase chaperone activity[19,24]. As a surrogate for chaperone activity, we measured the ability of Hsp27 to suppress aggregation of tau *in vitro*, as measured by thioflavin T (ThT) fluorescence. First, we confirmed previous observations that full length Hsp27 prevents aggregation of both 0N4R and K18 in the ThT assay (Figure 3.3A), significantly increasing the lag time and slowing the elongation rate. Presumably, WT Hsp27's ACD may be able to bind to tau under these conditions because the high local concentration of the client outcompetes the self-limiting IXI contacts. However, deletion of the NTD (ΔNTD) ablated Hsp27's ability to delay tau aggregation, showing that this region is essential to chaperone function. Consistent with this result, the ACD alone had no effect on tau aggregation, despite the fact that it would be predicted to (weakly) bind to the PHF6 and PHF6* motifs. The ACD is known to have chaperone activity in other amyloid-prone client systems[20], but it does not seem to be sufficient for tau. We speculate that the NTDs may be required to block PPIs between tau monomers, through steric/repulsive effects and/or coating the tau surface.

Next, we explored the effect of NTD phosphorylation on binding to tau. Specifically, we used a pseudo-phosphorylation mutant, termed 3D, in which three key serine residues (S15, S78 and S82) are replaced with aspartate as a phospho-isostere[32]. We first confirmed that oligomers of Hsp27 3D are more heterogeneous and generally smaller than oligomers of WT Hsp27, as measured by negative-stain EM and SEC-MALS

(Figure 3.3B). In both the intensity-based HSQC (Figure 3C) and the chemical shift-based, TROSY-HSQC (Figure S3.5) platforms, we found that Hsp27 3D binds to K18's aggregation motifs (PHF6 and PHF6*), while WT does not. This result is consistent with the idea that Hsp27 3D, unlike WT Hsp27, is better able to use its free NTDs to bind the client. Also, we found that Hsp27 3D retains the ability to prevent tau aggregation by ThT assays (Figure 3.3D). Given the variability of this assay (Figure S3.6), we were not able to confidently determine whether WT or 3D Hsp27 were the superior chaperone for 0N4R. Together, these results suggest that reducing oligomer size, through pseudo-phosphorylation of the NTD, releases the internal, self-limiting PPIs and activates tau binding and anti-aggregation activity.

The β4/β8 groove is a regulatory site of sHSP oligomerization and function.

Together, these results suggest a model in which the NTD is a major domain for chaperone function, at least for tau, while the β4-β8 groove of the ACD is a hot spot for regulatory PPIs. To further explore the role of the β4-β8 groove as a sensor, we wondered what effect weakening the self IPV-ACD interactions might have. Based on the alanine scanning and recent work[33], we mutated the isoleucine and valine residues in the IPV to glycine (Hsp27 GPG). Hsp27 GPG has an altered oligomeric structure as compared to WT (Figure S3.7B) and, as expected, it has a lower apparent melting temperature, as measured by differential scanning fluorimetry (DSF) (Figure 3.4A).

To understand whether the Hsp27 GPG mutant created additional opportunities for tau binding in the β4/β8 grooves, we first measured its affinity for IPV peptides by ITC

(Figure S3.2B). We used IPV peptides as a surrogate for binding site availability because they have tighter affinity than tau, so are more accurate to measure. As expected, we found that WT Hsp27 does not bind IPV peptide (Figure 3.4B), likely due to the high occupancy of the β4-β8 grooves. However, Hsp27 GPG bound to IPV with an affinity of ~ 10 μM, similar to that of an isolated ACD. This result suggests that easing the internal competition can, indeed, expose β4-β8 grooves and promote binding to client. However, Hsp27 GPG had a reduced binding stoichiometry (n = 0.2), indicating that not all β4-β8 grooves are available. To further probe the role of oligomeric interactions on the availability of β4/β8 grooves, we deleted the NTD from Hsp27 WT (ΔNTD) and Hsp27 GPG (ΔNTD GPG). These proteins were intended to release the NTD contacts entirely and create smaller oligomers. Indeed, the ΔNTD GPG construct is a dimer, consistent with the loss of both the NTD and IPV contacts. However, ΔNTD results in a heterogeneous mixture of 3-5mers (Figure S3.5C), likely because of the residual IXI-ACD contacts. Despite these slight differences, both ΔNTD and ΔNTD GPG had similar affinities for IPV peptides (11.4 and 14.3 μM, respectively). Thus, smaller oligomers of Hsp27 seemed to have more exposed β4-β8 grooves. Finally, we wondered whether Hsp27 3D would contain free β4/β8 grooves because of its smaller oligomeric size. However, Hsp27 3D bound poorly to IPV peptide (Kd > 50 μM), suggesting that there is still sufficient β4/β8 groove occupancy in this oligomer. Thus, the number of available β4-β8 grooves seems to be a product of both internal competition for IXI motifs, as well as less well understood contributions from relative oligomer size.

After using the IPV peptides as a surrogate for available tau binding sites, we confirmed that Hsp27 GPG could interact with K18 tau by NMR. We found that Hsp27 GPG bound to K18 by both the intensity- and chemical shift-based NMR (Figure 3.4C and S3.3), further highlighting the importance of competition between client and self in Hsp27.

Dynamic PPIs are important for anti-aggregation activity. These studies suggested that a series of competitive PPIs, driven by self- and client-interactions, as well as changes in phosphorylation and oligomerization, might coordinate Hsp27 function. This concept is in agreement with results from cryo-EM, mass spectrometry and SAXS studies of related systems, suggesting the importance of dynamics in sHSP oligomers[40–43] and sHSP-client interactions[23,29]. While it is difficult to accurately measure changes in Hsp27-tau dynamics during a chaperone cycle, we decided to cross-link Hsp27 and ask what effect this chemical modification would have on its ability to suppress tau aggregation. Specifically, we treated WT Hsp27 with gluteraldehyde and selected a concentration of crosslinker that would produce samples with a similar oligomeric size to the untreated protein by SEC-MALS (Figure 3.5A, S3.7D). Consistent with a role for dynamics, we found that the crosslinked sample (Hsp27 X) was severely compromised in suppressing aggregation of 0N4R or K18 tau (Figure 3.5B). Although further work is needed, this finding is supportive of the idea that shifting PPIs regulate sHSP function.

Discussion:

PPI-based model for sHSP chaperone function. Previous work had shown that the

ACD alone is sufficient to bind some clients but not others[12,20,44], suggesting that sHSPs may use different binding sites depending on the type of client. Here, we focused on mapping the interactions of Hsp27 with its native client, tau, which is important in AD and other neurodegenerative tauopathies[34]. We found that both the NTD and ACD of Hsp27 bind to the PHF6 and PHF6* aggregation motifs of tau, but that the accessibility of Hsp27's binding surfaces are limited by self-interactions within the oligomer. Importantly, each of these individual PPIs was relatively weak, with dissociation constants in the low to high micromolar.

Based on these results and the pioneering work of others[19,20,24,28,45], we propose a general model for Hsp27 function (Figure 3.6): in its "resting state" Hsp27's β4/β8 groove is occupied by its own IPV/IXI motifs and it is further auto-inhibited by additional oligomeric interactions with the NTD. We speculate that these self-limiting PPIs are important to preclude promiscuous client binding that might be detrimental to folding under normal, healthy conditions. However, under conditions of stress, the presence of higher affinity co-chaperones (i.e., BAG3)[37] and/or a large excess of clients is proposed to compete for these PPIs. In the case of tau, early stages of aggregation might generate locally high concentrations of putative Hsp27-binding sites, enhancing avidity. This change in state is likely further amplified by stress-responsive phosphorylation of the NTD which further de-oligomerizes the complex and reveals open β4-β8 grooves (see Figure 3.6). The result of these shifting PPI priorities is that client binding in now favored, along with partial Hsp27 oligomer disassembly and exposure of NTDs for chaperone activity. Moreover, this competing set of interactions might serve to facilitate

Hsp27 release from clients after cellular proteostasis is restored. In other words, as the levels of stress-responsive phosphorylation diminish and client levels drop, the internal IXI-ACD contacts might help restore Hsp27 to its "storage state". This step might be particularly important for sHSPs, because they lack the ATPase activity that other chaperones, such as Hsp70, use to promote cycles of reversible client release. In this way, the sHSPs might have more in common with non-enzymatic chaperones such as trigger factor [46] and Spy[47], which use dynamic, competitive PPIs to generate reversibility.

Putative "druggable" sites on sHSPs. There is great interest in either activating Hsp27 for the treatment of tauopathies[32] or inhibiting Hsp27 for the potential treatment of cancer[48] or cystic fibrosis[49]. Thus, it seems worth evaluating the implications of this model for translational research. This is especially true because Hsp27's lack of enzymatic activity implies that its PPIs may be the best sites for chemical perturbation[50]. Our findings here suggest that both the NTD and ACD contain potential sites for drug discovery.

We found that the β4/β8 groove of Hsp27 is an unexpected nexus for PPIs; a number of partners, including itself, clients and co-chaperones (*e.g.* BAG3) bind the same region. While the number and diversity of binding partners for this site highlight its functional importance, this scenario also creates a challenge for targeting the β4-β8 groove with small molecules. For example, compounds that bind this region might be counter-productive in some neurodegenerative disease settings because they would compete

for the client themselves. At the same time, such compounds might partially release the self-limiting IXI-ACD contacts and, potentially, reveal the NTDs. Thus, we anticipate that molecules targeting the β4-β8 groove could be either activators or inhibitors of Hsp27 activity, depending on occupancy of the site and concentration/identity of binding partners.

Alternatively, the NTD could be a potential site for chemical intervention. This region seemed to be essential in chaperone function, as least for tau, while also playing a role in Hsp27 oligomerization. However, due to the lack of structural knowledge about this disordered region, it will likely be difficult to find a molecule that selectively interacts with it. Rather, manipulation of the NTD might be best achieved through controlling the stress pathways that tune post-translational modifications. In that scenario, selectivity will likely become a major hurdle.

Due to the conceptual difficulty in targeting either the NTD or β4-β8 groove directly, we propose that targeting the dynamics of Hsp27 may be a more fruitful approach. For example, stabilizing specific PPIs might “trap” the chaperone in a specific state, favoring either client retention or release. In neurodegeneration or cancer, one might want to trap distinct states. For example, our work suggests that trapping the tau-bound Hsp27 complex might be a good way to limit tau aggregation. Thus, more broadly understanding how natural clients, in addition to tau, bind to Hsp27 and other sHSPs will likely be an important next step.

Methods:

Cloning and recombinant protein purification. Vectors for the expression of full-length human Hsp27 and Hsp27 ACD (residues Q80-S176) were a gift from the Klevit laboratory (University of Washington), and proteins were expressed and purified as described[51]. Hsp27 ACD L157A was generated using standard site-directed mutagenesis protocols. The vector for expression of Hsp27 3D was a gift from the Dickey laboratory (University of South Florida) and the protein was expressed and purified as described[32]. The Hsp27 NTD truncation, encompassing residues 1-88, was subcloned into a CMX3 vector using XhoI and Nde1 restriction enzymes. For all other Hsp27 constructs (GPG, ΔNTD consisting of residues 80-205), coding sequences were optimized for *Escherichia coli*, purchased from Integrated DNA Technologies, and LIC cloned into a PMCSG7 vector. All constructs were transformed in *E. coli* BL21 (DE3) cells, grown to an OD_{600} of 0.6 in Terrific Broth (TB), and induced with 0.5 mM IPTG overnight at 18 °C. Cells were pelleted and re-suspended in 50 mM Tris-HCl pH 8.0, 10 mM imidazole, 500 mM NaCl and lysed by sonication. The cleared lysate was applied Ni-NTA resin (Qiagen) and eluted with buffer containing 300 mM imidazole. Proteins were concentrated and further purified by size exclusion on a Superdex 200 16/600 column (GE Healthcare) equilibrated with SEC Buffer (50 mM sodium phosphate pH 7.5, 100 mM NaCl). Tau constructs, human 0N4R and unlabeled and ^{15}N-labeled K18 were purified as described previously[35]. All peptides were purchased from Genescript.

NMR spectroscopy. For Hsp27 ACD HSQC NMR experiments, all proteins were dialyzed into SEC Buffer (50 mM sodium phosphate, 100 mM NaCl, pH 7.4). Then,

samples containing 150 μM ACD and either 0N4R or K18 tau were prepared. Two-dimensional (2D) ^{1}H-^{15}N hetero-nuclear single quantum coherence (HSQC) spectra were required at 32 °C on a Bruker Avance III 500 MHz spectrometer equipped with a triple resonance, z-axis gradient probe. 256 scans were acquired per t1 value for a total of 200 t1s. Spectral widths of 6009 Hz and 1419 Hz were used in the ^{1}H and ^{15}N dimensions, respectively. Spectra were processed with NMRPipe and analyzed in Sparky. Chemical shift perturbations were calculated using the following equation,

$$CSP= \sqrt{((\Delta H)^2 + (\Delta N/5)^2)}$$

For ^{15}N K18 HSQC NMR experiments, all proteins were dialyzed overnight into NMR buffer (25 mM HEPES pH 7.4, 10 mM KCl, 5 mM $MgCl_2$, 1 mM TCEP, 10% (v/v) D_2O). Then, samples containing 50 μM ^{15}N-labeled tau and 50 or 100 μM unlabeled chaperone in NMR buffer were prepared. 2D HSQC spectra were acquired at 10 °C on a Bruker Avance AV800 spectrometer equipped with a cryoprobe. 16 scans were acquired per t1 value and spectral widths of 2100 Hz and 10416 Hz were used in the ^{1}H and ^{15}N dimensions, respectively. Spectra were processed using rNMR and Sparky based on deposited tau assignments (Barre 2013, BioMagResBank accession number 19253). Signal intensity ratios were calculated using Prism, by dividing the intensity of chaperone-bound peaks by intensity of the same peak in the unbound spectra.

The ^{15}N TROSY HSQC experiments were performed on a Bruker Avance 800 MHz spectrometer equipped with the TXO cryogenic probe at 283K. The [U-^{15}N] K18 proteins were dissolved at a concentration of 0.05 to 0.15 mM in 25 mM Hepes, 10 mM KCl, 5 mM $MgCl_2$, 1mM TCEP at pH 7.0 and titrated with the Hsp27 proteins in the same buffer. The K18:Hsp27 molar ratios in the samples are indicated in the figure

legends. The ^{1}H-^{15}N TROSY HSQC experiments were performed with 2048 direct (^{1}H) and 512 indirect (^{15}N) points with the spectral width of 16 ppm and 36 ppm, respectively. All NMR spectra were processed by Topspin 3.1, and analyzed with Sparky (Goddard and Kneller, SPARKY 3-NMR Assignment and Integration Software. University of California, San Francisco, CA).

Tau aggregation assay. Aggregation assays were performed as previously described[35]. Briefly, all proteins were dialyzed overnight at 4 °C into assay buffer (Dulbecco's PBS pH7.4, 2 mM $MgCl_2$, 1 mM DTT). 0N4R or K18 Tau (10 μM) was pre-incubated in the presence/absence of chaperones (5 μM to 20 μM) for 30 min at 37 °C. Thioflavin T (Sigma) at a final concentration of 10 μM was added and aggregation was induced by the addition of a freshly prepared heparin sodium salt solution (Santa Cruz) at a final concentration of 44 μg/mL. For non-induced controls, assay buffer was added in place of heparin solution. The aggregation reaction was carried out at 37 °C with continuous shaking and monitored via Thioflavin T fluorescence (excitation=444 nm, emission=485 nm, cutoff=480 nm) in a Spectramax M5 microplate reader (Molecular Devices). Readings were taken every 5 min for a minimum of 24 h. Baseline curves of non-induced controls (3 replicates) were subtracted from induced samples (3 replicates).

Electron Microscopy. Samples of Hsp27 (1 μM, in SEC Buffer) were negatively stained with uranyl formate (pH ~6.0) on thin-carbon layered 400-mesh copper grids (Ted Pella) that were glow discharged before sample was applied. Samples were imaged using a Tecnai T12 Spirit TEM (FEI) operated at 120 keV. Micrograph images

were acquired with ~1.5-µm defocus on a 4k x 4k CCD camera (Gatan) at a magnification of 67,000x with a pixel size of 1.73Å.

SEC-MALS. Solutions of Hsp27 were resolved by analytical SEC on a Shodex 804 column on an Ettan LC (GE Healthcare). Molecular weights were determined by multi-angle laser light scattering using an in-line DAWN HELEOS detector and an Optilab rEX differential refractive index detector (Wyatt Technology Corporation). The column was equilibrated overnight in SEC Buffer. Samples were analyzed at the indicated concentrations. Calculation of molecular weights was performed using the ASTRA software package (Wyatt Technology Corporation).

Isothermal Titration Calorimetry. For experiments with BAG3, proteins were dialyzed overnight against ITC buffer (25 mM Hepes, 5 mM $MgCl_2$, 100 mM KCl, pH 7.5). For experiments with peptides, sHSPs were dialyzed overnight against SEC Buffer, and peptides were dissolved in dialysis buffer. Concentrations were determined using BCA assays (Thermo Scientific), and the ITC experiment was performed with a MicroCal ITC200 (GE Healthcare) at 25 °C. In BAG3 experiments, sHSP (200 µM) in the syringe was titrated into a 10 µM cell solution of BAG3 protein. For peptide binding experiments, peptide (1 mM) was titrated into a cell containing Hsp27 proteins (100 µM). Calorimetric parameters were calculated using Origin® 7.0 software and fit with a one-site binding model.

Thermal shift assay. Samples of Hsp27 (25 µL; 0.3 mg/mL) in DSF buffer (50mM

NaPi pH 7.4, 700mM NaCl, 50mM LiCl) with a 5x final concentration of SYPRO Orange (Sigma) were placed into a white 96-well plate with optically clear caps. Melt curves were acquired on a Stratagene Mx300P RT-PCR using the SYPRO filter set. Samples were heated from 25 °C to 95 °C in 1 °C increments for 2 minutes, cooled to 25 °C at each cycle, and fluorescence was measured. The melting temperature was determined using a Boltzmann fit in Prism.

Crosslinking of Hsp27. Samples of Hsp27 in SEC Buffer (20uM) were cross-linked in the presence of 0.04% gluteraldehyde for 20 minutes, followed by quenching with 2M Tris pH7.4. Samples were dialyzed into SEC buffer post crosslinking.

Acknowledgements: We thank Rachel Klevit and Chad Dickey for plasmids and Matthew Ravalin for biotinylated peptides. This work was supported by NIH grant NS059690 and grants from Brightfocus Foundation and the Tau Consortium.

References:

1. Powers, E. T. & Balch, W. E. Diversity in the origins of proteostasis networks — a driver for protein function in evolution. *Nat. Rev. Mol. Cell Biol.* **14,** 237–248 (2013).

2. Jakob, U., Gaestel, M., Engel, K. & Buchner, J. Small heat shock proteins are molecular chaperones. *J. Biol. Chem.* **268,** 1517–20 (1993).

3. Ehrnsperger, M., Gräber, S., Gaestel, M. & Buchner, J. Binding of non-native protein to Hsp25 during heat shock creates a reservoir of folding intermediates for reactivation. *EMBO J.* **16,** 221–229 (1997).

4. Haslbeck, M. & Vierling, E. A first line of stress defense: small heat shock proteins and their function in protein homeostasis. *J. Mol. Biol.* **427,** 1537–48 (2015).

5. Ungelenk, S. *et al.* Small heat shock proteins sequester misfolding proteins in near-native conformation for cellular protection and efficient refolding. *Nat. Commun.* **7,** 13673 (2016).

6. Duennwald, M. L., Echeverria, A. & Shorter, J. Small Heat Shock Proteins Potentiate Amyloid Dissolution by Protein Disaggregases from Yeast and Humans. *PLoS Biol.* **10,** e1001346 (2012).

7. Mymrikov, E. V., Daake, M., Richter, B., Haslbeck, M. & Buchner, J. The Chaperone Activity and Substrate Spectrum of Human Small Heat Shock Proteins. *J. Biol. Chem.* **292,** 672–684 (2017).

8. Shimura, H., Miura-Shimura, Y. & Kosik, K. S. Binding of Tau to Heat Shock Protein 27 Leads to Decreased Concentration of Hyperphosphorylated Tau and Enhanced Cell Survival. *J. Biol. Chem.* **279,** 17957–17962 (2004).

9. Wyttenbach, A. *et al.* Heat shock protein 27 prevents cellular polyglutamine

toxicity and suppresses the increase of reactive oxygen species caused by huntingtin. *Hum. Mol. Genet.* **11,** 1137–51 (2002).

10. Perrin, V. *et al.* Neuroprotection by Hsp104 and Hsp27 in lentiviral-based rat models of Huntington's disease. *Mol. Ther.* **15,** 903–11 (2007).

11. Rajagopal, P., Liu, Y., Shi, L., Clouser, A. F. & Klevit, R. E. Structure of the α-crystallin domain from the redox-sensitive chaperone, HSPB1. *J. Biomol. NMR* **63,** 223–228 (2015).

12. Hochberg, G. K. A. *et al.* The structured core domain of B-crystallin can prevent amyloid fibrillation and associated toxicity. *Proc. Natl. Acad. Sci.* **111,** E1562–E1570 (2014).

13. Pasta, S. Y., Raman, B., Ramakrishna, T. & Rao, C. M. The IXI/V motif in the C-terminal extension of alpha-crystallins: alternative interactions and oligomeric assemblies. *Mol. Vis.* **10,** 655–62 (2004).

14. Delbecq, S. P., Jehle, S. & Klevit, R. Binding determinants of the small heat shock protein, αB-crystallin: recognition of the 'IxI' motif. *EMBO J.* **31,** 4587–4594 (2012).

15. Jehle, S. *et al.* Solid-state NMR and SAXS studies provide a structural basis for the activation of αB-crystallin oligomers. *Nat. Struct. Mol. Biol.* **17,** 1037–1042 (2010).

16. Delbecq, S. P., Rosenbaum, J. C. & Klevit, R. E. A Mechanism of Subunit Recruitment in Human Small Heat Shock Protein Oligomers. *Biochemistry* **54,** 4276–4284 (2015).

17. Bova, M. P., McHaourab, H. S., Han, Y. & Fung, B. K. Subunit exchange of small heat shock proteins. Analysis of oligomer formation of alphaA-crystallin and Hsp27 by

fluorescence resonance energy transfer and site-directed truncations. *J. Biol. Chem.* **275,** 1035–42 (2000).

18. Haslbeck, M. *et al.* A Domain in the N-terminal Part of Hsp26 is Essential for Chaperone Function and Oligomerization. *J. Mol. Biol.* **343,** 445–455 (2004).

19. Jovcevski, B. *et al.* Phosphomimics Destabilize Hsp27 Oligomeric Assemblies and Enhance Chaperone Activity. *Chem. Biol.* **22,** 186–195 (2015).

20. Mainz, A. *et al.* The chaperone αB-crystallin uses different interfaces to capture an amorphous and an amyloid client. *Nat. Struct. Mol. Biol.* **22,** 898 (2015).

21. Friedrich, K. L., Giese, K. C., Buan, N. R. & Vierling, E. Interactions between small heat shock protein subunits and substrate in small heat shock protein-substrate complexes. *J. Biol. Chem.* **279,** 1080–9 (2004).

22. Jaya, N., Garcia, V. & Vierling, E. Substrate binding site flexibility of the small heat shock protein molecular chaperones. *Proc. Natl. Acad. Sci.* **106,** 15604–15609 (2009).

23. Stengel, F. *et al.* Quaternary dynamics and plasticity underlie small heat shock protein chaperone function. *Proc. Natl. Acad. Sci. U. S. A.* **107,** 2007–12 (2010).

24. Peschek, J. *et al.* Regulated structural transitions unleash the chaperone activity of αB-crystallin. *Proc. Natl. Acad. Sci. U. S. A.* **110,** E3780-9 (2013).

25. Basha, E., Friedrich, K. L. & Vierling, E. The N-terminal Arm of Small Heat Shock Proteins Is Important for Both Chaperone Activity and Substrate Specificity. *J. Biol. Chem.* **281,** 39943–39952 (2006).

26. Arbach, H., Butler, C. & McMenimen, K. A. Chaperone activity of human small heat shock protein-GST fusion proteins. *Cell Stress Chaperones* **22,** 503–515 (2017).

27. McDonald, E. T., Bortolus, M., Koteiche, H. A. & Mchaourab, H. S. Sequence, structure, and dynamic determinants of Hsp27 (HspB1) equilibrium dissociation are encoded by the N-terminal domain. *Biochemistry* **51,** 1257–68 (2012).

28. Jaya, N., Garcia, V. & Vierling, E. Substrate binding site flexibility of the small heat shock protein molecular chaperones. *Proc. Natl. Acad. Sci.* **106,** 15604–15609 (2009).

29. Cheng, G., Basha, E., Wysocki, V. H. & Vierling, E. Insights into small heat shock protein and substrate structure during chaperone action derived from hydrogen/deuterium exchange and mass spectrometry. *J. Biol. Chem.* **283,** 26634–42 (2008).

30. Fu, X., Shi, X., Yan, L., Zhang, H. & Chang, Z. In vivo substrate diversity and preference of small heat shock protein IbpB as revealed by using a genetically incorporated photo-cross-linker. *J. Biol. Chem.* **288,** 31646–54 (2013).

31. Cox, D., Selig, E., Griffin, M. D. W., Carver, J. A. & Ecroyd, H. Small Heat-shock Proteins Prevent α-Synuclein Aggregation via Transient Interactions and Their Efficacy Is Affected by the Rate of Aggregation. *J. Biol. Chem.* **291,** 22618–22629 (2016).

32. Abisambra, J. F. *et al.* Phosphorylation dynamics regulate Hsp27-mediated rescue of neuronal plasticity deficits in tau transgenic mice. *J Neurosci* **30,** 15374–15382 (2010).

33. Baughman, H. E. R., Clouser, A. F., Klevit, R. E. & Nath, A. HspB1 and Hsc70 chaperones engage distinct tau species and have different inhibitory effects on amyloid formation. *J. Biol. Chem.* **293,** 2687–2700 (2018).

34. Holtzman, D. M. *et al.* Tau: From research to clinical development. *Alzheimer's*

Dement. **12,** 1033–1039 (2016).

35. Mok, S.-A. *et al.* Mapping interactions with the chaperone network reveals factors that protect against tau aggregation. *Nat. Struct. Mol. Biol.* **25,** 384–393 (2018).

36. Jinwal, U. K. *et al.* Imbalance of Hsp70 family variants fosters tau accumulation. *FASEB J.* **27,** 1450–1459 (2013).

37. Rauch, J. N. *et al.* BAG3 Is a Modular, Scaffolding Protein that physically Links Heat Shock Protein 70 (Hsp70) to the Small Heat Shock Proteins. *J. Mol. Biol.* **429,** (2017).

38. von Bergen, M. *et al.* Assembly of tau protein into Alzheimer paired helical filaments depends on a local sequence motif ((306)VQIVYK(311)) forming beta structure. *Proc. Natl. Acad. Sci. U. S. A.* **97,** 5129–34 (2000).

39. Takeuchi, K., Arthanari, H., Shimada, I. & Wagner, G. Nitrogen detected TROSY at high field yields high resolution and sensitivity for protein NMR. *J. Biomol. NMR* **63,** 323–331 (2015).

40. Franzmann, T. M., Menhorn, P., Walter, S. & Buchner, J. Activation of the Chaperone Hsp26 Is Controlled by the Rearrangement of Its Thermosensor Domain. *Mol. Cell* **29,** 207–216 (2008).

41. White, H. E. *et al.* Multiple Distinct Assemblies Reveal Conformational Flexibility in the Small Heat Shock Protein Hsp26. *Structure* **14,** 1197–1204 (2006).

42. Baldwin, A. J. *et al.* Quaternary dynamics of αB-crystallin as a direct consequence of localised tertiary fluctuations in the C-terminus. *J. Mol. Biol.* **413,** 310–20 (2011).

43. Palmieri, V., Maulucci, G., Maiorana, A., Papi, M. & De Spirito, M. α-crystallin

modulates its chaperone activity by varying the exposed surface. *Chembiochem* **14,** 2362–70 (2013).

44. Kulig, M. & Ecroyd, H. The small heat-shock protein αB-crystallin uses different mechanisms of chaperone action to prevent the amorphous versus fibrillar aggregation of α-lactalbumin. *Biochem. J.* **448,** 343–352 (2012).

45. Jehle, S. *et al.* N-terminal domain of alphaB-crystallin provides a conformational switch for multimerization and structural heterogeneity. *Proc. Natl. Acad. Sci. U. S. A.* **108,** 6409–14 (2011).

46. Martinez-Hackert, E. & Hendrickson, W. A. Promiscuous Substrate Recognition in Folding and Assembly Activities of the Trigger Factor Chaperone. *Cell* **138,** 923–934 (2009).

47. Horowitz, S. *et al.* Visualizing chaperone-assisted protein folding. *Nat. Struct. Mol. Biol.* **23,** 691–7 (2016).

48. Jego, G., Hazoumé, A., Seigneuric, R. & Garrido, C. Targeting heat shock proteins in cancer. *Cancer Lett.* **332,** 275–285 (2013).

49. Ahner, A. *et al.* Small heat shock proteins target mutant cystic fibrosis transmembrane conductance regulator for degradation via a small ubiquitin-like modifier–dependent pathway. *Mol. Biol. Cell* **24,** 74–84 (2013).

50. Freilich, R., Arhar, T., Abrams, J. L. & Gestwicki, J. E. Protein-Protein Interactions in the Molecular Chaperone Network. *Acc. Chem. Res.* **51,** (2018).

51. Clouser, A. F. & Klevit, R. E. pH-dependent structural modulation is conserved in the human small heat shock protein HSBP1. *Cell Stress Chaperones* **22,** 569–575 (2017).

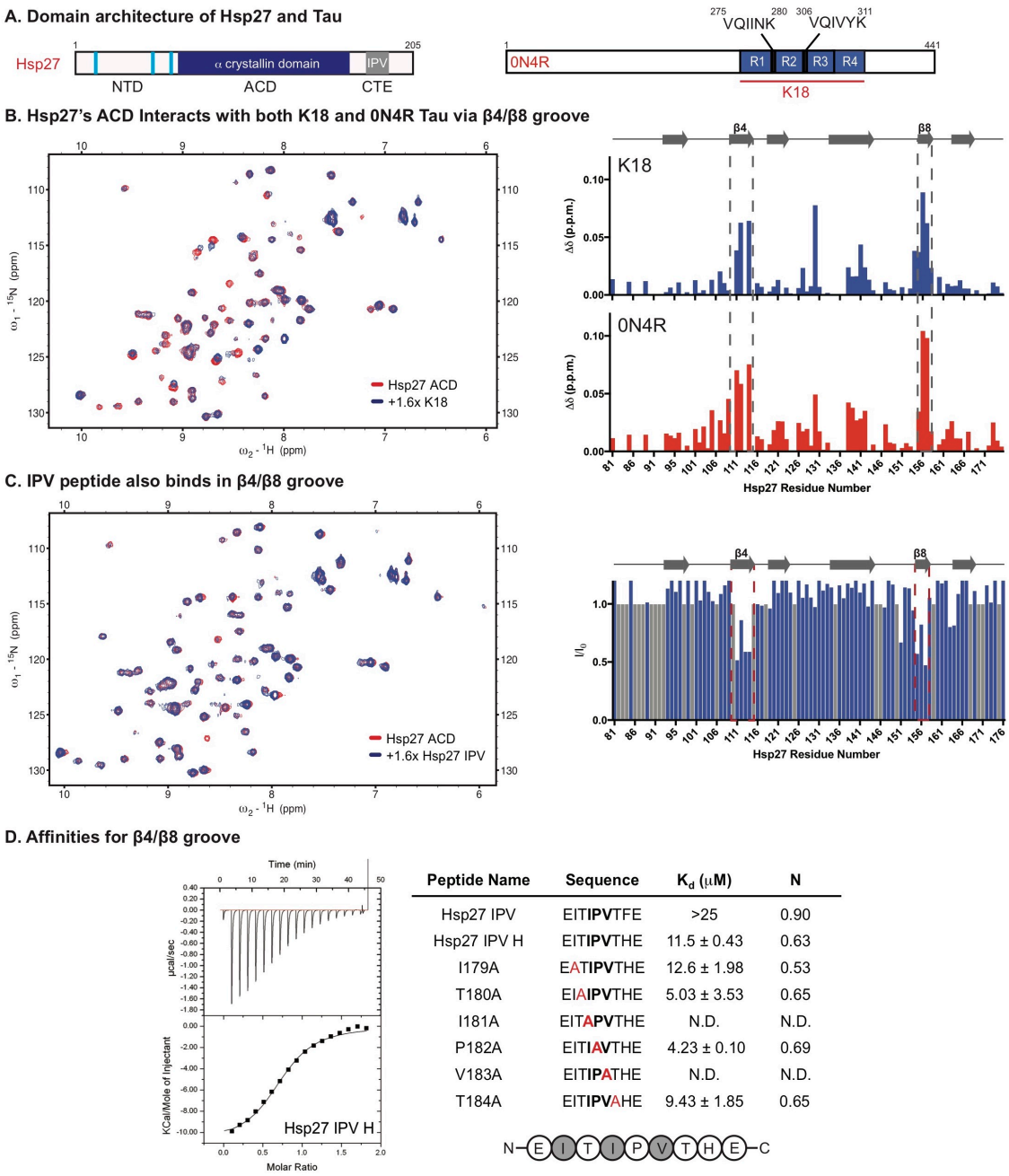

Peptide Name	Sequence	K_d (μM)	N
Hsp27 IPV	EIT**IPV**TFE	>25	0.90
Hsp27 IPV H	EIT**IPV**THE	11.5 ± 0.43	0.63
I179A	EA**TIPV**THE	12.6 ± 1.98	0.53
T180A	EI**AIPV**THE	5.03 ± 3.53	0.65
I181A	EIT**APV**THE	N.D.	N.D.
P182A	EITI**AV**THE	4.23 ± 0.10	0.69
V183A	EIT**IPA**THE	N.D.	N.D.
T184A	EIT**IPV**AHE	9.43 ± 1.85	0.65

Figure 3.1. Hsp27's β4/β8 groove is a PPI hotspot for both client- and self-interactions. (A) Domain architecture of Hsp27 and Tau isoforms. (B) Left, HSQC spectra of ^{15}N Hsp27 ACD alone (150 μM, red) or in the presence of 250 μM K18 (blue). Right, chemical shift perturbations in ACD upon binding of 250 μM K18 (top) or 0N4R (bottom). (C) Left, intensity ratios upon binding of Hsp27 IPV peptide, with unassigned residues shown in gray. Right, HSQC spectra of ^{15}N Hsp27 ACD alone (150 μM, red) or in the presence of 250 μM Hsp27 IPV peptide (blue). (D) Isothermal calorimetry of Hsp27 ACD with IPV-derived peptides. Left, representative ITC curve for Hsp27 IPV H peptide. Right, table of affinity values. ND, no detectable binding. Values are

represented as mean ± standard error of the mean (SEM) determined from a minimum of three independent experiments.

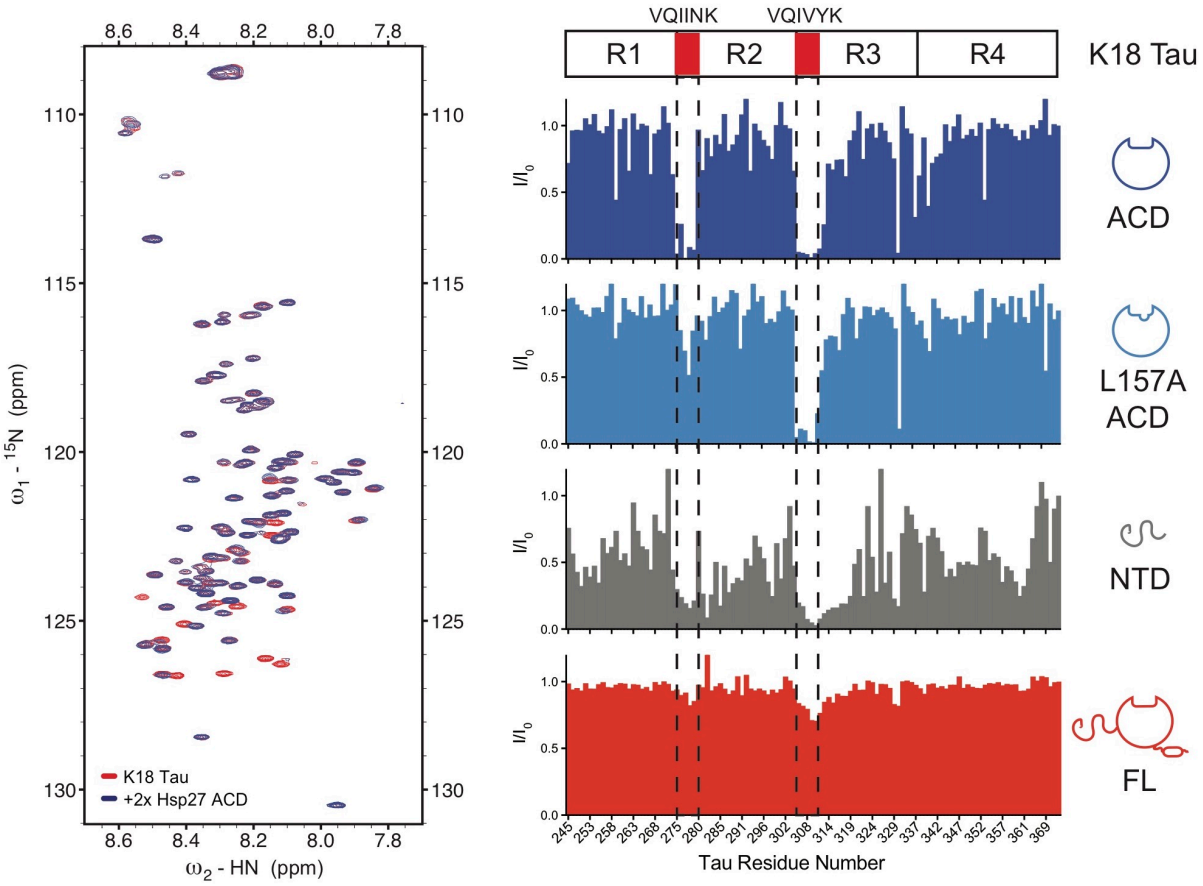

Figure 3.2. Binding of Hsp27 and its individual domains to K18. Left, HSQC spectra of ^{15}N K18 alone (50 μM, red) or in the presence of 100 μM ACD (blue). Right, intensity ratios upon binding of listed Hsp27 constructs at a 2:1 molar ratio.

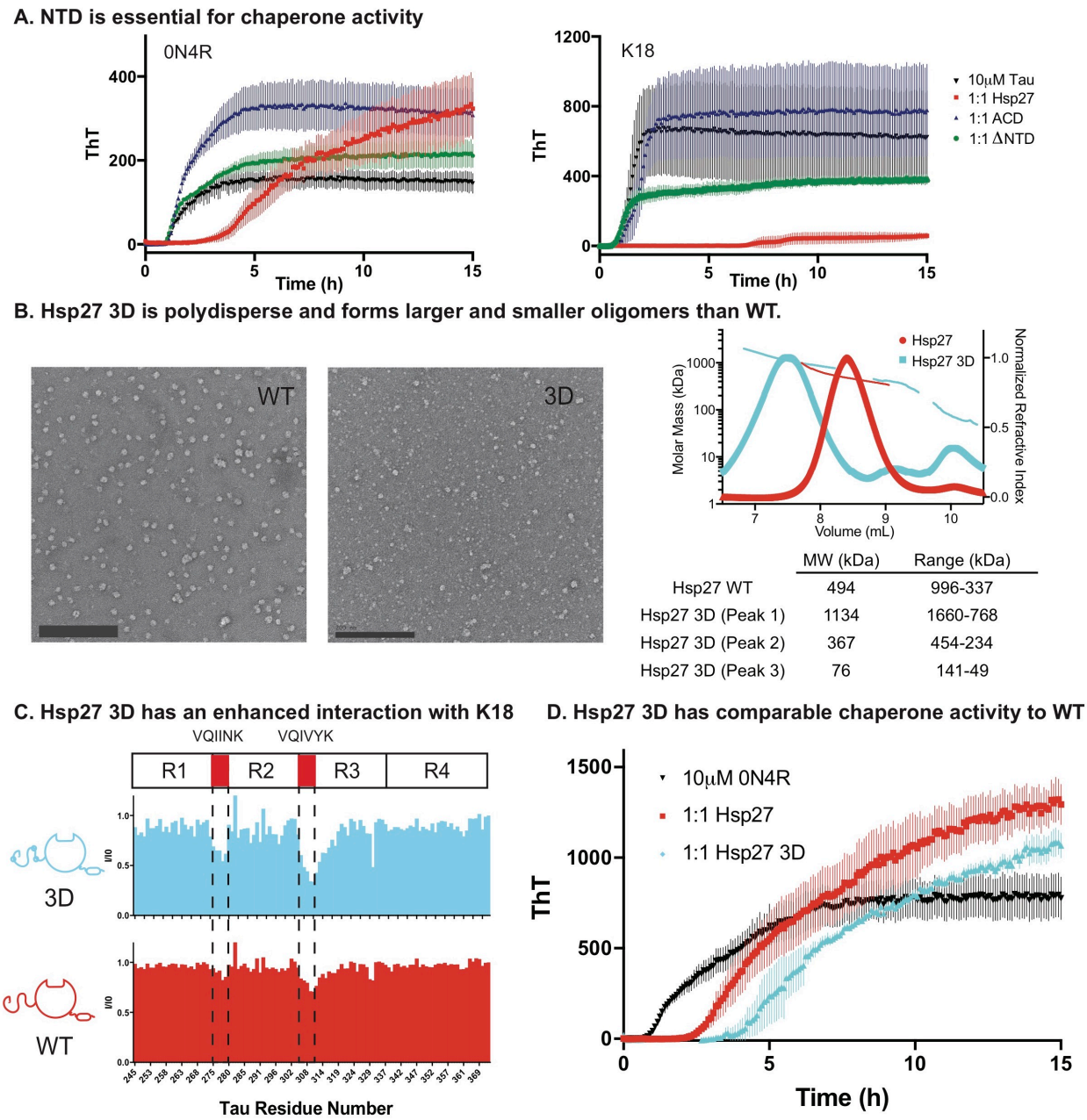

Figure 3.3. Hsp27's NTD plays an important role in chaperoning Tau. (A) Representative tau aggregation curves in the presence of truncated Hsp27 constructs. Aggregation of 0N4R (left) or K18 (right) in the presence of listed chaperones at a 1:1 molar ratio (10μM). Data points are the mean ± SEM of 3 technical replicates. RFU, relative fluorescence units. (B) Left, Negative stain EM images of WT (left) and 3D (right) Hsp27. Images are representative of a minimum of 12 random fields. Scale bar is 200 nm. Right, SEC-MALS trace of Hsp27 WT and 3D (40 μM). (C) Intensity ratios of 50 μM ^{15}N K18 in the presence of of 100 μM Hsp27 WT or 3D (2:1 molar ratio). (D) Representative 0N4R aggregation curves in the presence of Hsp27 WT or 3D at a 1:1 molar ratio (10 μM).

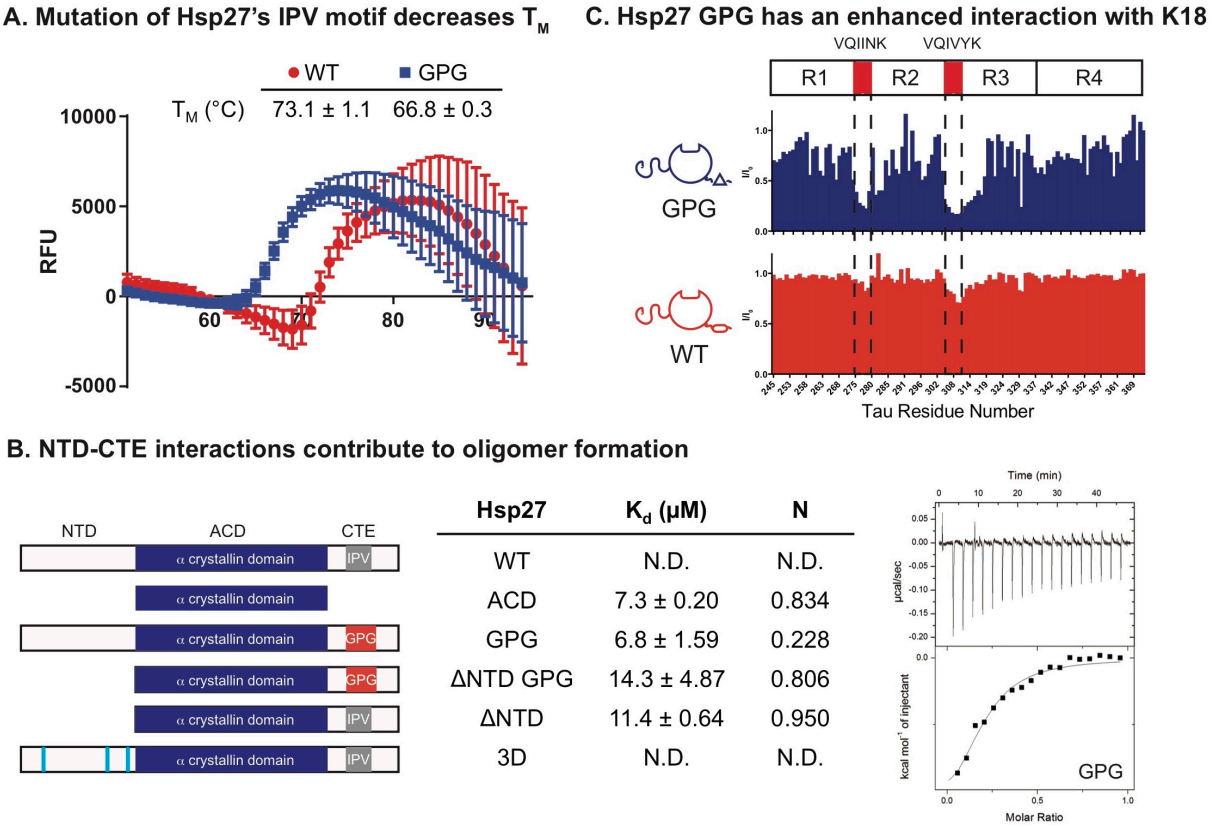

Figure 3.4. The β4/β8 groove is a regulatory site of sHSP oligomerization and function. (A) Differential scanning fluorimetry melting curves of Hsp27 WT and GPG. Data points are the mean ± SEM of three technical replicates. Listed melting temperatures are the mean ± SD of three independent experiments. (B) ITC binding experiments of optimized IPV peptide with listed constructs of Hsp27. Left, cartoon representation of Hsp27 constructs used in this experiment. Middle, table of affinity and stoichiometry values obtained from ITC experiments. Values in table are mean ± SEM determined from a minimum of three independent experiments. Right, representative ITC curve of peptide binding to Hsp27 GPG. (C) Intensity ratios of ^{15}N K18 in the presence of 100 μM Hsp27 WT or GPG (2:1 molar ratio).

A. Hsp27 and Hsp27 X form comparable oligomers.

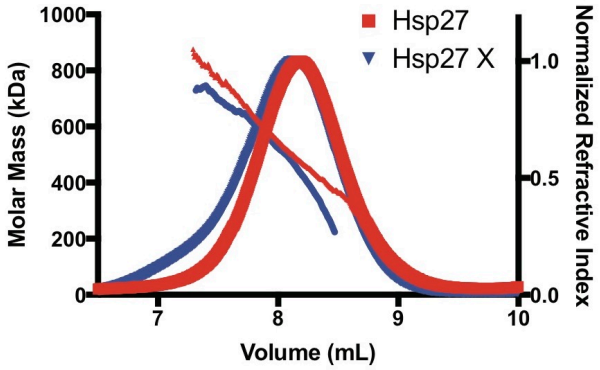

	MW (kDa)	Range (kDa)
Hsp27	535	876-294
Hsp27 X	528	729-224

B. Hsp27 X is deficient at chaperoning Tau.

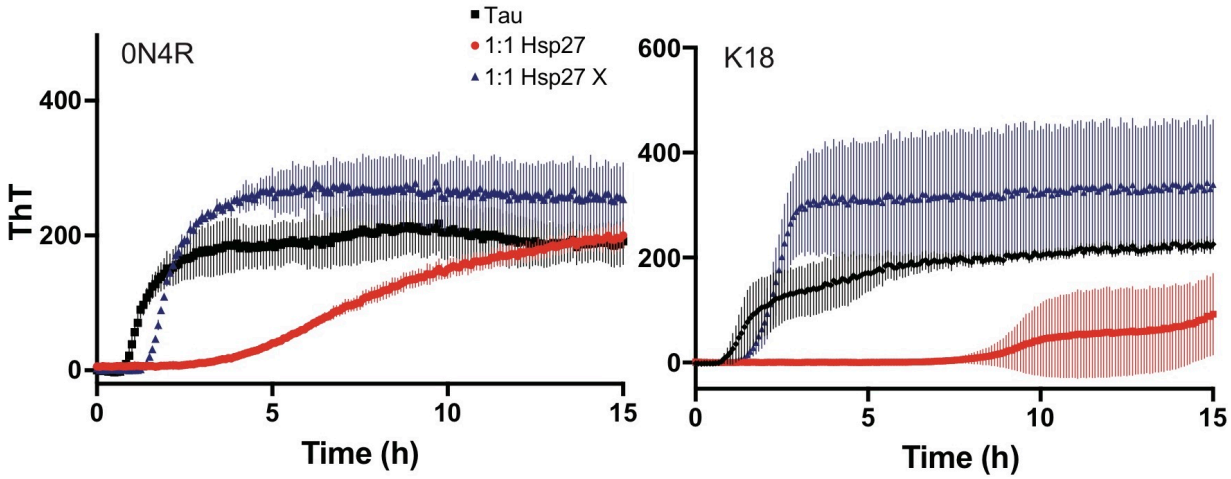

Figure 3.5. Dynamics of Hsp27 are critical to limit tau aggregation. (A) SEC-MALS trace of Hsp27 and Hsp27X (40 μM). (B) Representative aggregation curves of 0N4R (left) or K18 (right) Tau in the presence of 1:1 molar ratio of Hsp27 and Hsp27X (10 μM).

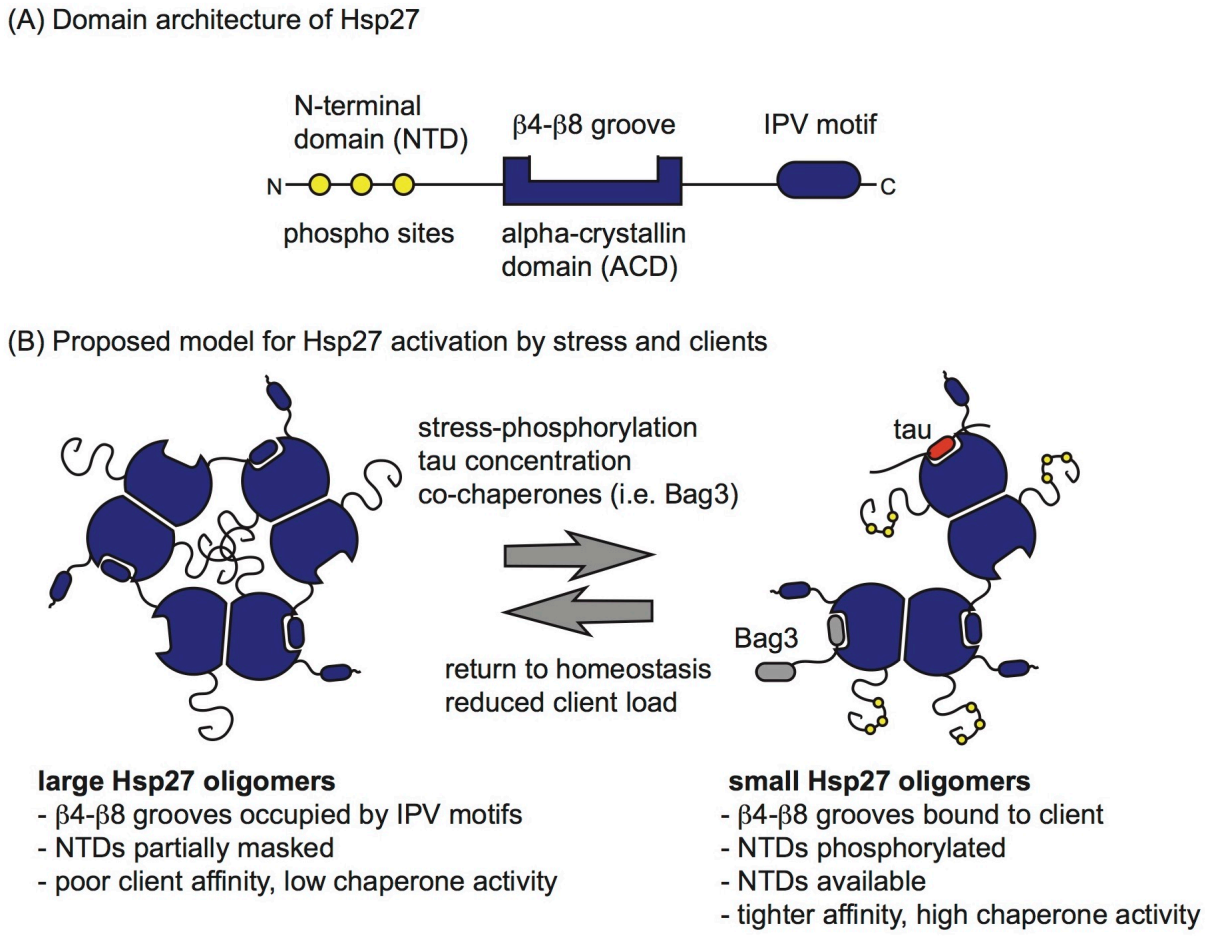

Figure 3.6. Schematic model for the activation of Hsp27. (A) Major domains of Hsp27, highlighting the sites of protein-protein interactions (PPIs). (B) Schematic summary of the model. Large Hsp27 oligomers are held together by multiple PPIs: (i) ACD-ACD interactions (ii) self-limiting IPV contacts between dimers and (ii) NTD interactions. Under conditions of stress, phosphorylation of the NTD, combined with competitive interactions for the b4-b8 grooves, drives oligomer disassembly and reveals the active NTDs. The contact with tau takes place within the aggregation-prone regions of the microtubule-binding repeats (red), while Bag3 uses its own IPV motifs (gray). When conditions improve, the restored self-IPV contacts would re-set the system and release the client (i.e. tau).

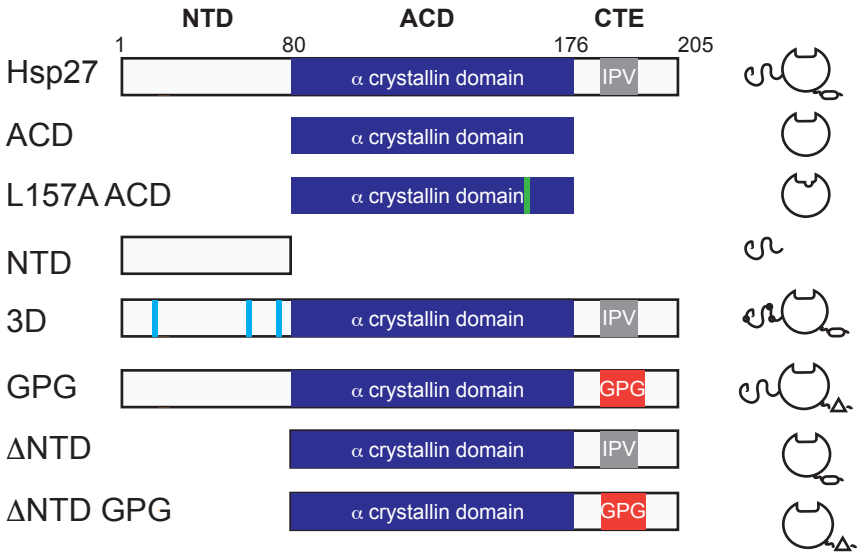

Figure S3.1. Schematic of all Hsp27 constructs used in this work.

A. Representative ITC curves from Figure 1D, alanine scan of IPV peptides.

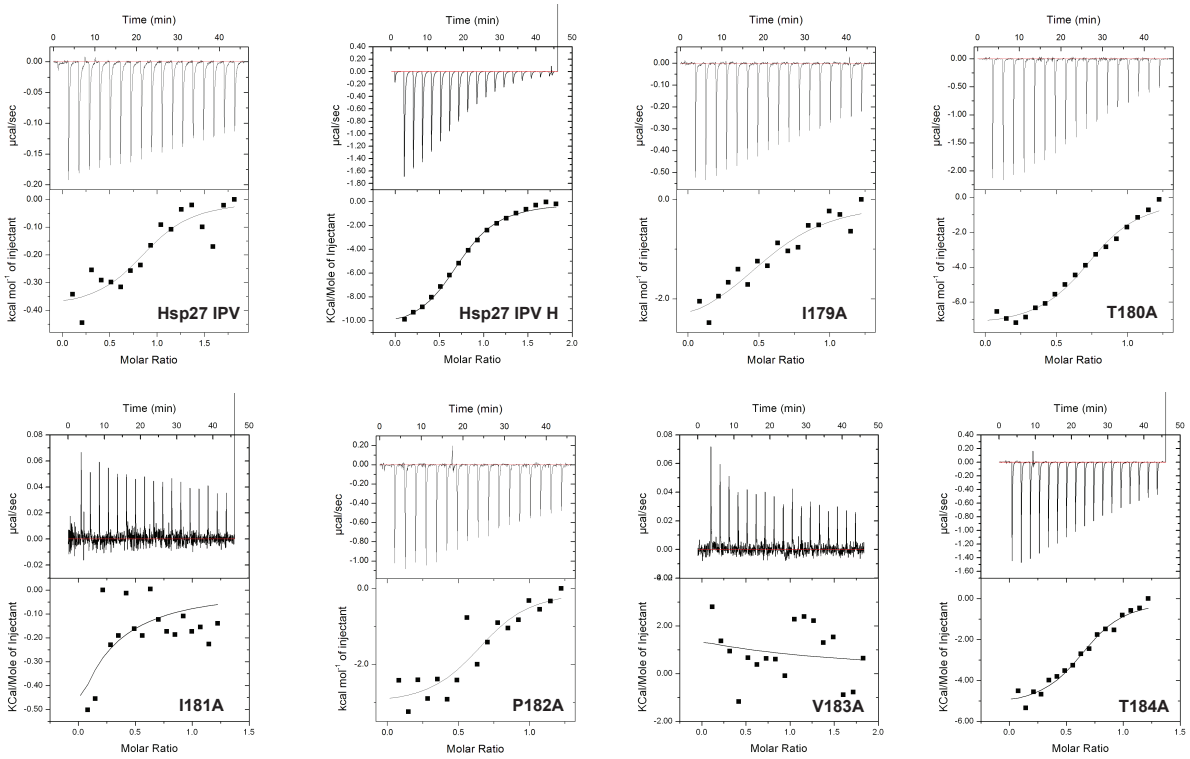

B. Representative ITC curves from Figure 4B, optimized IPV peptide with various Hsp27 constructs.

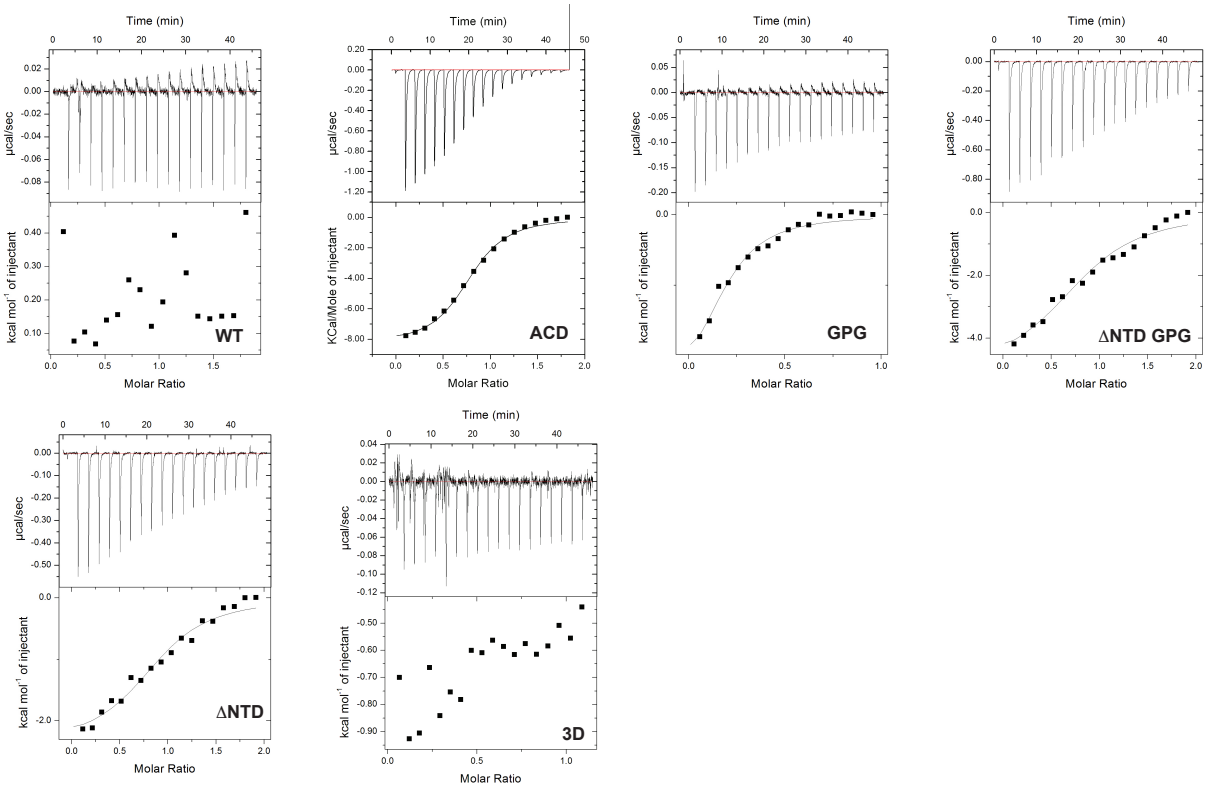

Figure S3.2. Representative ITC curves from figures 3.1D and 3.4B.

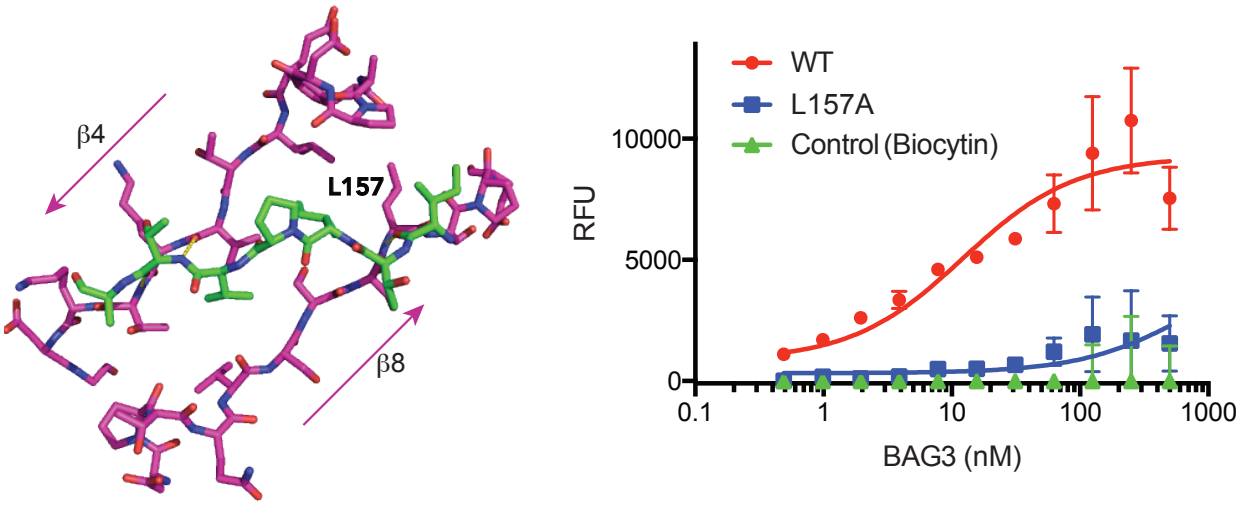

Figure S3.3. L157A ACD is deficient in BAG3 binding. Left, crystal structure (PDB: 4MJH) of Hsp27's IPV peptide bound to the β4/β8 groove of the ACD. Residue L157 is labeled. Right, interaction of Hsp27 ACD (WT and L157A) with BAG3 as measured by FCPIA[37].

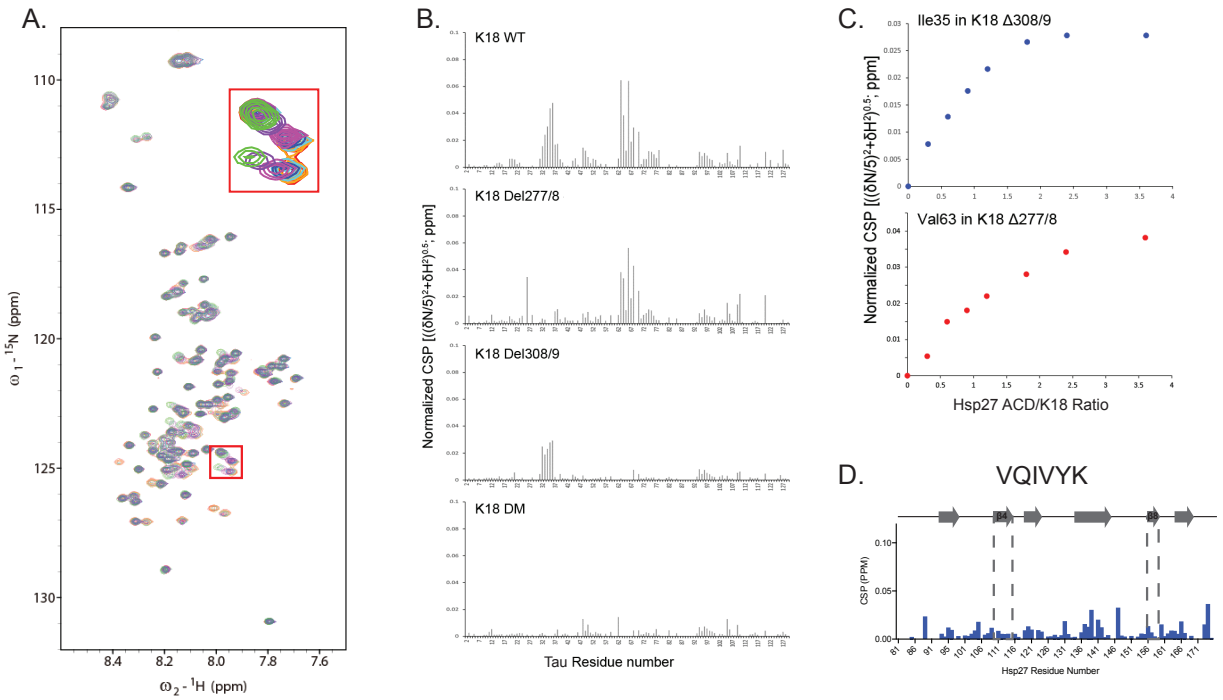

Figure S3.4. Interaction of Hsp27's ACD with K18 Tau. (A) TROSY HSQC spectra of ^{15}N WT K18 Tau (red) in the presence of increasing concentrations of ACD. (B) Chemical shift perturbations of listed Tau constructs in the presence of 2:1 molar ratio of ACD (120 μM). K18 DM, double mutant. (C) Concentration dependence of CSPs for listed residues and constructs in the presence of increasing concentrations of ACD. (D) CSPs of Hsp27 ACD in the presence of 3.3-fold molar excess of PHF6* peptide (500 μM).

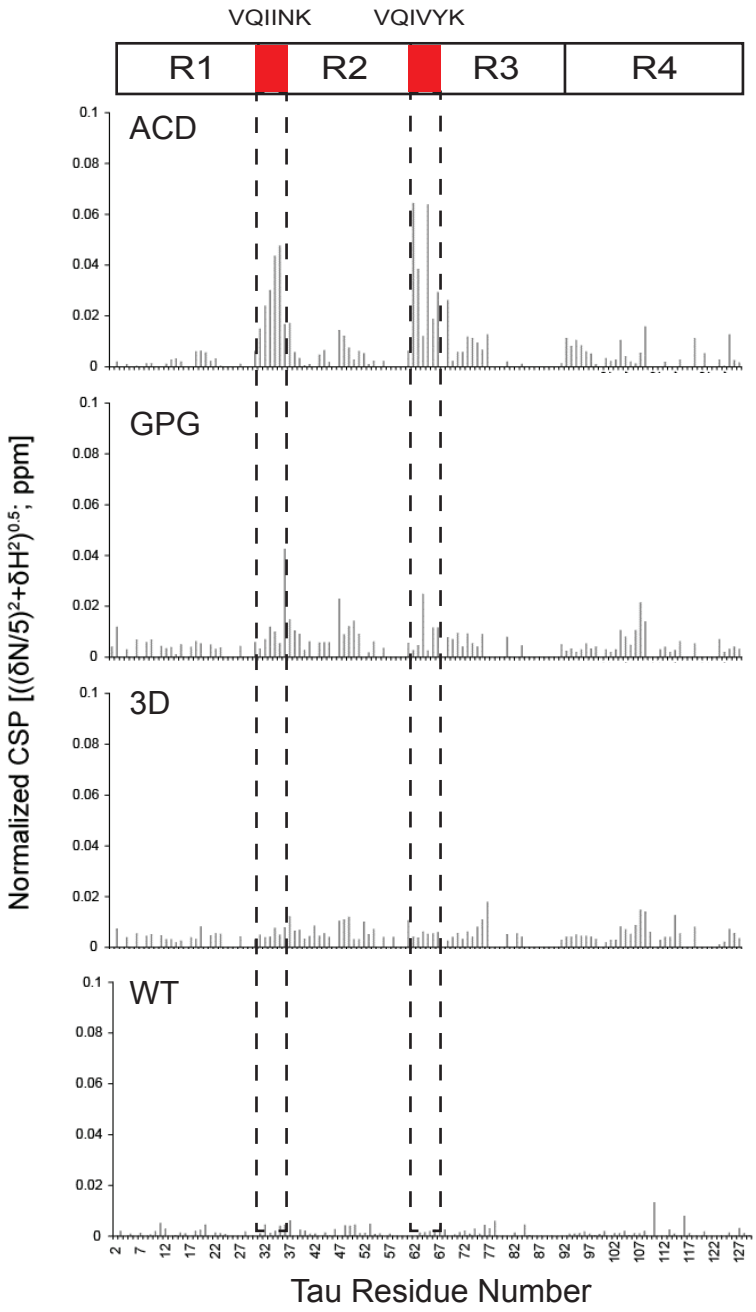

Figure S3.5. TROSY HSQC of full length Hsp27 constructs with WT K18. CSPs of WT K18 in the presence of 3.6-fold molar excess of listed Hsp27 constructs.

A. 0N4R curves have more consistent replicates, with a lesser overall chaperone effect. Hsp27 3D is slightly better than or the same as WT.

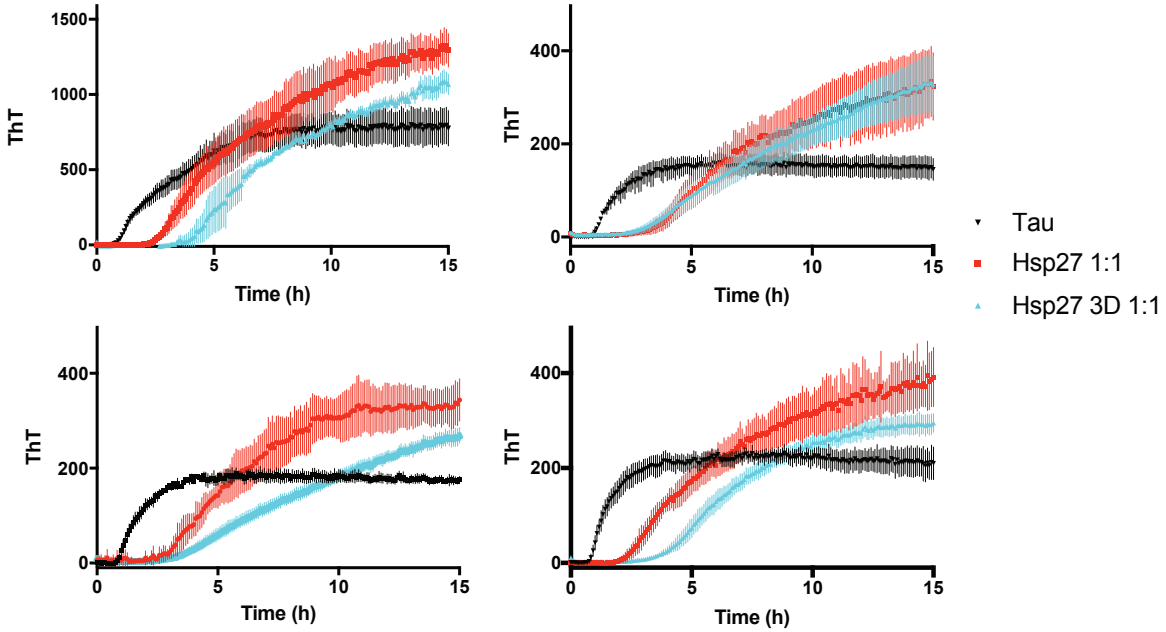

B. K18 curves have high replicate variability and larger effects on Tau aggregation. WT Hsp27 is better than 3D.

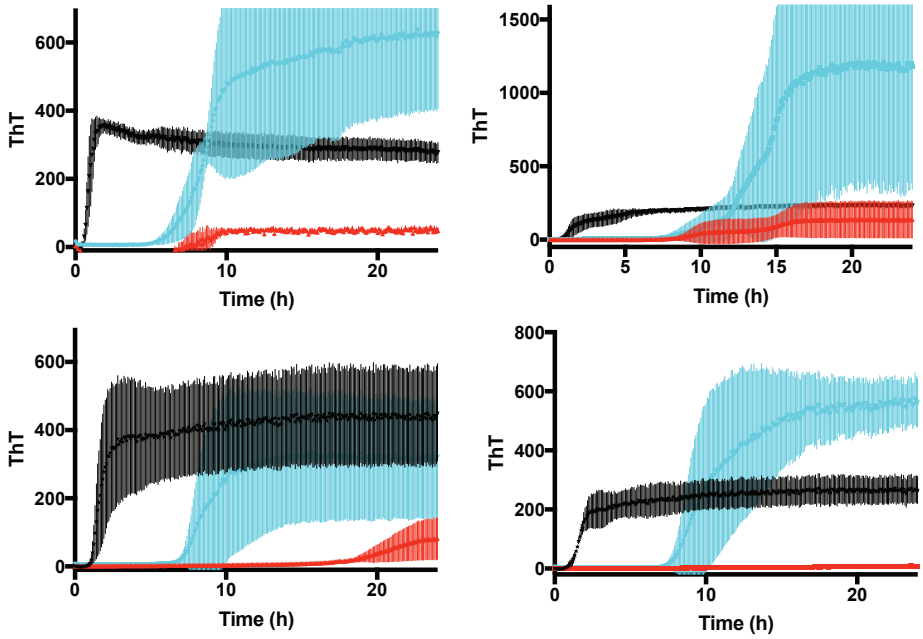

Figure S3.6. Sample Aggregation curves of Tau constructs with full-length Hsp27 constructs. Four independent replicates of K18 (A) or 0N4R (B) (both, 10 μM) in the presence of equimolar Hsp27 WT (red) or 3D (cyan). Data points are the mean ± SEM of 3 technical replicates.

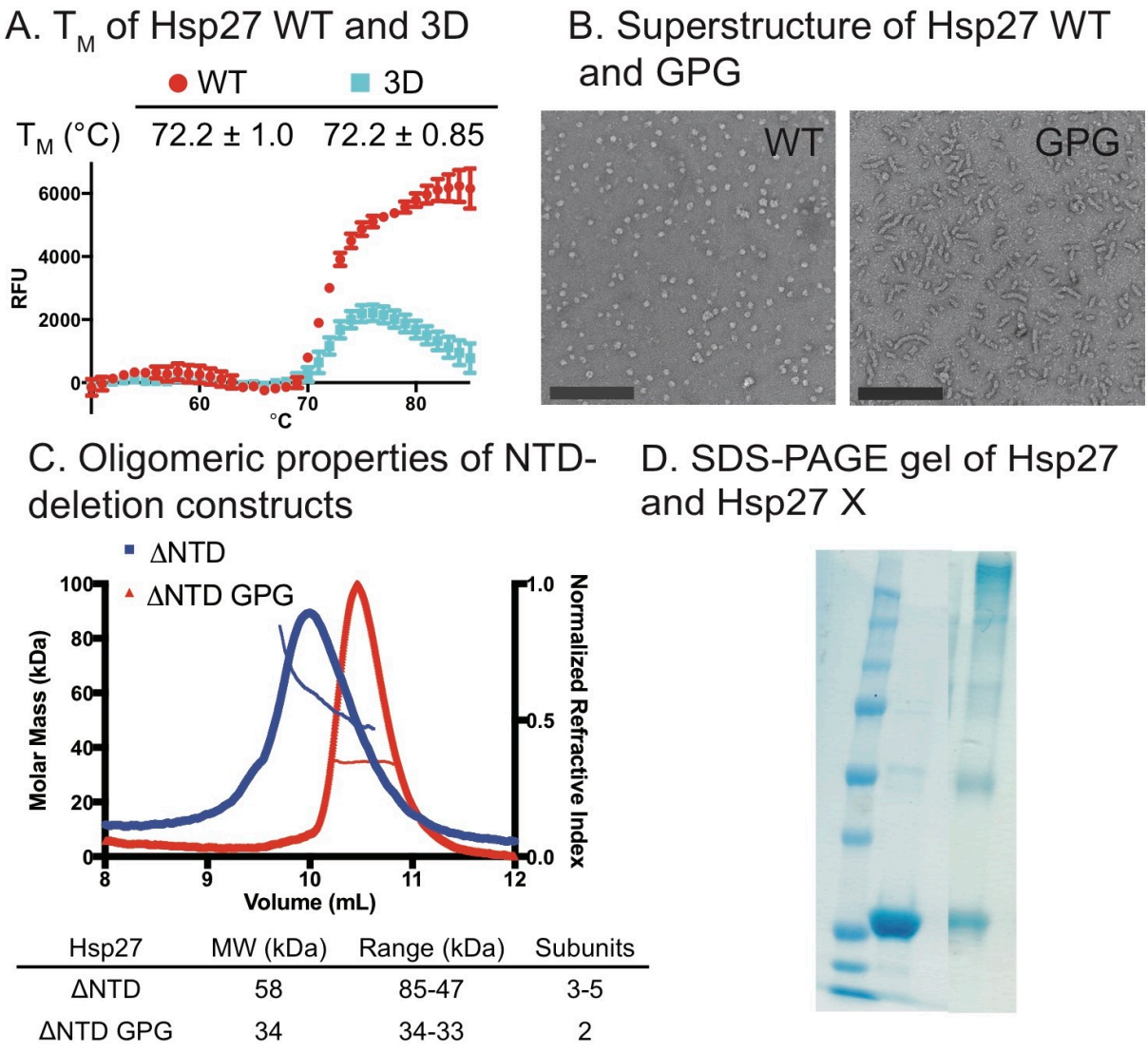

Hsp27	MW (kDa)	Range (kDa)	Subunits
ΔNTD	58	85-47	3-5
ΔNTD GPG	34	34-33	2

Figure S3.7. Oligomeric properties of Hsp27 constructs. (A) Differential scanning fluorimetry melting curves of Hsp27 WT and 3D. Data points are the mean ± SEM of three technical replicates. Listed melting temperatures are the mean ± SD of three independent experiments. (B) Negative stain EM images of WT (left) and GPG (right) Hsp27. Images are representative of a minimum of 12 random fields. Scale bar is 200 nm. (C) SEC-MALS trace of N-terminal deletion constructs (60 μM). (D) SDS-PAGE gel of Hsp27 and Hsp27X.

Publishing Agreement

It is the policy of the University to encourage the distribution of all theses, dissertations, and manuscripts. Copies of all UCSF theses, dissertations, and manuscripts will be routed to the library via the Graduate Division. The library will make all theses, dissertations, and manuscripts accessible to the public and will preserve these to the best of their abilities, in perpetuity.

Please sign the following statement:

I hereby grant permission to the Graduate Division of the University of California, San Francisco to release copies of my thesis, dissertation, or manuscript to the Campus Library to provide access and preservation, in whole or in part, in perpetuity.

Author Signature

9/3/18

Date